

**INVESTIGATION OF RAPID THERMAL ANALYSIS
PROCEDURES FOR PREDICTION OF THE SERVICE
LIFE OF PCCP CARBONATE COARSE AGGREGATE**

PHASE I PROGRESS REPORT

APRIL 30, 1992

IOWA DOT PROJECT HR-337
ERI PROJECT 3473

Sponsored by the Highway Division of the
Iowa Department of Transportation and the
Iowa Highway Research Advisory Board

ENGINEERING RESEARCH INSTITUTE

IOWA STATE UNIVERSITY

ISU-ERI-AMES 92-409

**INVESTIGATION OF RAPID THERMAL ANALYSIS
PROCEDURES FOR PREDICTION OF THE SERVICE
LIFE OF PCCP CARBONATE COARSE AGGREGATE**

PHASE I PROGRESS REPORT

APRIL 30, 1992

**S. SCHLORHOLTZ
B.V. ENÜSTÜN
K.L. BERGESON**

**IOWA DOT PROJECT HR-337
ERI PROJECT 3473
ISU-ERI 92-409**

Sponsored by the Highway Division of the
Iowa Department of Transportation and the
Iowa Highway Research Advisory Board

"The opinions, findings and conclusions expressed in this publication are those of the authors and not necessarily those of the Highway Division of the Iowa Department of Transportation."

TABLE OF CONTENTS

ABSTRACT.....	iii
INTRODUCTION.....	1
RESEARCH APPROACH.....	1
Sampling Scheme.....	1
Equipment and Methods.....	1
CURRENT STATUS.....	3
RESULTS AND DISCUSSION.....	4
X-ray Studies.....	4
Thermal Analysis Studies.....	11
FURTHER DISCUSSION.....	15
Particle Size Effect.....	23
SUMMARY.....	36
Field Performance of Limestone Aggregates.....	36
ACKNOWLEDGMENTS.....	37
REFERENCES.....	37
APPENDIX I (X-ray Diffractograms)	
APPENDIX II (Crystallite Size Study)	
APPENDIX III (Thermal Curves)	

ABSTRACT

The major objective of this research project is to utilize thermal analysis techniques in conjunction with x-ray analysis methods to identify and explain chemical reactions that promote aggregate related deterioration in portland cement concrete.

The first year of this project has been spent obtaining and analyzing limestone and dolomite samples that exhibit a wide range of field service performance. Most of the samples chosen for the study also had laboratory durability test information (ASTM C 666, method B) that was readily available.

Preliminary test results indicate that a strong relationship exists between the average crystallite size of the limestone (calcite) specimens and their apparent decomposition temperatures as measured by thermogravimetric analysis. Also, premature weight loss in the thermogravimetric analysis tests appeared to be related to the apparent decomposition temperature of the various calcite test specimens:

INTRODUCTION

The following report summarizes research activities conducted on Iowa Department of Transportation Project HR-337, for the period May 1, 1991 through April 30, 1992. The objective of this research project is to utilize thermal analysis techniques in conjunction with x-ray analysis techniques to identify and explain chemical reactions that promote aggregate related deterioration in portland cement concrete.

RESEARCH APPROACH

Sampling Scheme

Twenty coarse aggregate samples were selected for the first phase of this study. The samples were selected based on availability, homogeneity and service record. A summary of the samples that were selected is given in Table 1. The table also lists the aggregates service record and durability factor (ASTM C 666, method B) when used in IDOT C-3 concrete mixes [1,2].

A sample size of 200 to 300 pounds of crushed stone was taken from the various quarries. One third of the sample (about 100 pounds) was crushed in a jaw mill to obtain a maximum particle size of about 1/4 inch. A representative sub sample of this crushed material was then obtained by riffle splitting. This sample was used for the chemical and physical tests conducted in this research project. The remaining (uncrushed) sample was placed in storage.

Equipment and Methods

All of the aggregate samples were subjected to detailed chemical and mineralogical analysis. X-ray methods were utilized for bulk composition (both bulk chemistry and bulk mineralogy). Also, thermal analytical techniques and scanning electron microscopy were used to study the thermal stability and morphology, respectively, of the various stone samples.

X-ray diffraction (XRD) was used to identify the major and minor crystalline compounds present in each sample. The identification of minor constituents was enhanced by an acid

Table 1. Summary of the Coarse Aggregate Samples Studied in Phase I

Sample Identification	Quarry Location	Service Record, Years to Visible Deterioration	C 666 Durability Factor
Eldorado	SW17 T095 R08W	40	97
Maryville	SE24 T091 R07W	40	96
Alden (tan, bed 3)	NW20 T089 R21W	40	96
Crescent (beds 25 d, e)	35 T076 R44W	07	75
Menlo (bed 15)	SE17 T077 R31W	10	88
Montour (beds 1-7)	NW09 T083 R16W	40	84
Garrison (beds 12-16)	NE33 T085 R11W	15	100
Pesky (bed 5)	SW01 T088 R12W	15	90
Lamont (bed 4)	NW14 T090 R07W	40	96
Cedar Rapids South-Gray	NW07 T082 R07W	N/A	N/A
Cedar Rapids South-Tan	NW07 T082 R07W	40	99
Plower (beds 1-9)	SE36 T086 R06W	10	88
Early Chapel (bed 15)	NW10 T076 R29W	10	65
Linwood	SW13 T077 R02E	30	94
Bryan	Minnesota	15	93
Conklin (beds 6-9)	NW33 T080 R06W	30	88
Skyline (beds 1-3)	SE10 T098 R08W	25-30	92
Gassman	SE07 T088 R03E	40?	N/A
Huntington	Missouri	20-25	92
Le Claire	NW35 T079 R05E	25	98

N/A = Not Available

? = Questionable

digestion process which removed the major (carbonate) minerals from the test specimen. A Siemens D 500 x-ray diffractometer was used throughout this study. The diffractometer was controlled by a PDP 11/23 computer via an LC 500 interface. A copper x-ray tube was used for all diffraction work. The diffractometer was equipped with a diffracted beam monochromator. Normally the diffractometer was operated with the various slits in a medium resolution

configuration; however, the slits were placed in a high resolution configuration for some of the crystallite size measurements.

X-ray fluorescence (XRF) analysis was used to quantify the major, minor and selected trace elements present in the various samples. A Siemens SRS 200 sequential x-ray spectrometer was used for all the analyses. The spectrometer was fully computer controlled via an IBM compatible microcomputer and a LC 200 interface. The spectrometer was operated in vacuum mode, and, depending on the element of interest, employed either a chromium or tungsten x-ray tube.

The thermal analysis studies utilized a TA Instruments 2000 thermal analysis system. The system employed a TA Hi-Res. TGA thermogravimetric analyzer module and a DSC 2910 module for either a differential scanning calorimeter (DSC) cell or a high temperature (1600°C) differential thermal analyzer (DTA) cell. The TGA system is equipped with a 16 sample carousel. A typical TGA experiment used the following analytical parameters: (1) a scanning rate of 40° per minute, resolution = 5; (2) a sample mass of 55 ± 2 milligrams; (3) a dynamic nitrogen or carbon dioxide atmosphere (depending on the goal of the experiment), purged at 100 ml per minute; (4) test specimens were heated from 100°C to about 970°C.

A JEOL JSM-840 scanning electron microscope (SEM) was used to examine the morphology of the coarse aggregate samples. The SEM is interfaced to both a KEVEX Delta V Microanalyzer and a WDX-2A wavelength dispersive x-ray spectrometer, this allows researchers to supplement morphological features with detailed chemical information.

CURRENT STATUS

All of the crushed stone samples have been obtained and processed. Hand specimens have been obtained from LeClaire, Plower, Garrison, Montour, South Cedar Rapids, Early Chapel and Pesky. The remaining hand specimens should be obtained early in the second year of the research project.

The bulk chemistry has been obtained for all the stone samples included in this study. Work is still continuing on the determination of trace elements in the various rock samples.

The initial mineralogical investigation of the bulk rock samples has been completed. Also, the acid insoluble residue from each sample has been subjected to XRD analysis to help identify the minor constituents that are present. The preliminary crystallite size determinations have been completed for the limestones studied in this project. However, several refinements will need to be made in the experimental procedure to enhance the reliability of the measurements.

The preliminary thermal stability studies have been completed on all the stone samples. The detailed studies (i.e., sodium chloride and calcium chloride treatments) should be completed by the late summer or early fall of 1992. This should put the project slightly ahead of the activity schedule listed in the proposal. Hence, this may allow for the investigation of additional rock specimens as described in Task #9 in the research proposal. Discussion with Wendell Dubberke, Geologist, at the Iowa Department of Transportation, has indicated that research project HR-336 has uncovered several different coarse aggregate sources that merit more investigation.

RESULTS AND DISCUSSION

X-ray Studies

The results of the bulk XRD scans are summarized in Table 2. X-ray diffractograms of all the samples can be found in Appendix I. The JCPDS database information that was used to identify the various diffractograms has also been placed in Appendix I.

The preliminary results of the acid insoluble residue tests are also summarized in Table 2. The tests were performed in a manner similar to the standard procedure described in ASTM D 3042; however, the test specimens were ground to passing a 100 mesh sieve to reduce the time needed to dissolve the carbonate fraction of the sample. Also, the samples were dried at 50°C (rather than 110°C) to allow for identification of the clay minerals present in the acid-insoluble

material. Further work is currently being conducted on the acid-insoluble material which should enhance the identification of the clay minerals that are present in the various samples.

Table 2. Minerals Identified in the Various Test Specimens by using XRD Analysis

Sample	Mineral						Acid Insoluble Residue (wt %)
	Calcite	Dolomite	Quartz	Pyrite	Clay	Feldspar	
Calaites							
Alden	M	-	-	-	T	-	0.38
Crescent	M	T	m	-	T	-	?8.4
Conklin	M	-	-	-	-	-	0.90
Early Chapel	M	m	m	-	T	-	3.76
Eldorado	M	-	T	-	T	-	1.01
Linwood	M	T	m	-	-	-	?2.1
Menlo	M	-	m	-	T	-	4.46
Montour	M	T	-	T	-	-	1.48
Skyline	M	M	m	-	T	-	?16.0
Huntington	M	m	m	-	-	-	2.13
Dolomites							
Maryville	m	M	T	-	-	-	?9.1
Bryan	m	M	m	-	T	T	10.3
Cedar Rapids-Gray	T	M	m	T	T	-	2.94
Cedar Rapids-Tan	T	M	T	-	-	T	1.29
Garrison	m	M	T	T	-	-	?6.8
Gassman	m	M	m	-	T	-	2.34
Lamont	T	M	T	-	-	-	1.59
LeClaire	T	M	T	-	-	T	3.87
Pesky	m	M	T	-	-	-	2.15
Plower	M	M	m	-	-	-	2.47

M = major component; m = minor component; T = trace/uncertain

? = experimental difficulties, the test is being repeated and the test results will be updated in future reports.

Several of the acid-insoluble test results appear to be erroneously high, this may be due to incomplete digestion. These tests are currently being repeated.

The results of the bulk XRF tests are summarized in Table 3. The loss-on-ignition (LOI) values listed in the table were obtained from the thermal analysis phase (100 - %Residue, N₂ gas atmosphere) of this study. All of the assays have been expressed as oxides. This allows one to quickly check the overall reliability of the analysis since the oxide totals should approximate 100 percent. Several of the chemical assays appear to be quite poor (for instance, see the test results

Table 3. Results of Bulk XRF Analyses on the Carbonate Stone Specimens

Oxide (wt.%)	Calaites										Dolomites									
	Early Chapel	Menlo	Conklin	Montour	Crescent	Eldorado	Skyline	Huntington	Linwood	Alden	Maryville	Gassman	Ced. Rapids-Gray	Bryan	LeClaire	Lamont	Garrison	Plower	Pesky	Ced. Rapids-Tan
SiO ₂	2.77	3.99	0.62	0.27	2.41	1.20	1.87	1.50	0.79	0.16	2.16	2.07	2.83	7.67	1.46	1.46	2.27	2.56	1.69	0.76
Fe ₂ O ₃	0.60	0.33	0.19	0.60	0.18	0.16	0.31	0.12	0.22	0.20	0.27	0.93	0.30	2.74	0.35	0.20	0.84	0.94	0.46	0.53
Al ₂ O ₃	0.40	0.37	0.12	0.05	0.25	0.26	0.28	0.13	0.16	0.23	0.42	0.42	0.24	0.77	0.33	0.23	0.48	0.44	0.31	0.16
TiO ₂	0.02	0.02	0.01	<0.01	0.02	0.02	0.02	0.01	0.01	0.02	0.03	0.03	0.02	0.04	0.03	0.02	0.03	0.03	0.02	0.01
P ₂ O ₅	0.02	0.02	<0.01	<0.01	0.01	<0.01	0.03	0.04	<0.01	<0.01	0.01	0.01	0.01	0.08	0.01	<0.01	0.02	0.02	<0.01	0.01
MnO	0.04	0.03	0.05	0.02	0.02	0.01	0.02	0.02	0.05	0.02	0.04	0.04	0.03	0.20	0.04	0.02	0.04	0.04	0.02	0.03
CaO	52.39	52.56	53.44	53.13	52.94	54.89	47.40	52.72	52.96	53.75	52.39	52.96	30.34	28.92	30.08	30.34	32.39	31.91	34.38	30.12
SiO	0.04	0.04	0.02	0.02	0.04	0.02	0.02	0.02	0.02	0.03	0.04	0.02	0.02	0.20	0.04	0.02	0.04	0.02	0.02	0.03
MgO	0.71	0.35	0.44	0.41	0.42	0.29	4.34	1.18	0.32	0.30	0.71	0.35	18.84	15.72	18.43	18.52	15.62	16.72	13.18	18.54
K ₂ O	0.08	0.08	0.04	0.01	0.06	0.08	0.14	0.04	0.04	0.01	0.08	0.04	0.11	0.31	0.09	0.07	0.15	0.16	0.10	0.06
SO ₃	0.04	<0.01	0.04	0.20	0.05	0.03	<0.01	0.04	0.09	<0.01	0.04	0.04	0.06	0.04	0.03	0.02	0.03	0.03	0.02	0.01
LOI	42.6	42.3	43.7	42.9	42.9	43.4	44.0	43.6	43.2	44.1	42.6	42.3	43.7	42.9	42.9	43.4	44.0	43.6	43.2	44.1
SUM	99.7	100.1	98.7	97.6	99.3	100.4	98.4	99.4	97.9	98.6	99.7	100.1	98.7	97.6	99.3	100.4	98.4	99.4	97.9	98.6

for Lamont, Maryville and Gassman) because the test results are much higher than 100 percent. However, all three of these specimens exhibited premature weight loss in the thermal analysis portion of this study. In fact, the error in the chemical assays of the three samples appears to be proportional to the magnitude of the premature weight loss. Also, the reliability of the XRF test method was evaluated by inserting standards into the spectrometer along with the test specimens. Two of the standards were certified reference materials of National Institute of Standards and Technology (NIST, previously known as the NBS) or British Chemical Society (BCS) quality. The remaining standard was high purity calcite from Fisher Scientific Company. One of the standards (NBS 1c) had been included in the original development of the calibration curves for the various elements; and hence, cannot be used to estimate the bias in the method. This standard was used only to monitor drift in the XRF spectrometer. The remaining standards (BCS 368 and Fisher Calcite) had not been used in the calibration procedure and can be used to estimate the potential bias in the analytical method. The test results obtained from the various standards are summarized in Table 4. The measured values are in reasonably good agreement with the

Table 4. Comparison of Measured (by XRF) and Certified Values for Three Standards

Oxide (wt.%)	NBS 1c*		BCS 368		Fisher Calcite	
	Measured	Certified	Measured	Certified	Measured	Certified
SiO ₂	6.90	6.84	0.86	0.92	0.02	N/M
Fe ₂ O ₃	0.57	0.55	0.25	0.23	0.00	<0.005
Al ₂ O ₃	1.20	1.30	0.10	0.17	0.02	N/M
TiO ₂	0.07	0.07	0.01	<0.01	0.01	N/M
P ₂ O ₅	0.04	0.04	0.01	-	0.00	N/M
MnO	0.02	0.025	0.05	0.06	0.01	N/M
CaO	50.68	50.3	30.85	30.8	55.01	56
SrO	0.025	0.03	0.017	<0.01	0.021	0.02
MgO	0.45	0.42	20.80	20.9	0.23	0.01
K ₂ O	0.27	0.28	0.02	<0.01	0.00	<0.01
Na ₂	N/M	0.02	N/M	<0.01	N/M	<0.01
LOI	N/M	39.9	N/M	46.7	43.8	44
SUM	-	99.8	-	99.8	99.1	100.0

* This standard was used in the calibration process for the elements (oxides) measured in this study.
N/M = not measured

certified (or specified) values. Therefore, we have concluded that there is either a particle size or matrix effect problem present in the XRF test results that we are currently not correcting for. This problem is currently being worked on and the accuracy of the XRF assays will be improved during Phase II of the project.

The crystallite size of the various samples is currently being measured using XRD techniques. The measurements for the calcite samples have been completed and will be described in this report. Crystallite size is important because it may influence the sample decomposition temperature that is observed in the thermal analysis experiments.

Two different crystallite size studies were conducted. The first study consisted of XRD scans over the calcite (104) peak (i.e., the largest peak in the patterns, located at 3.04\AA) for the various samples. The second study was much less precise but it investigated the influence of heat treatments on the calcite crystallite size.

The first crystallite size study consisted of a very slow, high resolution scan over the primary (3.04\AA) calcite peak. The study employed high resolution slits, a step size of $0.01^\circ 2\theta$ and a counting time of ten seconds at each step. The results obtained from a typical scan are illustrated in Figure 1. The plots of the scans for the other test specimens are located in Appendix II. The pertinent properties of the diffraction peak are also illustrated in Figure 1. The purpose of the study was to determine the full-width-at-half-maximum (FWHM) of the diffraction peak for the various specimens because this can be related to the average crystallite size. The preliminary results obtained from the study are summarized in Table 5. Please note, that the measurements have been corrected for peak broadening due to the $K\alpha$ doublet; however, the results have not been corrected for instrument broadening. The numbers will be corrected for instrument broadening when a suitable standard is found that can be used to accurately adjust the observed values. In general, the preliminary test results indicate a small increase in FWHM with decreasing service record. Further work is being conducted to: (1) define the precision and accuracy of the crystallite size determinations and (2) extending the study to include the dolomite samples.

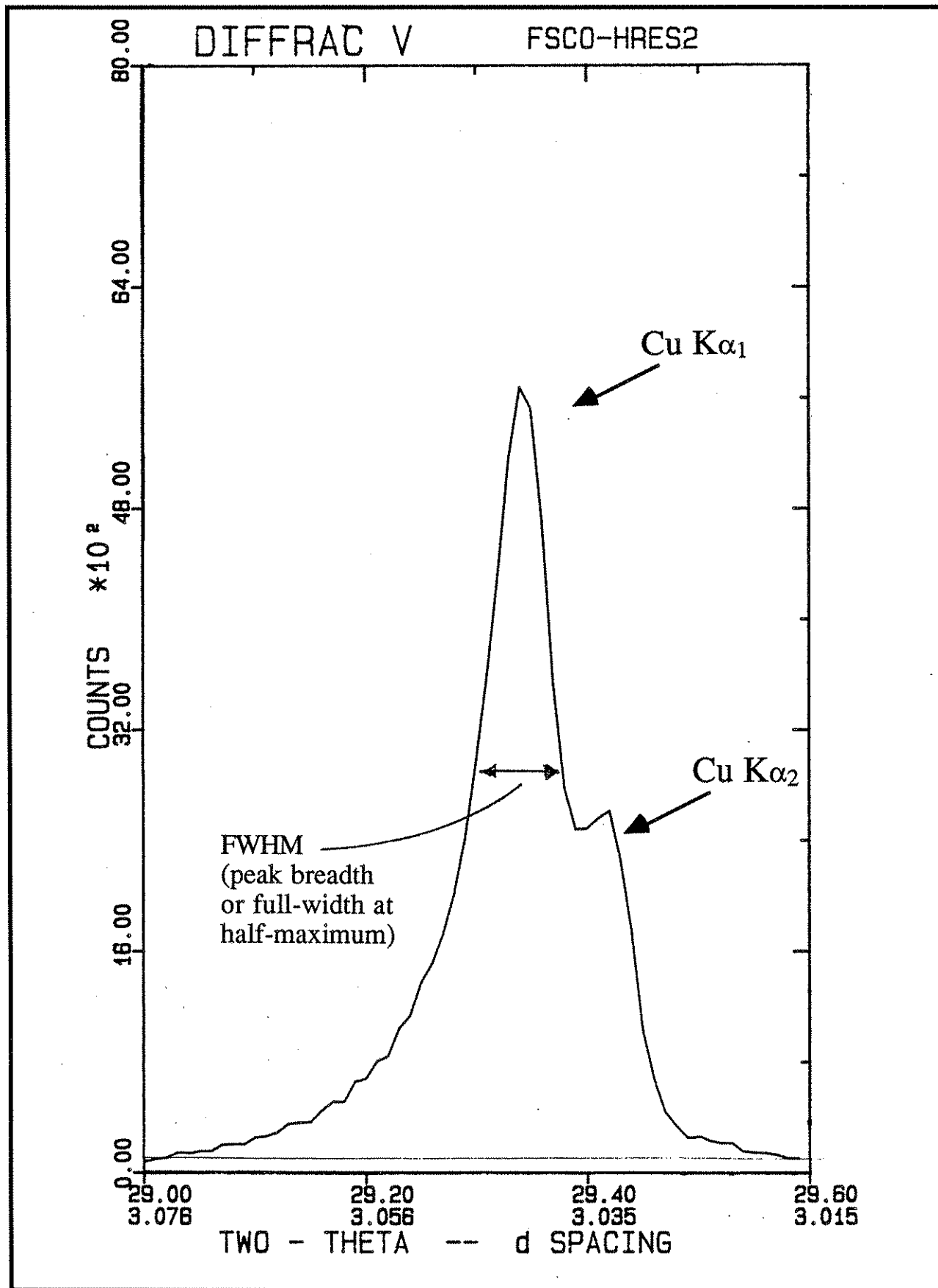


Figure 1. Diffraction profile for a high resolution scan of Fisher calcite.

Table 5. Preliminary Results of the Crystallite Size Study Conducted on Calcite Specimens

Sample	FWHM (measured, mm)	FWHM (degrees 2 θ)	FWHM ($^{\circ}2\theta$) (corrected for $K\alpha$ doublet broadening)
Montour	27.0	0.135	0.097
Skyline	26.0	0.130	0.090
Menlo	27.5	0.138	0.102
Linwood	25.5	0.128	0.087
Eldorado	25.0	0.125	0.084
Early Chapel	28.0	0.140	0.105
Conklin	27.0	0.135	0.097
Crescent	26.5	0.133	0.093
Alden	25.0	0.125	0.084
Fisher Calcite	16.0*	0.080	0.080

* $K\alpha$, peak resolved, no doublet broadening correction needed

The second crystallite size study was conducted on samples that had been subjected to a series of heat treatments in a carbon dioxide atmosphere. For the purpose of discussion the results obtained from a good limestone (Montour, 40 year service life), a poor limestone (Crescent, 7 year service life), and a standard calcite sample (Fisher calcite; used as a control specimen) will be discussed in detail.

The experimental procedure was as follows: (1) a one gram portion of each test specimen was weighed into a porcelain crucible; (2) the crucible was placed in a warm muffle furnace (temperature about 200°C) that was continuously purged with carbon dioxide; (3) the temperature was increased to the desired temperature (440, 550 or 810) and held constant ($\pm 20^{\circ}\text{C}$) for 15 ± 1 hours; (4) after treatment the crucibles were covered with lids and then removed from the muffle furnace; (5) the various samples were cooled to room temperature and then subjected to a series of tests (i.e., weight loss, XRD, crystallite size, etc.).

The results of the weight loss and XRD tests are summarized in Table 6. The general trend indicated by the test results suggests that the full-width-at-half-maximum tends to decrease during the heat treatments. The decrease is very small for the Fisher calcite but quite measurable for either the Crescent or Montour samples. Also, the change in FWHM appeared to take place

even at the lowest temperature used in this study (440°C). All three of the calcite specimens have very similar FWHM values (about $0.18^\circ 2\theta$) after the heat treatment at 810°C.

Table 6. Results of Heat Treatment Tests Conducted on Several Calcite Specimens

Sample	Treatment Temperature (°C)			
	Initial (25)	440	550	810
Crescent				
Weight loss, %	0.00	0.24	0.14	2.93
3.04Å FWHM, °2θ	0.241	0.209	0.214	0.176
2.28Å FWHM, °2θ	0.269	0.255	0.245	0.207
Montour				
Weight Loss, %	0.00	0.23	0.07	0.71
3.04Å FWHM, °2θ	0.214	0.193	0.208	0.177
2.28Å FWHM, °2θ	0.264	0.241	0.236	0.189
Fisher Calcite				
Weight Loss, %	0.00	0.02	0.03	0.03
3.04Å FWHM, °2θ	0.187	0.169	0.173	0.167
2.28Å FWHM, °2θ	0.191	0.183	0.200	0.183

Thermal Analysis Studies

The results of the thermogravimetric analysis (TGA) studies have been summarized in Tables 7 and 8. The various parameters listed in the two tables are defined in Figures 2 and 3. Please note, that each table contains information pertaining to tests that were conducted in either a carbon dioxide or a nitrogen atmosphere. The parameters for the samples tested in a nitrogen atmosphere were similar to those shown in Figure 2. However, the calcite and dolomite decompositions were not resolved by the tests and only an average decomposition temperature, denoted as DT_{Both} in Tables 7 and 8, has been listed for each of the test specimens. The actual thermal curves that were observed for the various test specimens can be found in Appendix III.

There are several trends that are readily apparent in Tables 7 and 8, and also in the thermal curves listed in Appendix III. First, the carbon dioxide atmosphere was essential for distinguishing calcite samples from dolomite samples in the TGA tests. Without the carbon

Table 7. Results of TGA Tests Conducted on Calcites

Sample	CO ₂ Atmosphere			N ₂ Atmosphere		
	DT _{CAL}	Loss from 600° to 900° C	Residue	DT _{CAL}	Loss from 400° to 650° C	Residue
Alden	930.5	0.38	55.55	688.9	0.76	55.94
Crescent	922.2	1.62	56.86	700.5	0.34	57.11
Conklin	923.0	0.75	56.33	694.2	0.36	56.33
Early Chapel	919.0	2.59	57.06	700.4	0.38	57.44
Eldorado	928.5	0.87	56.44	696.5	0.35	56.58
Linwood	925.4	0.65	56.42	702.3	0.33	56.79
Menlo	919.9	2.54	58.00	696.3	0.50	57.71
Montour	927.8	0.39	56.64	704.0	0.59	57.11
Skyline	919.0	0.63*	55.60	688.5	1.02	55.98
Huntington	925.2	0.31*	56.22	696.0	1.18	56.43
FSCO	947.1	0.00	56.19 ± 0.14**	684.8	0.43	56.06
Wards-Calcite	933.7	0.08	56.14	681.8	0.49	56.00
Synthetic- Calcite	911.0	0.65	55.98	N/M	N/M	N/M

* loss from about 800° to 900° C used because of presence of dolomite

** test result based on 5 repetitions

N/M = not measured

Table 8. Results of TGA Tests Conducted on Dolomites

Sample	CO ₂ Atmosphere					N ₂ Atmosphere		
	DT _{DOL}	DT _{CAL}	Residue	Loss from 400° to 700°C	Loss from 800° to 900°C	DT _{Both}	Residue	Loss from 400° to 650°C
Maryville	743.3	916.2	49.09	9.71	0.82	676.1	48.71	10.65
Bryan	730.6	916.1	53.77	7.51	1.78	682.9	57.01	3.15
Cedar Rapids-Gray	733.4	916.0	52.60	3.93	0.84	678.4	52.80	3.39
Cedar Rapids-Tan	738.2	917.1	52.26	2.38	0.68	679.4	52.46	1.95
Garrison	724.8	911.9	54.21	2.23	2.25	684.5	54.71	1.60
Gassman	724.2	913.3	47.92	14.19	1.10	676.5	48.11	12.67
Lamont	726.6	917.2	45.93	15.67	0.65	673.2	46.81	14.1
LeClaire	736.5	916.2	52.51	2.61	0.93	678.9	52.90	2.20
Pesky	728.1	911.7	53.90	2.16	1.33	684.0	53.97	1.29
Plower	736.5	914.8	54.54	1.44	1.06	683.1	54.26	1.35

dioxide atmosphere (i.e., see test results in nitrogen) both calcites and dolomites decomposed within a temperature range of about 25°C, although the calcite samples tended to decompose closer to 700°C than did the dolomite samples. Secondly, the residue values obtained for calcite

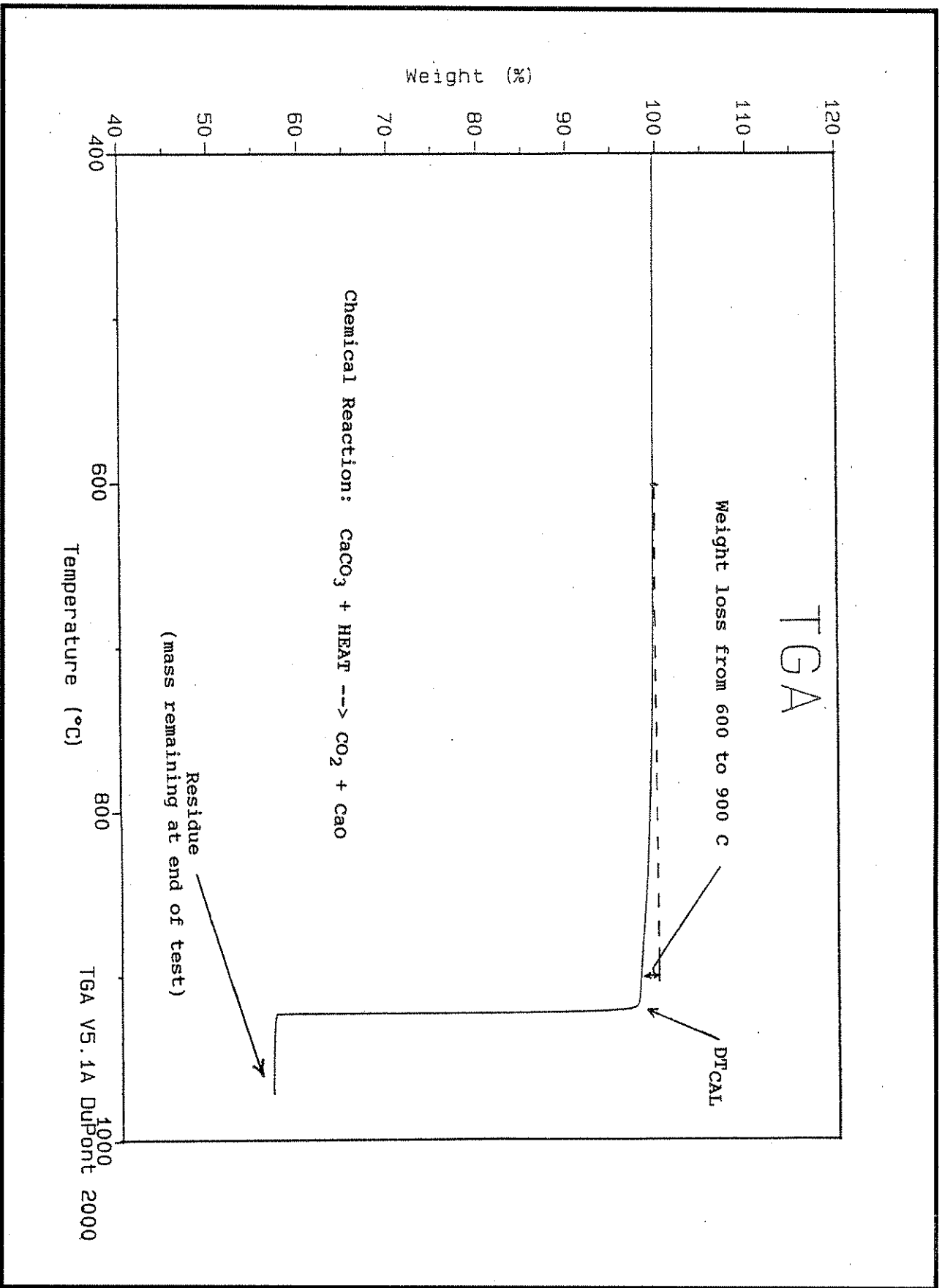


Figure 2. Illustration of the various parameters used to characterize calcite.

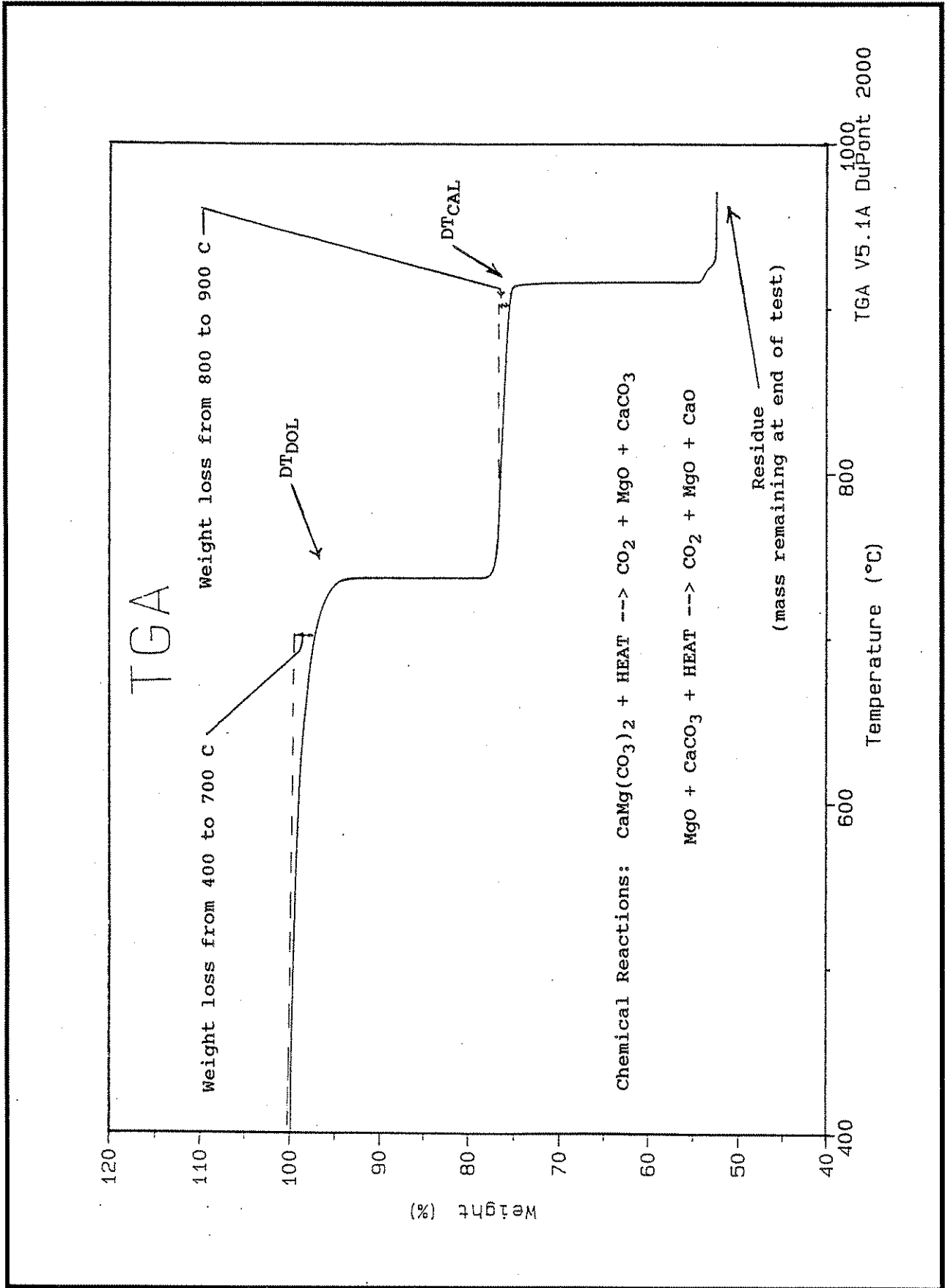
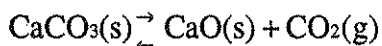


Figure 3. Illustration of the various parameters used to characterize dolomites.

samples tested in a nitrogen atmosphere tended to be slightly larger than those observed from the same samples that had been tested in a carbon dioxide atmosphere. This trend was also observed for many of the dolomite samples. And finally, several of the dolomite samples (Lamont, Maryville, Gassman, and to some extent, Bryan) exhibited a very gradual weight loss during early stages of the TGA scans. The purge gas had only a minor influence on this decomposition reaction because neither the onset nor the weight loss of the reaction changed dramatically when carbon dioxide gas was substituted for nitrogen gas (see Figure 4). Therefore, one may conclude that the decomposition reaction did not release carbon dioxide as a product. The exact nature of this early decomposition reaction is currently being studied.

FURTHER DISCUSSION

Chemical thermodynamics tells us that decomposition of a pure crystalline compound under a constant (atmospheric) pressure into two or more products, each forming a new pure phase, constitutes an "invariant" system. For instance, applying the "phase rule" to thermally decomposing calcite



one finds that the "degree of freedom" of the system at constant pressure is zero. This means that if the decomposition reaction is carried out with an infinitesimal rate, the temperature of this system should remain constant. Only when all CaCO_3 is gone, i.e., when the system consists of $\text{CaO}(\text{s}) + \text{CO}_2(\text{g})$, the system becomes "monovariant." Only then its temperature can be increased.

The thermodynamic (equilibrium) decomposition temperature can be computed from the literature values of standard free energies and enthalpies of formation and the specific heats of the species involved in the reaction. Using recent data [3], such a computation gives 853°C for the thermodynamic decomposition temperature of calcite.

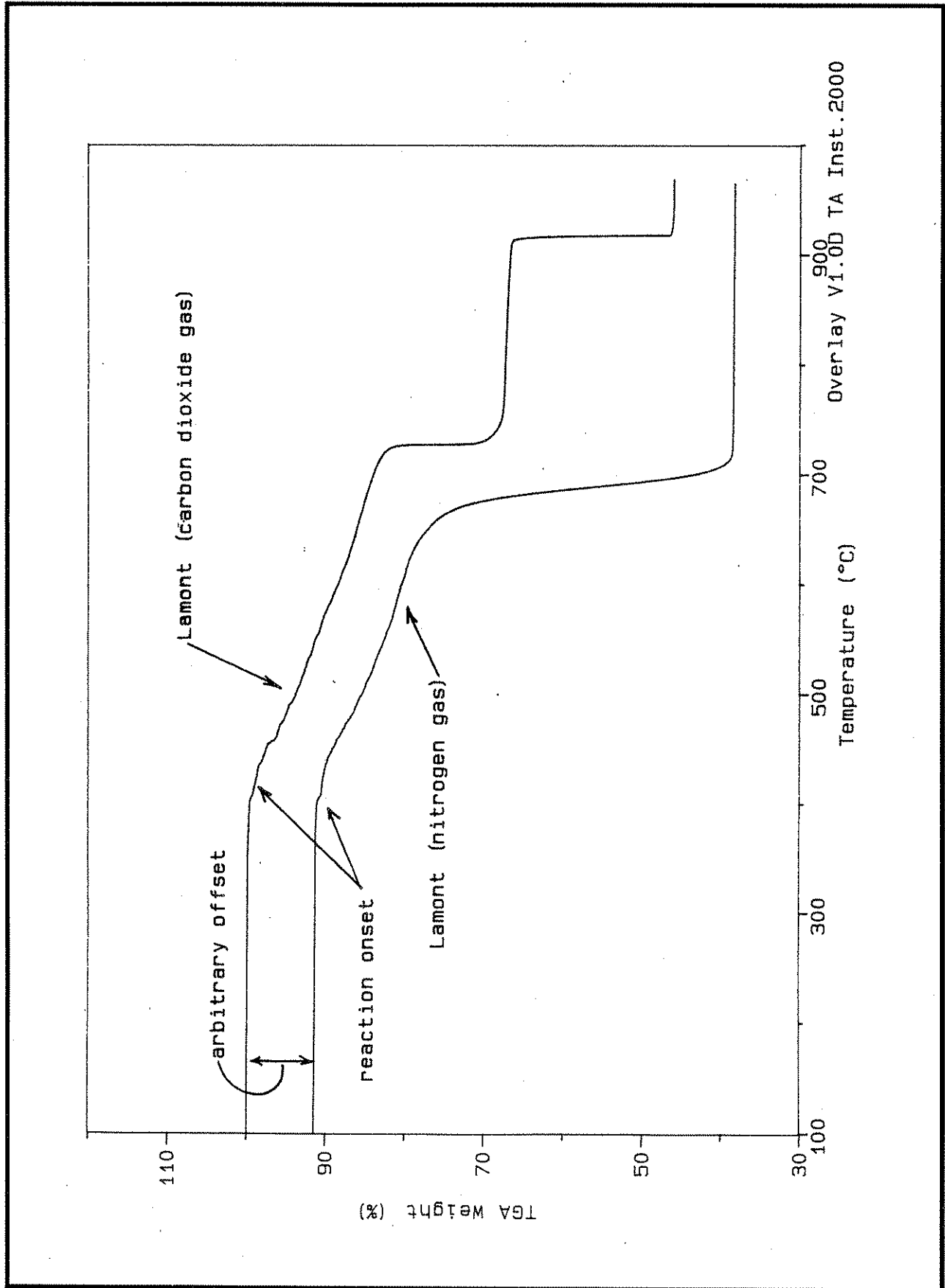


Figure 4. Thermal curves for the decomposition of Lamont dolomite in nitrogen or carbon dioxide atmospheres.

Therefore, if the scanning were infinitesimally slow, the thermogravimetric analysis (TGA) chart for a pure calcite sample purged with CO_2 gas would look like as represented by the dashed line in Figure 5.

At a finite rate of heating, however, the picture is more complex. In the first place, there will be a difference between the measured furnace temperature and the sample temperature at any time during scanning, depending on the scanning rate. When the sample reaches the decomposition temperature, it will start decomposing. As regards to the rate of reaction, we may consider two cases:

- (1) If the reaction is endothermic, as in decomposition of CaCO_3 , and fast enough, the rate is controlled by heat transfer from the furnace to the sample. During decomposition the sample temperature will remain constant. Therefore, linearly rising furnace temperature is expected to accelerate the heat transfer and, thus, also the rate of reaction in a linear fashion. Then, the actual TGA plot will be a parabola concave downwards as shown by the solid line in Figure 5. (A rounded, rather than a sharp, beginning of the parabola signifies a finite rate of warming up of the whole mass of sample to come to the decomposition temperature.) In this case, the dashed line will represent the sample temperature. Near the end of reaction, i.e., when only a small amount of CaCO_3 is left over, to maintain the thermodynamic decomposition temperature, the rate of reaction per unit surface area of the reactant must (and will) increase tremendously. However, it cannot increase above that imposed by the absolute specific rate of reaction (i.e., per unit surface area of the solid reactant) which is controlled by the activation energy. From this moment on, the reaction becomes rate-controlled, and slows down, allowing the sample temperature to rise slightly as represented by dotted line in Figure 5. This shapes the parabolic TGA curve to end with a short tail, as shown in the figure, creating an inflection point. Needless to say, the location of this point on the temperature axis is far from the thermodynamic decomposition temperature or from the sample temperature.

HR - 337

Calcite Standards -- Normal TGA Scan

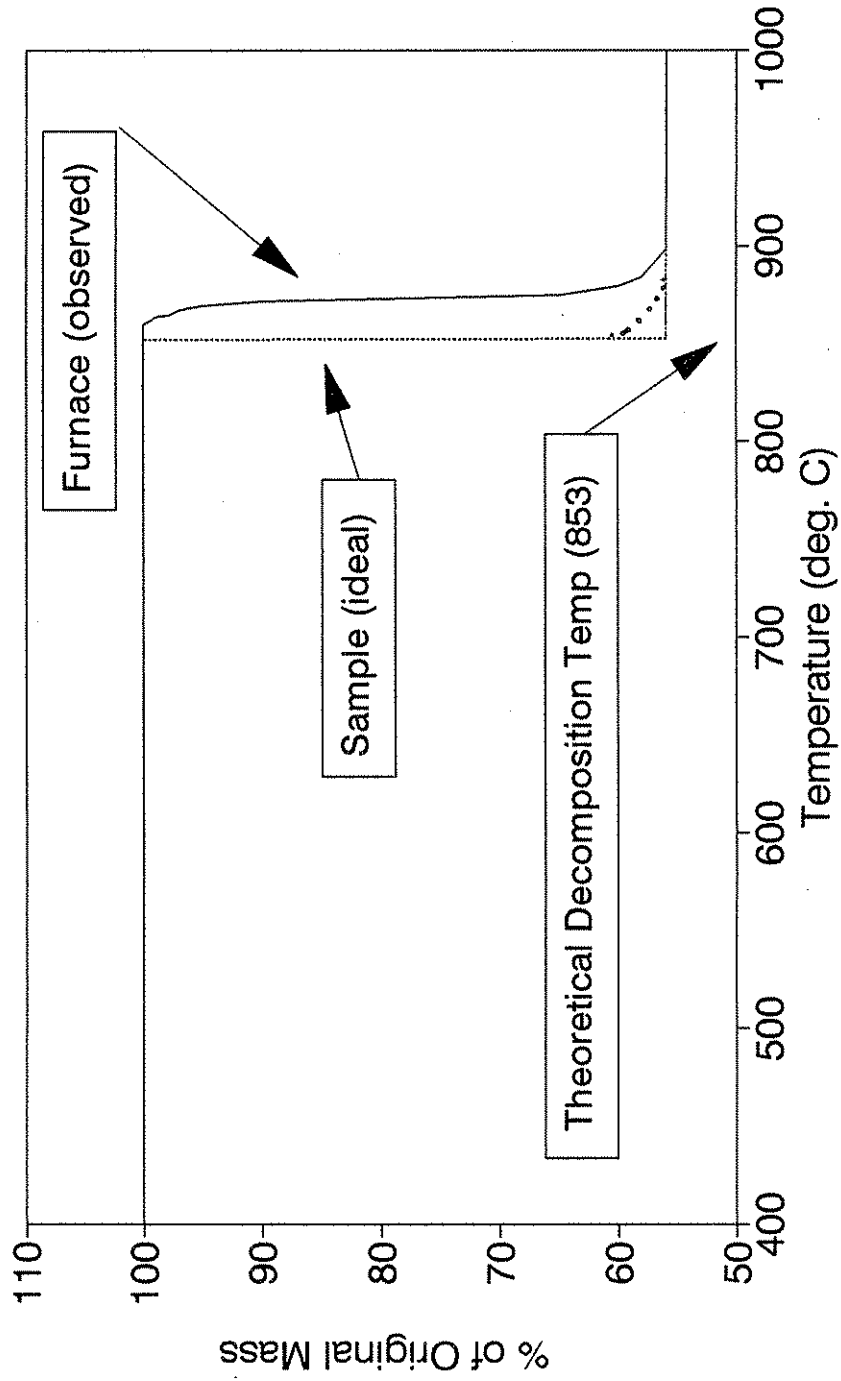


Figure 5. Thermal curve for the decomposition of calcite (fast reaction) in a normal TGA scan.

- (2) If the endothermic reaction is very slow due to small specific rate, then it is rate-controlled right from the beginning. In this case an insignificant fraction of heat transferred from furnace to the sample is consumed by the reaction, and the sample temperature runs practically at the same rate as the furnace temperature, and the difference between the furnace and the sample temperatures remains constant. As the temperature is increased linearly, the rate of reaction slightly but progressively increases as required by the Arrhenius equation. Using a finite rate of scanning, the reaction may not go to completion at the maximum scanning temperature, and the TGA plot may look like what is shown in Figure 6. In this figure the solid line again represents the measured furnace temperature, and the dashed line originating from a point at the decomposition temperature represents the sample temperature.

When the TGA unit is operated in Hi-Res. mode (high resolution mode) as was done throughout most of this study, the module monitors the rate of weight loss while the normal scanning goes on, and when this rate reaches a preset minimal value it holds the furnace temperature constant at that point, until the rate falls back to that value again due to partial or total consumption of the reactant.

Then, if the reaction is fast, the high resolution version of the TGA chart shown in Figure 5 for calcite will be that shown in Figure 7 with a perfectly vertical decomposition line. However, because of the usual temperature difference between the furnace and the sample the abscissa of this vertical line has no thermodynamic significance. All it means is that the thermodynamic (equilibrium) decomposition temperature is somewhere below this temperature. In this case, the unknown sample temperature should follow the theoretical path as shown in Figure 7 by the dashed line, practically with no end-tail.

If the reaction is moderately slow, the high resolution version of the plot in Figure 6 will look like as shown in Figure 8, exhibiting at least a short vertical section with a long end-tail having a finite slope. In this case, since the rate of consumption of heat is small, the sample will

HR - 337

Incomplete Reaction -- Normal TGA Scan

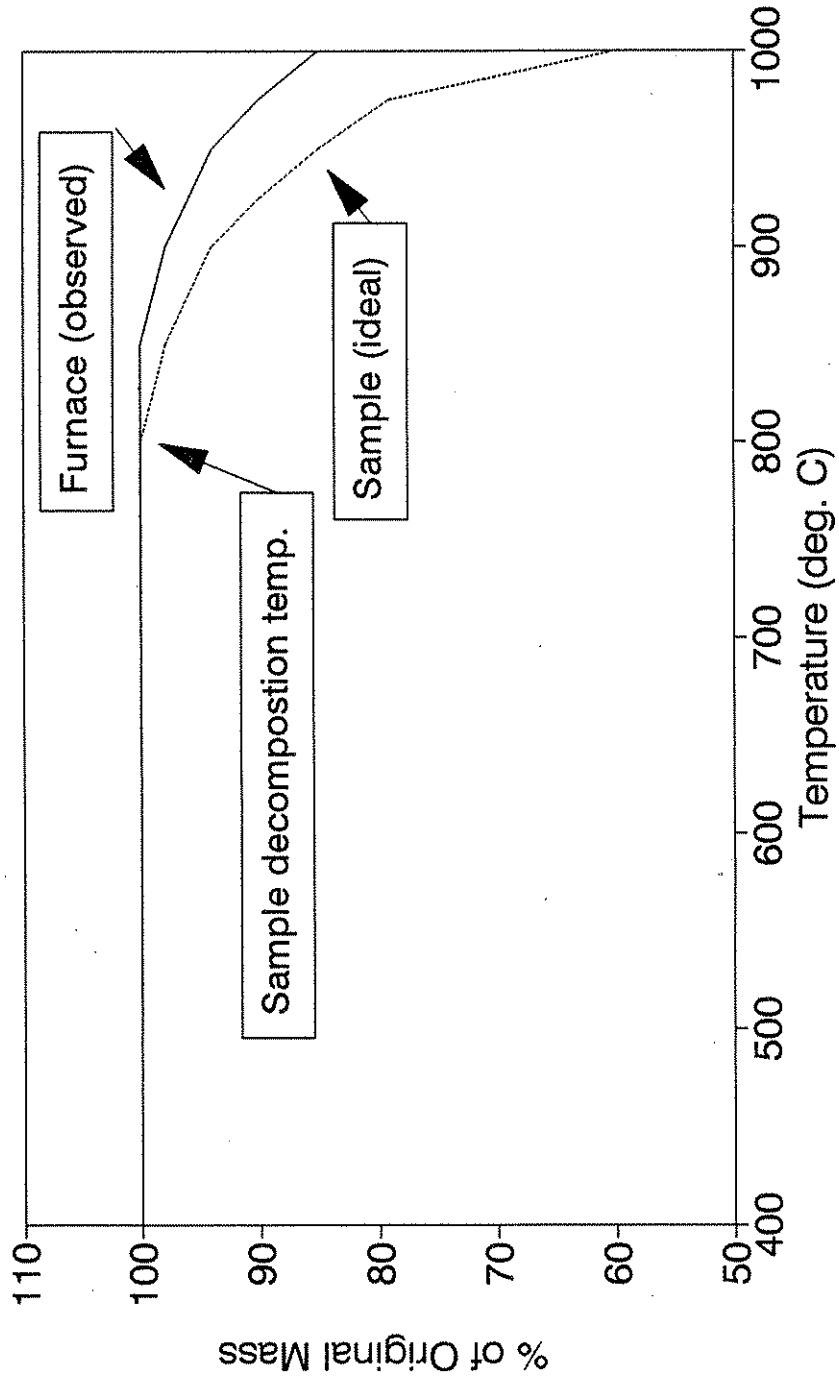


Figure 6. Thermal curve for the decomposition of a sample that does not reach completion.

HR - 337

Calcite Standards -- Hi Res Mode

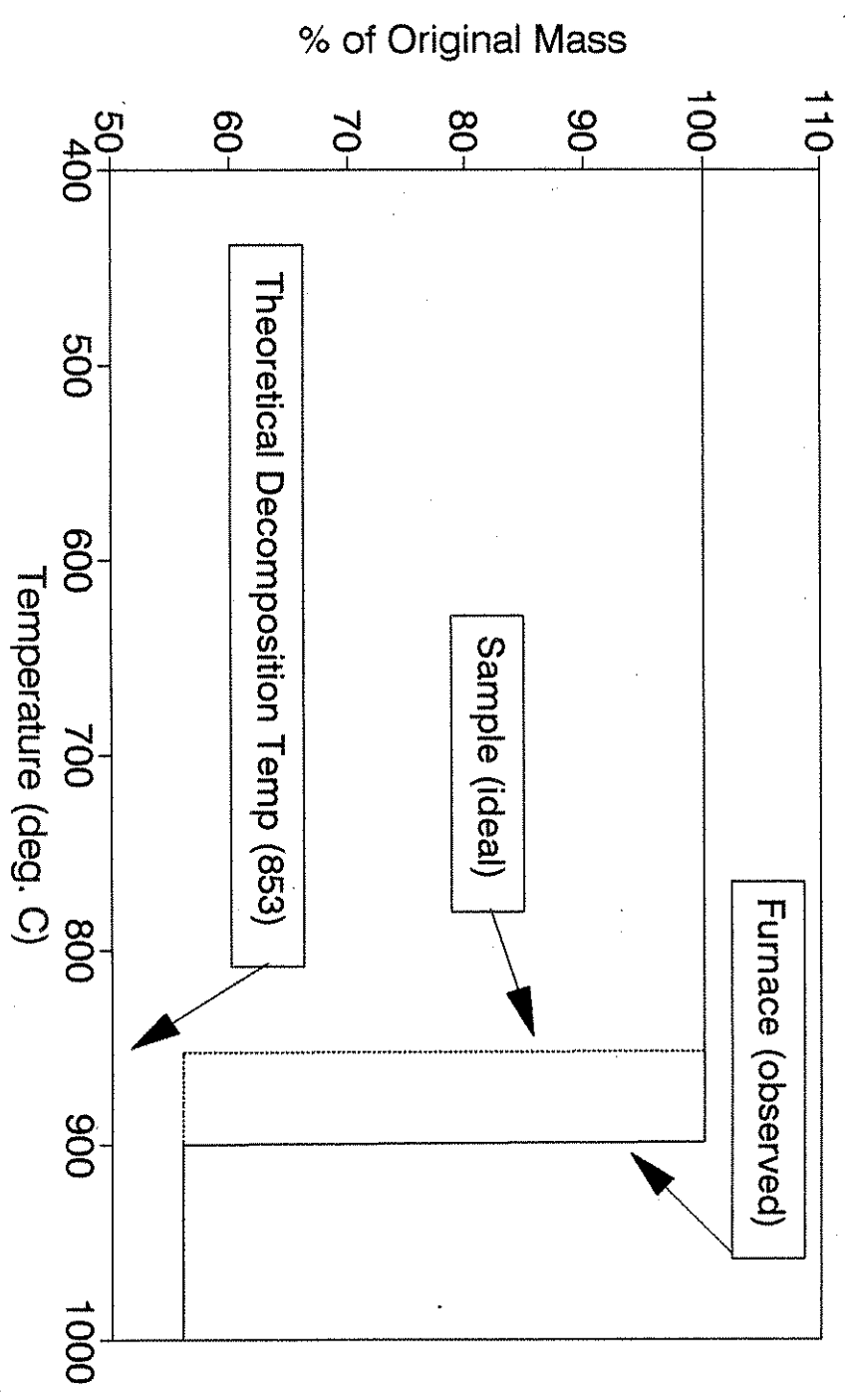


Figure 7. Thermal curve for the decomposition of calcite (fast reaction) in a Hi-Res. TGA scan.

HR - 337

Moderate Reaction -- Hi-Res TGA Mode

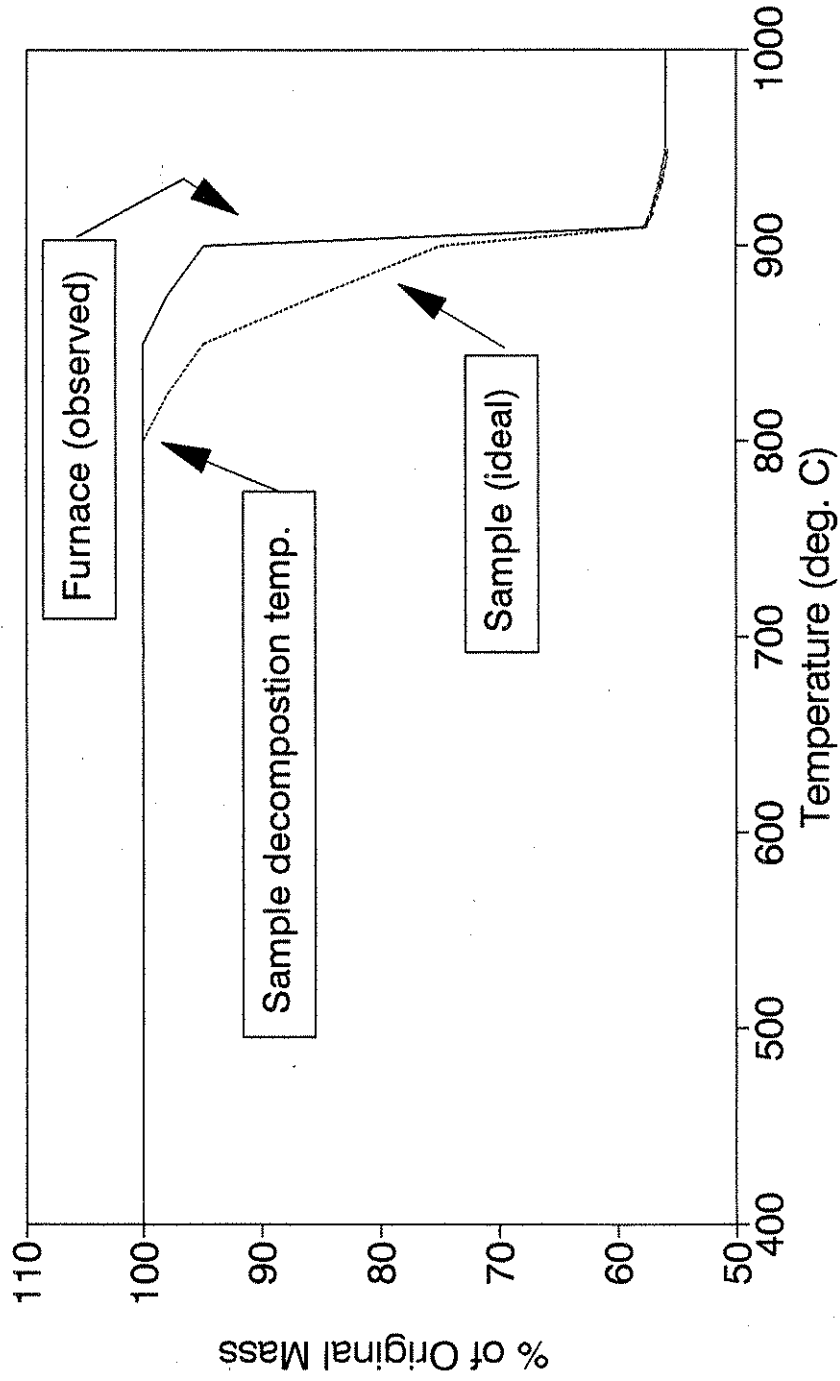


Figure 8. Thermal curve for a test specimen that decomposes at a moderate rate in a Hi-Res. TGA scan.

HR - 337

Slow Reaction -- Hi-Res TGA Mode

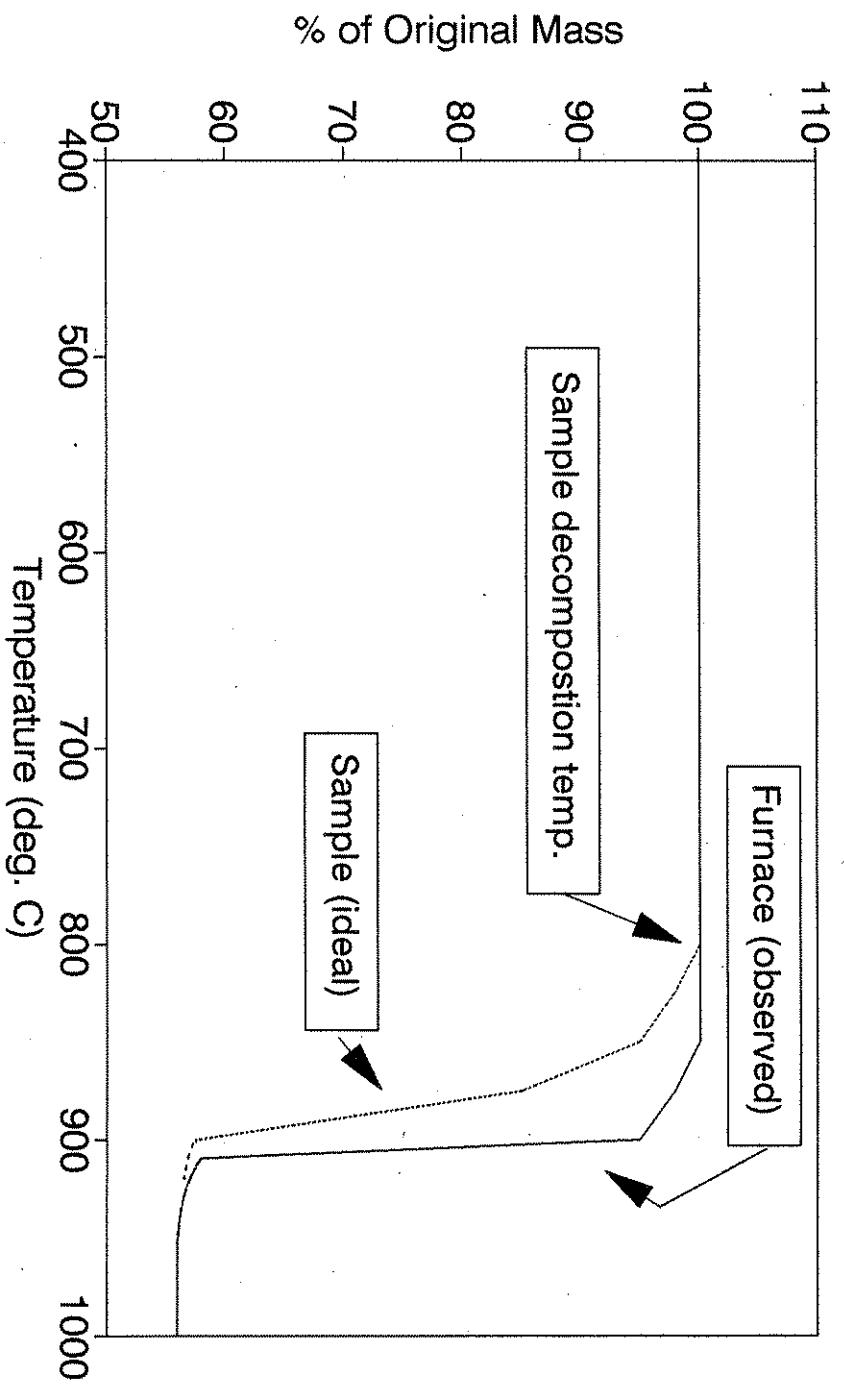


Figure 9. Thermal curve for a test specimen that decomposes at a slow rate in a Hi-Res. TGA scan.

HR - 337

Moderate Reaction -- Hi-Res TGA Mode

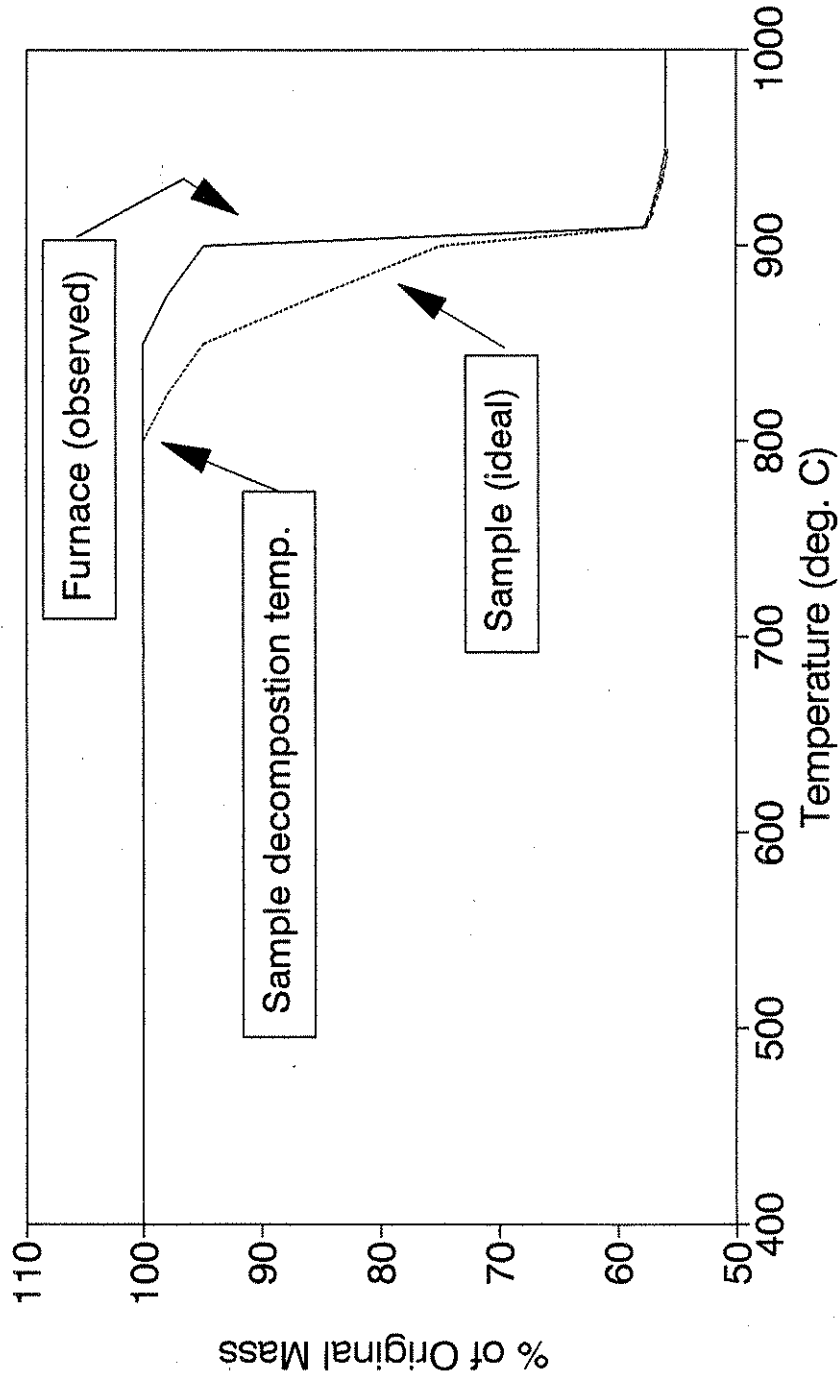


Figure 8. Thermal curve for a test specimen that decomposes at a moderate rate in a Hi-Res. TGA scan.

probably find time to come to the furnace temperature at least when the vertical section is reached, as shown by the dashed line in Figure 8. Even then the location of the vertical section is far from the thermodynamic decomposition temperature. This time it is because the sample is at a higher temperature than the latter.

If the reaction is extremely slow, the Hi-Res. TGA profile will either be the same as in Figure 6, or will look like what is shown in Figure 9 exhibiting just an inflection point instead of a vertical section, depending on the reaction rate. This is because transition of the module to the temperature holding mode is preceded by an intermediate mode in which the scanning rate decreases to lower values inversely proportional to the rate of weight loss. This mode generates wide and rounded upper and lower shoulders, and enhances the manifestation of a slow reaction.

Particle Size Effect

The foregoing discussion is valid if the reaction system is invariant, so that during the whole course of the reaction the temperature may remain constant. When the sample contains submicron particles of graded sizes i.e., when the surface effects come into play the system is no longer in true equilibrium. The phase rule becomes inapplicable. If the solid products form in large sizes so that they are free of measurable surface effects, each small reactant particle will decompose at a temperature characteristic for its size.

The simplest way of deriving an expression relating the decomposition temperature to the particle size is assuming that the particles are spherical. Then, the problem becomes analogous to that of depression of melting point of ice in capillaries [4]. This analogy leads to the equation

$$T = T_0 - \frac{2M\gamma}{\Delta s \rho r} \quad (1)$$

where T is the decomposition temperature of a particle of radius r , T_0 is that of an infinitely large particle, M is the formula weight of the reactant, γ is its surface tension, Δs is the entropy of decomposition of one mole of reactant, and ρ is its density. According to this equation, the decomposition temperature of a small particle is lower than the normal decomposition

HR - 337

Slow Reaction -- Hi-Res TGA Mode

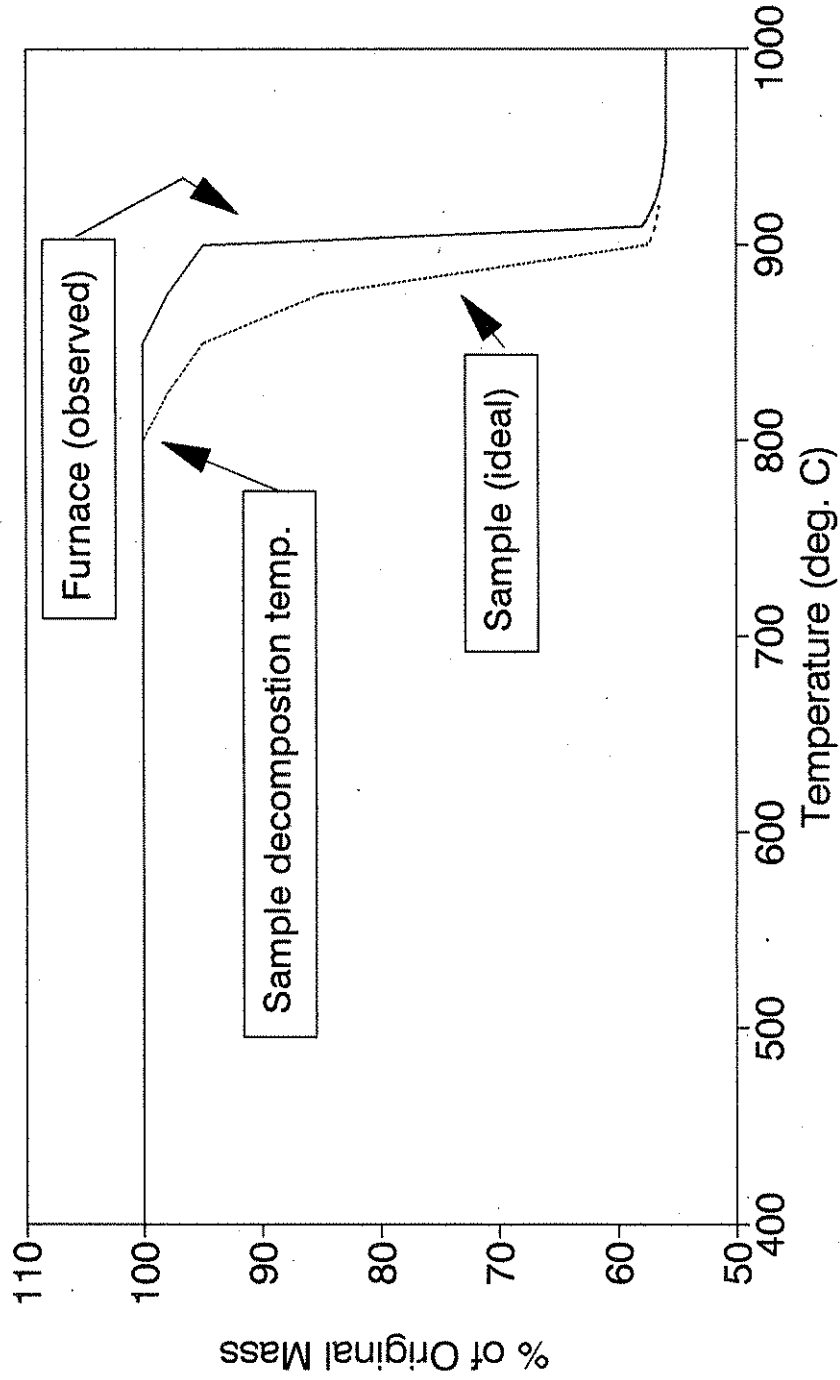
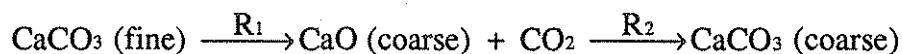


Figure 9. Thermal curve for a test specimen that decomposes at a slow rate in a Hi-Res. TGA scan.

temperature T_0 by an amount inversely proportional to its size. If heat is supplied gradually to a particulate sample of graded sizes, when the decomposition temperature of the smallest particles is reached, the sample starts decomposing. In contrast to a sample exclusively consisting of large particles, the sample temperature of a specimen containing a variety of sizes gradually increases as larger and larger particles decompose, until the turn comes for the largest particles to decompose, which would occur at the normal decomposition temperature. One further assumption implicit in this discussion must also be stressed here. When the solid product or products of the reaction are formed as coarse crystals as assumed, they are thermodynamically unstable at temperatures below T_0 , and are prone to reverse the decomposition reaction. For instance, coarse particles of CaO formed by decomposition of fine particles of CaCO_3 may reform large particles of CaCO_3 at temperatures below 853°C in an atmosphere of CO_2 as follows:



The net process is the growth of CaCO_3 crystals. Then the foregoing discussion is valid only if the rate R_2 of the reverse reaction is incomparably smaller than the rate R_1 of the forward reaction. Since the rates of these heterogeneous reactions are proportional to the surface area of the respective reactants, in reality this requirement is fulfilled (i.e., $R_1 \gg R_2$).

If the decomposition reaction is fast, the Hi-Res. TGA plot will look like as in slow decomposition (Figure 8 or 9) at the beginning with a wide rounded upper shoulder, but as in fast decomposition (Figure 7) with no tail at the end. For instance, with a CaCO_3 sample containing some submicron particles the solid curve shown in Figure 10 is the expected TGA profile. If the reaction were slow, the plot would look very much like that of a slowly decomposing sample of large crystals (Figure 8 or 9).

A Hi-Res. TGA curve obtained with 55 mg of reagent grade CaCO_3 supplied by Fisher Company at a scanning rate of 40 deg/min under CO_2 purged at a rate of 100 ml/min is shown in Figure 11. Absence of a shoulder at the beginning of decomposition and a tail at the end shows

HR - 337

Particle Size Effects - Hi-Res TGA Mode

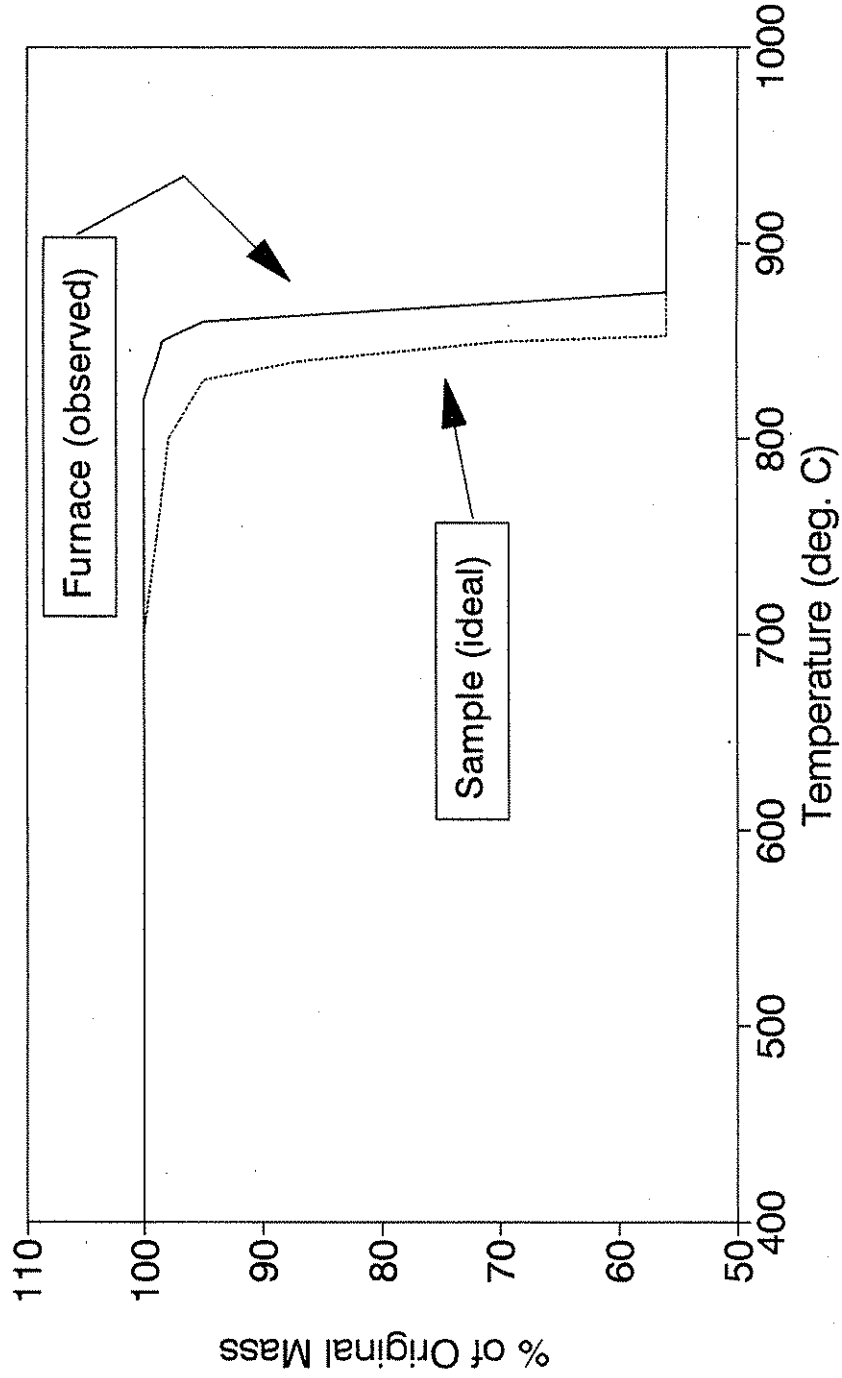


Figure 10. Predicted thermal curve for a calcite test specimen that contains submicron-sized particles.

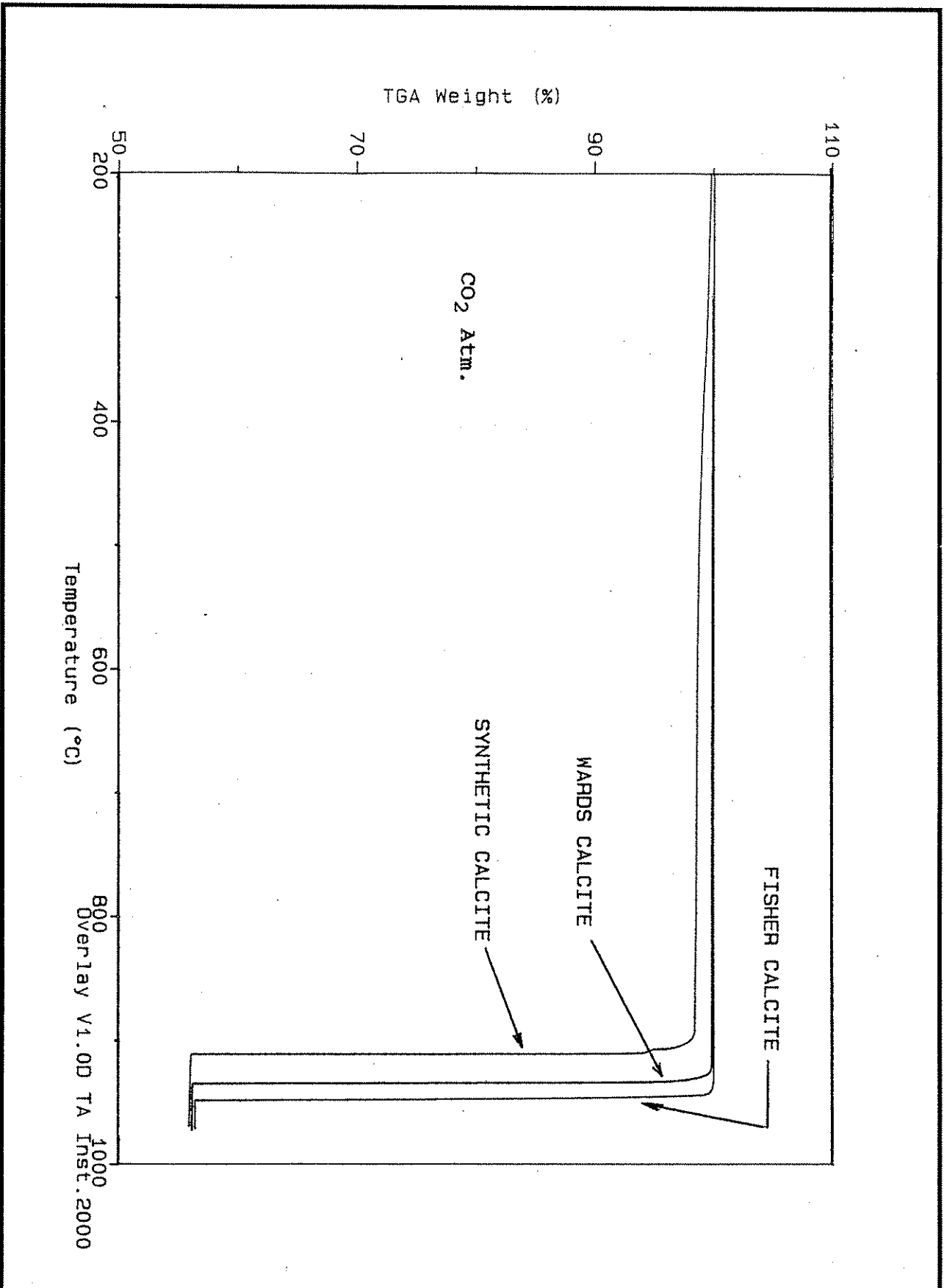


Figure 11. Thermal curves that were experimentally observed for several calcites used in this study.

that the reaction is fast and takes place sharply at a furnace temperature of 947° (without triggering an intermediate scanning mode mentioned above). A SEM micrograph of this sample reveals that it exclusively consists of crystals coarser than about $2\ \mu\text{m}$, with an average size of about $6\ \mu\text{m}$ (see Figure 13). Therefore, it is expected to decompose at the normal thermodynamic temperature of 853° . The difference between the measured decomposition temperature 947° and 853° (i.e., 94°) must be the usual temperature difference between the furnace and the sample under these conditions. Can this difference be used to translate the measured location of a vertical line in a Hi-Res. TGA plot to the real decomposition temperatures of other samples? The answer would be yes, if not only the sample sizes (55 mg) were the same, but also the scanning rate (40 deg/min) remained constant up to the decomposition temperature. If there is a noticeable sloping shoulder preceding the vertical line, the latter condition is not fulfilled because of the intermediate scanning mode has been triggered as mentioned earlier. In such a case the temperature difference is expected to be less. In other words, existence of a sloping shoulder pulls the vertical line to the left.

A ground sample of natural Iceland spar (Wards calcite) run under the same conditions has given the plot shown in Figures 11 and 12, with a slightly sloping and more rounded shoulder than the first sample. The measured decomposition temperature was 934°C . The SEM pictures of this sample indicated that it contained some crystalline particles as small as $0.3\ \mu\text{m}$. The average size was about $1.5\ \mu\text{m}$.

A third sample of pure CaCO_3 was prepared deliberately to contain much smaller particles. The method of preparation was similar to that used previously to synthesize fine particles of SrSO_4 by precipitation [5]. The procedure was as follows:
10 ml 0.25 M $\text{Ca}(\text{NO}_3)_2$ solution was added gradually to a mixture of 250 ml methanol, 50 ml water, and 10 ml 0.25 M Na_2CO_3 solution while it was vigorously stirred by a magnetic stirrer. The mixture was stored overnight and centrifuged to expel the mother liquor. The precipitate was washed five times with 6 ml water, and centrifuged each time. The product was dried to a constant weight in an oven at 105°C .

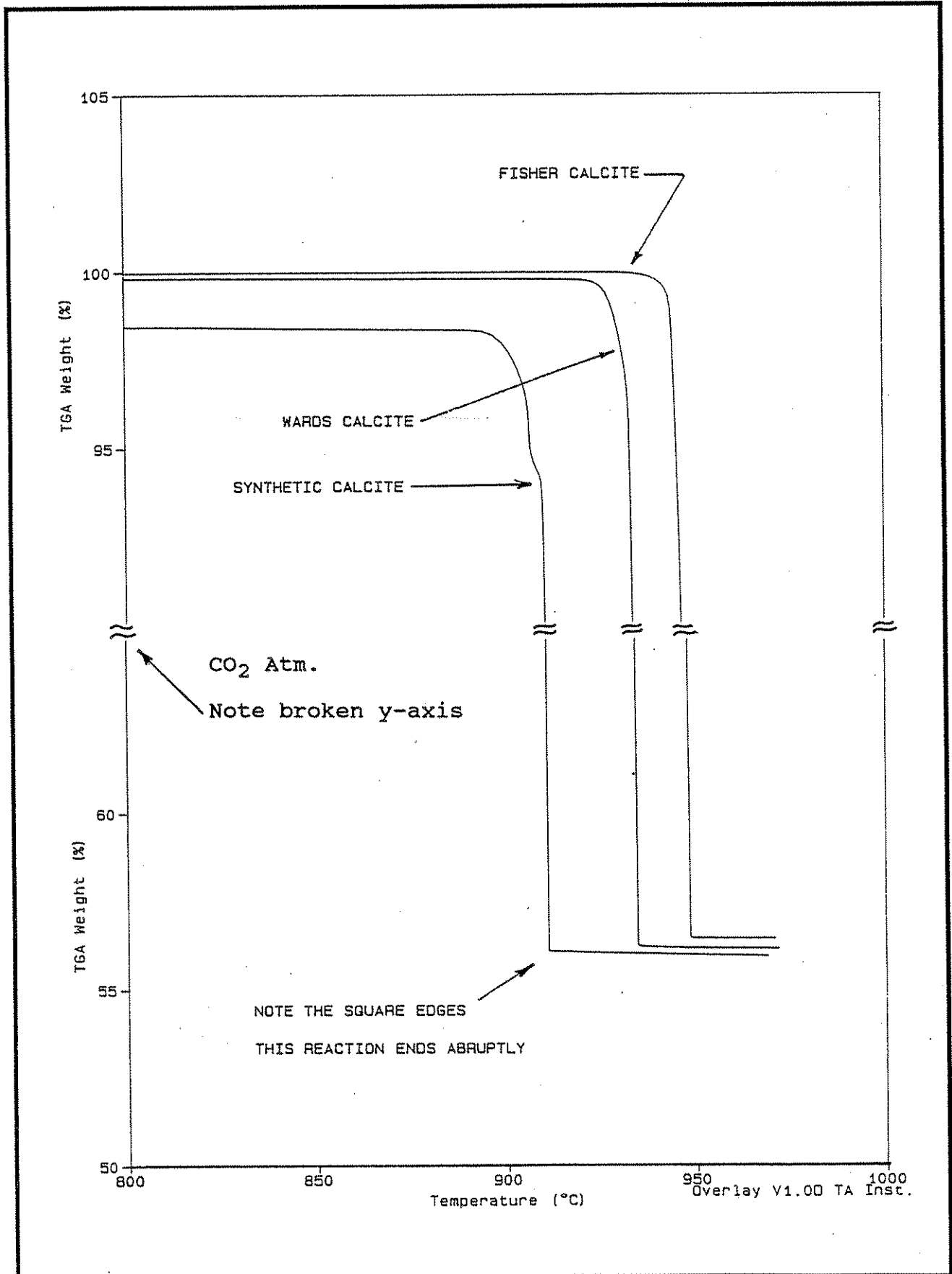


Figure 12. Enlarged view of Figure 11 that accentuates the differences between the various calcite samples.

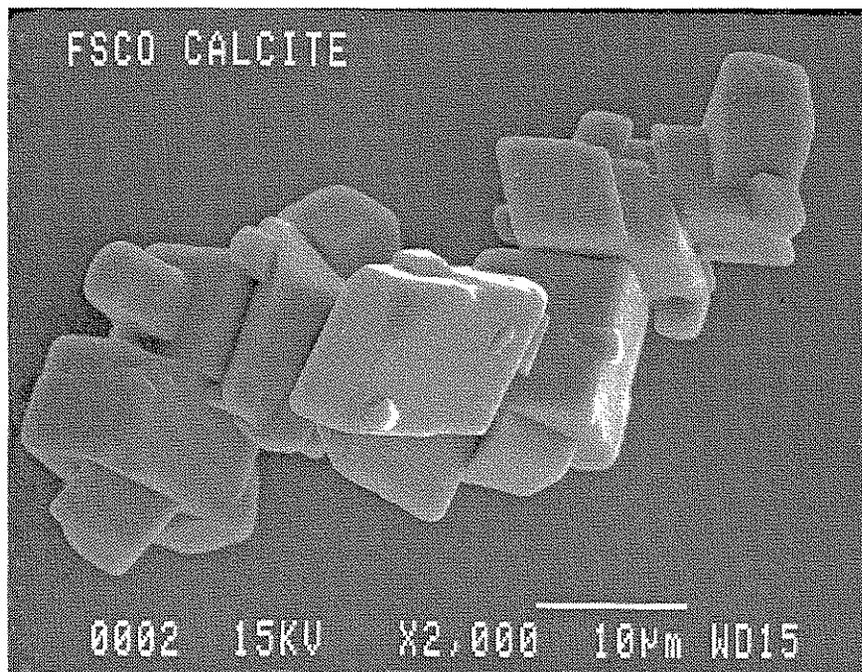
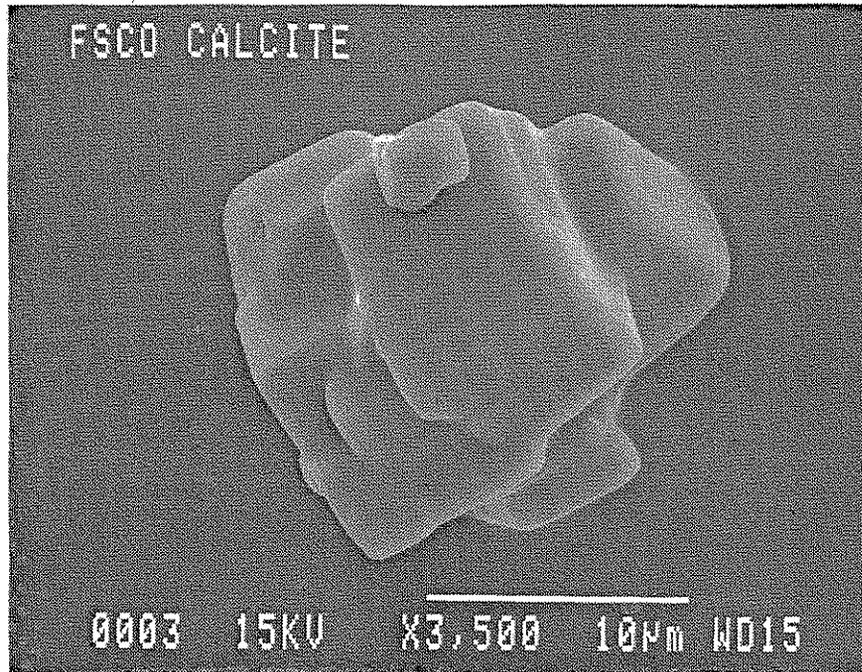


Figure 13. Scanning electron micrograph of the Fisher calcite used in this study.

A SEM micrograph of this sample showed rhombohedral calcite crystals of about 2 μm average size, plus needle-like crystals characteristic for aragonite ranging from 0.15 μm to 1.1 μm in width (see Figure 14). X-ray diffraction analysis also showed that it contained about 20 to 30 percent aragonite.

The TGA plot of this sample is also shown in Figures 11 and 12. The measured decomposition temperature was 911°C, much lower than the first two samples. The shoulder slope of the decomposition profile was also larger (see Figure 12).

As far as the instrumental response is concerned, what generates a sloping shoulder in a Hi-Res. TGA plot is a slow weight loss preceding a faster weight loss. It is not possible to distinguish whether it is due to a low absolute rate of reaction, or due to presence of small amount of fine particles of graded sizes decomposing before the bulk of the sample. As a rule of thumb, the particle size effect is measurable only in the case of submicron particles. The average particle sizes of all three pure CaCO_3 samples described above were greater than 1 μm . Therefore the bulk of all three samples are expected to decompose at the normal thermodynamic temperature of 853°C. Why then, they decompose at different furnace temperatures is because of the "shoulder effect" discussed earlier.

The next question is what causes the sloping shoulder with the second and the third samples. Since the only reaction involved is the decomposition of CaCO_3 , which is a fast reaction as the TGA results indicate, then the only reason for these shoulders is the presence of submicron particles in these samples. Indeed, if we compare the sizes of detectable smallest particles, the premature weight losses at the beginning of fast decomposition as measures of shoulder slopes, and the measured apparent decomposition temperatures of these three samples, we observe significant correlations between these data, as tabulated in Table 9. These correlations mean that a sloping shoulder before a fast decomposition indicates presence of submicron particles, and affects the apparent decomposition temperature as discussed earlier.

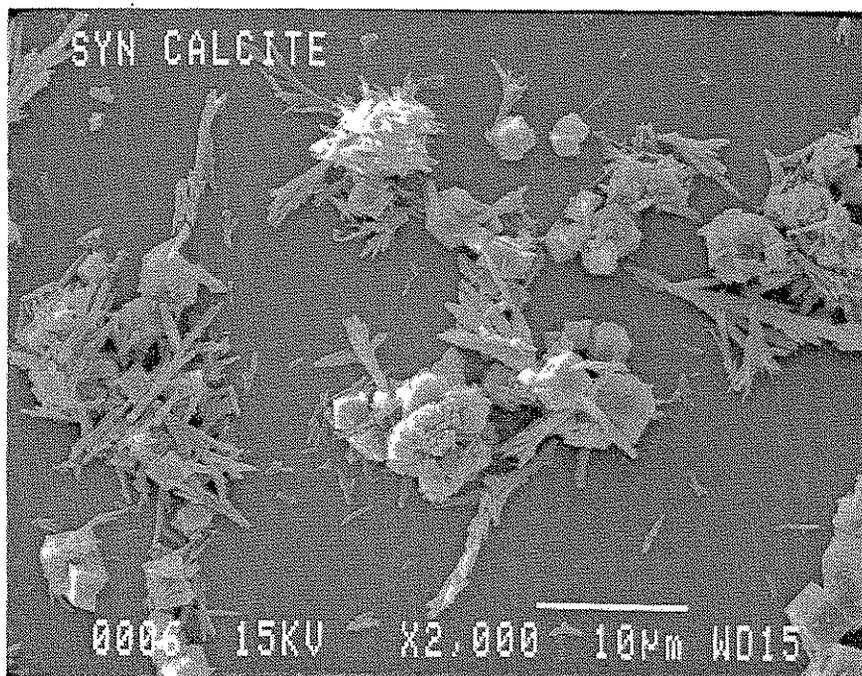
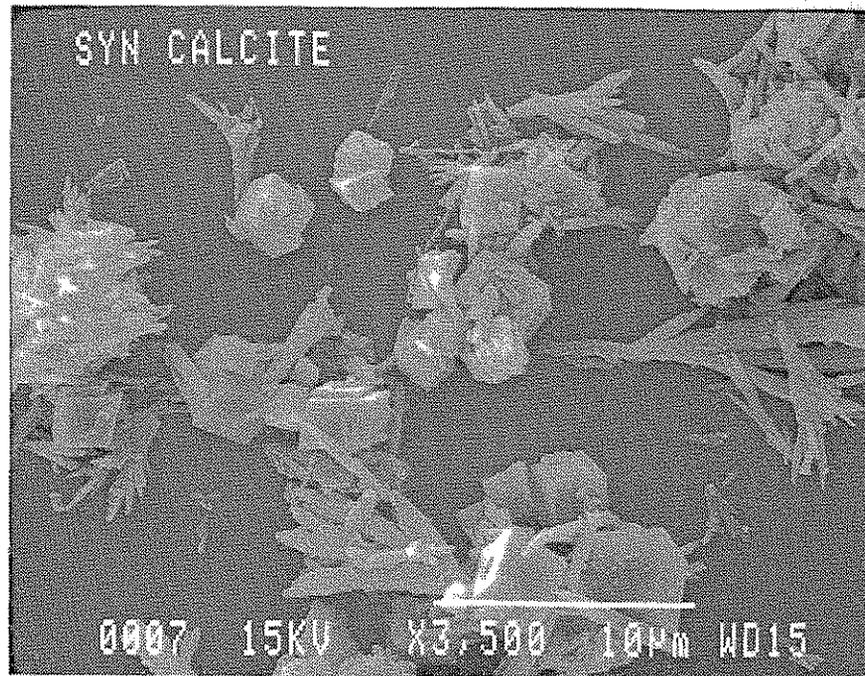


Figure 14. Scanning electron micrograph of synthetic calcite used in this study.

Table 9. Summary of Details for the Standard Calcite Samples Used in this Study

Sample	Minimum Particle Size, μm	Premature Weight Loss, %	Apparent Decomposition Temperature, $^{\circ}\text{C}$
Fisher CaCO_3	2	0	947
Iceland Spar	0.3	0.08	934
Synthetic CaCO_3	0.15	0.65	911

This observation lead us to look for a similar correlation between the extent of premature decomposition of limestone aggregate samples and their apparent decomposition temperatures measured under identical conditions. It is important to mention that the various limestone specimens used in this study are not purely composed of calcite; and therefore, the decomposition of additional minerals may tend to bias the TGA test results. However, the majority of the limestones included in the study were reasonably pure (see Tables 2 and 3), and the trend depicted in Figure 15 indicates a correlation between premature weight loss and apparent decomposition temperature. In fact, a plot of apparent decomposition temperature (DT_{CAL}) versus full-width-at-half-maximum (FWHM) shown on Figure 16 indicates a similar trend (although FWHM data was not available for the Iceland spar or the synthetic calcite).

Also included in Figure 15 are the three calcite samples of Table 9. While the points for the first and second samples appear to be compatible with the general trend of distribution of other points, the third sample (synthetic calcite) significantly deviates from this trend. We believe this anomaly is due to the presence of submicron size aragonite crystals in this sample. It undergoes with an exceedingly premature, but temporary, decomposition at a furnace temperature of about 360°C (Figure 11). We believe this is because of the presence of fine aragonite crystals possibly of almost a uniform size, coupled with the fact that the normal decomposition temperature of aragonite is about 75°C below that of calcite [4]. Apparently, this group of aragonite particles decompose at such a low temperature. It is known that aragonite is not stable at high temperature, and it transforms into calcite at 520°C [4]. However because of fast heating, some large crystals of aragonite may survive this transformation and find time to

HR - 337

calcite specimens -- CO2 atmosphere

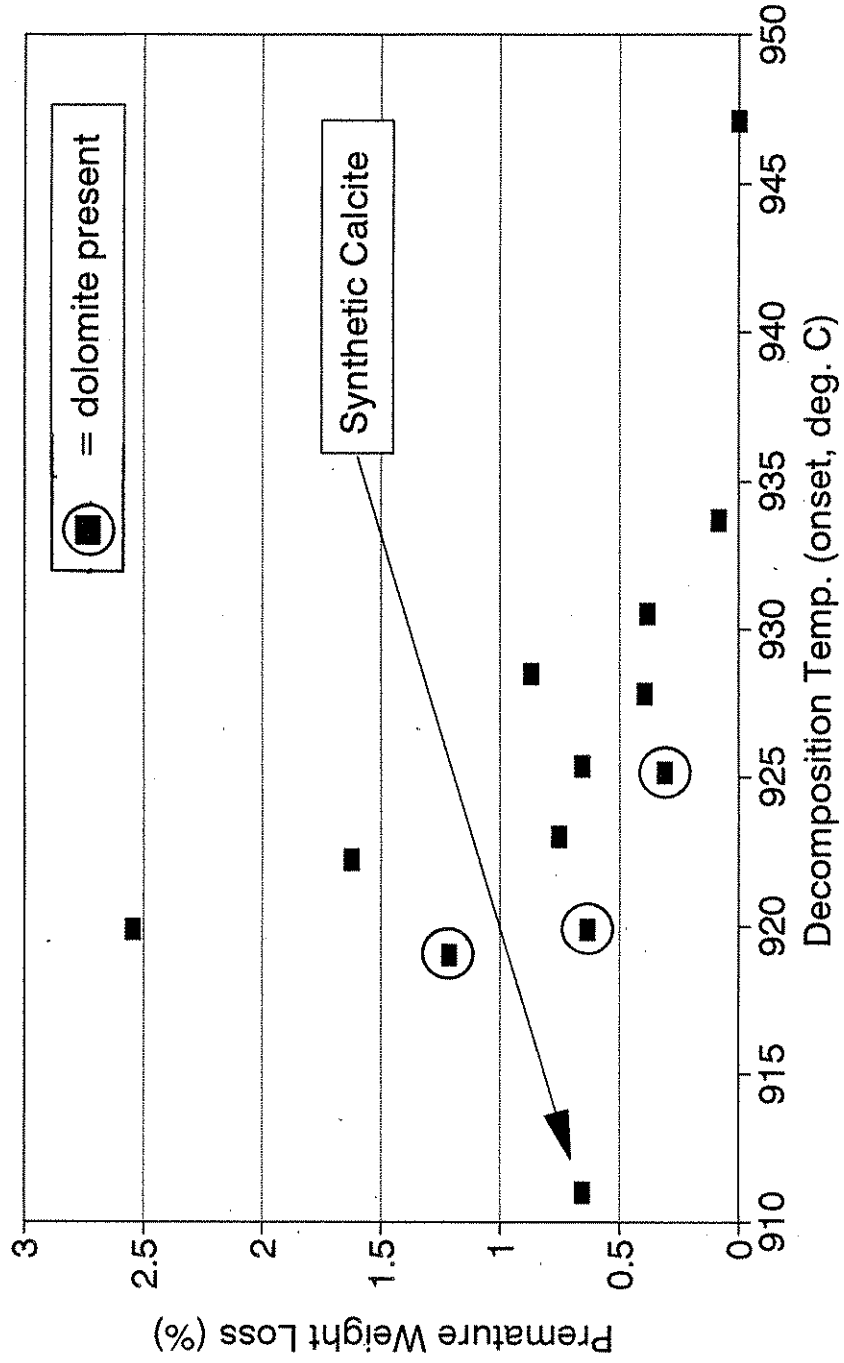


Figure 15. Plot of premature weight loss versus apparent decomposition temperature for the limestone and for the standard calcite specimens used in this study.

HR - 337

calcite specimens -- CO₂ atmosphere

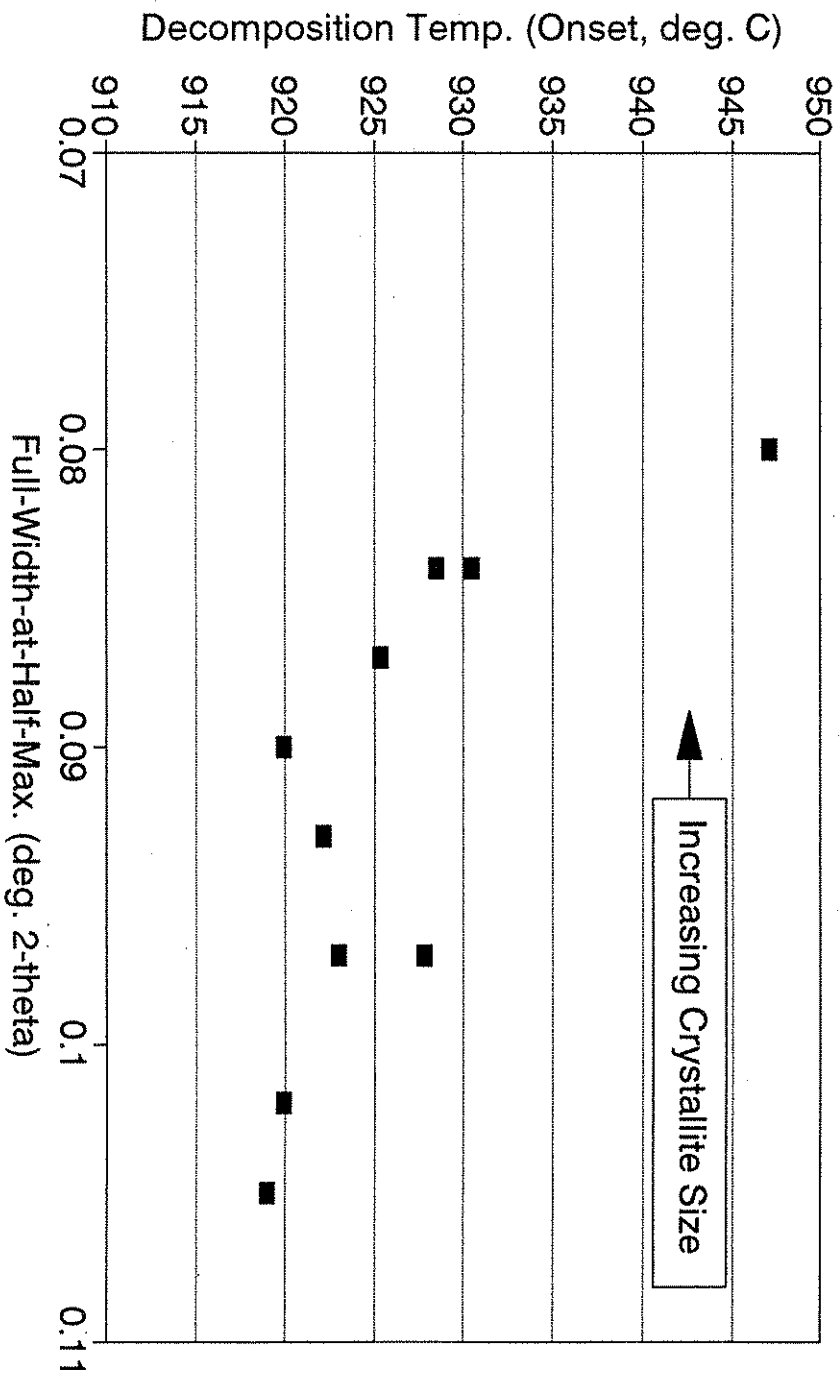


Figure 16. Plot of apparent decomposition temperature versus full-width-at-half-maximum for the limestone specimens and for the Fisher calcite.

decompose just before decomposition of calcite. A short vertical section seen in the plot shown in Figure 9 a few degrees ahead of the main decomposition line is probably a reflection of this decomposition on the TGA profile of this sample. Although the synthesized submicron particles were not calcite, but aragonite, this preparation served the purpose of deliberate enhancement of premature decomposition due to particle size effect.

SUMMARY

In summary, the first year of this project has been spent obtaining and analyzing the carbonate stone samples. The preliminary experimental findings indicate that fundamental characteristics of the limestone specimens can influence the thermal decomposition of any given test specimen. The relevance of these findings can be surmised as follows.

Field Performance of Limestone Aggregates

We may conclude from the foregoing discussion that continuous premature thermal decomposition of limestones, which has been correlated to poor performance of such samples as concrete aggregates by W. Dubberke, is because they contain submicron size crystallites. Another finding of W. Dubberke was that fine grain size also correlates with poor performance. We understand now that fine grain size and premature thermal decomposition are not two independent variables, but that the latter is a consequence of the former.

Fine grained structure of limestone aggregates may contribute to poor performance in two ways.

- (1) Interaction with Deicers: It is well known that the solubility of CaCO_3 in a concentrated electrolyte solution (e.g. NaCl) is greater than in water, because a high-ionic-strength-medium lowers the activity coefficients of the dissolving ions of Ca^{2+} and CO_3^{2-} . This effect is enhanced if the solid phase, i.e., CaCO_3 , consists of fine particles; because the

chemical potential of fine particles is larger than that of large crystals [5]. Therefore, presence of fine grains may cause a severe erosion of the aggregate in the presence of deicing salts.

- (2) Frost Susceptibility: Presence of fine grains means fine pore structure which, in turn, increases the rate of saturation of the aggregate when immersed in water. It has been established that the rate of saturation of concrete is a critical property to increase its frost susceptibility [7].

ACKNOWLEDGMENTS

We would like to thank all the people who helped to contribute to this project during its first year. A special thanks to IDOT personnel who have helped to procure materials. Without their help this research project would not have been possible.

REFERENCES

1. Dubberke, W. and Marks, V.J., Thermogravimetric Analysis of Carbonate Aggregate, presented at the Transportation Research Board 71st Annual Meeting, January 12-16, 1992.
2. Personal Communication with Wendell Dubberke, 04/22/92.
3. Carpenter, A.B., "The Chemistry of Dolomite Formation I: The Stability of Dolomite," Soc. of Economic Paleontologists and Mineralogists, Spec. Pub. No. 28, 111-121, November 1980.
4. Enüstün, B.V., Sentürk, H.S., and Yurdakul, O., "Capillary Freezing and Melting," J. Colloid Interface Sci., 65, 509-516 (1978).

5. Enüstün, B.V., and Turkevich, J., "Solubility of Fine Particles of Strontium Sulfate," J. Am. Chem. Soc., 82, 4502-4509 (1960).
6. Handbook of Chemistry and Physics, 59th Ed., p. B-105, CRC Press Inc., W. Palm Beach, FL, 1978.
7. Enüstün, B.V., Bergeson, K.L., and Soo, K.S., "Frost Susceptibility of Concrete in Near-Saturated States," NSF Final Report CES-8713443, 5-21-1990.

APPENDIX I

5-0586 JCPDS-ICDD Copyright 1988 Quality: i
 CaCO₃ Calcite, syn
 Calcium Carbonate

Rad: CuKα1 wl: 1.5405 Filter: Ni d-sp:
 Cutoff: Int: Diffractometer I/Icor: 2.00
 Ref: Swanson, Fuyat, Natl. Bur. Stand. (U.S.), Circ. 539, II 51 (1953)

Sys: Rhombohedral (Hex) Space Group: R-3c (167)
 a: 4.989 b: c: 17.062 A: C: 3.4199
 α: β: γ: v: Z: 6
 Ref: Ibid.
 mp: Dx: 2.71 Dm: 2.71 SS/FOM: F(30)=49.9(.0163,37)

α: 1.487 n_{wb}: 1.659 ε_v: Sign: - 2v:
 Ref: Dana's System of Mineralogy, 7th Ed., 2 142

Color: Colorless.
 X-ray pattern at 26 C. Sample from Mallinckrodt Chemical Works. CAS RN:
 13397-26-7. Spectroscopic analysis: <0.1% Sr; <0.01% Ba; <0.001% Al, B, Cs,
 Cu, K, Mg, Na, Si, Sn; <0.0001% Ag, Cr, Fe, Li, Mn. Merck Index, 8th Ed., p.
 190. Other form: aragonite. PSC: hr10.

*Not permitted by space group

d A	Int	h k l	d A	Int	h k l
3.86	12	0 1 2	1.1538	3	1 3 4
3.035	100	1 0 4	1.1425	1	2 2 6
2.845	3	0 0 6	1.1244	<1	1 2 11
2.495	14	1 1 0	1.0613	1	2 0 14
2.285	18	1 1 3	1.0473	3	4 0 4
2.095	18	2 0 2	1.0447	4	3 1 8
1.927	5	0 2 4	1.0352	2	1 0 16
1.913	17	0 1 8	1.0234	<1	2 1 13
1.875	17	1 1 6	1.0118	2	3 0 12
1.626	4	2 1 1	0.9895	<1	3 2 1
1.604	8	1 2 2	0.9846	1	2 3 2
1.587	2	1 0 10	0.9782	1	[1 3 10]
1.525	5	2 1 4	0.9767	3	1 2 14
1.518	4	2 0 8	0.9655	2	3 2 4
1.510	3	1 1 9	0.9636	4	4 0 8*
1.473	2	1 2 5	0.9562	<1	2 0 16*
1.440	5	3 0 0	0.9429	2	4 1 0
1.422	3	0 0 12	0.9376	2	2 2 12
1.356	1	2 1 7			
1.339	2	0 2 10			
1.297	2	1 2 8			
1.284	1	3 0 6			
1.247	1	2 2 0			
1.235	2	1 1 12			
1.1795	3	2 1 10			

36-0426

JCPDS-ICDD Copyright 1988

Quality: *

CaMg(CO₃)₂

Calcium Magnesium Carbonate

Dolomite

Rad: CuK α λ : 1.54178 Filter: Graph Mono. d-sp: Diffractometer
 Cutoff: Int: Diffractometer I/I_{cor}:
 Ref: Keller, L., McCarthy, G., North Dakota State University, Fargo, North
 Dakota, USA, JCPDS Grant-in-Aid Report (1985)

Sys: Rhombohedral (Hex) Space Group: R-3 (148)
 a: 4.8092(2) b: c: 16.020(5) A: C: 3.3311
 α : β : γ : Z: 3
 Ref: Ibid.
 mp: Dx: 2.86 Dm: 2.86 SS/FOM: F(30)=148.1(.0063,32)

ρ_x : n_w : 1.680 n_D : 1.503 Sign: - 2v:
 Ref: Howie, Broadhurst, Am. Mineral., 43 1210 (1958)

Color: Tan
 Specimen from Baxter Springs, Arkansas, USA. Chemical analysis by EDX at
 University of North Dakota (wt.%): CaO 30.18, MgO 21.10, FeO 0.44, MnO 0.11,
 CO₂ 47.18, Na₂O 0.17, Al₂O₃ 0.13, SiO₂ 0.47 (chiefly from traces of quartz and
 plagioclase); Ca(Mg_{0.977}Fe_{0.011}Na_{0.005}Mn_{0.003}Ca_{0.004})(CO₃)₂. Optical data on
 specimen from Haley, Ross Township, Ontario, Canada. Silicon used as internal
 standard. PSC: hR10. To replace 11-78.

d Å	Int	h	k	l	d Å	Int	h	k	l
4.033	1	1	0	1	1.3350	1	0	0	12
3.699	4	0	1	2	1.2970	1	2	1	7
2.888	100	1	0	4	1.2698	1	0	2	10
2.670	4	0	0	6	1.2374	1	1	2	8
2.539	3	0	1	5	1.2318	<1	3	0	6
2.404	7	1	1	0	1.2022	1	2	2	0
2.193	19	1	1	3	1.1935	<1	2	0	11
2.065	3	0	2	1	1.1817	<1	1	0	13
2.015	10	2	0	2	1.1729	<1	2	2	3
2.006	1	1	0	7	1.1672	1	1	1	12
1.8473	3	0	2	4	1.1433	<1	3	1	2
1.8049	10	0	1	8	1.1228	1	2	1	10
1.7870	13	1	1	6	1.1099	<1	1	3	4
1.7800	2	0	0	9	1.1034	<1	0	1	14
1.7461	<1	2	0	5	1.0963	1	2	2	6
1.5667	2	2	1	1	1.0947	<1	3	0	9
1.5446	4	1	2	2					
1.5403	<1	0	2	7					
1.4955	<1	1	0	10					
1.4652	2	2	1	4					
1.4435	2	2	0	8					
1.4308	1	1	1	9					
1.4129	1	1	2	5					
1.3885	2	3	0	0					
1.3436	<1	3	0	3					

34-0517

JCPDS-ICDD Copyright 1988

Quality: i

Ca(Mg_{0.67}Fe_{0.33})(CO₃)₂

Calcium Magnesium Iron Carbonate

Dolomite, ferroan

Rad: CuK α wl: 1.5418 Filter: Ni

d-sp:

Cutoff: Int: Diffractometer

I/Icor:

Ref: Howie, Broadhurst, Am. Mineral., 43 1210 (1958)

Sys: Rhombohedral (Hex) Space Group: R-3 (148)

a: 4.819

b:

c: 16.10

A:

C: 3.3409

 α : β : γ :

Z: 3

Ref: Ibid.

mp:

Dx: 3.00

Dm: 2.97

SS/FOM: F(30)=14.7(0.044,47)

 $\epsilon\alpha$: 1.515nw β : 1.710 $\epsilon\gamma$:

Sign: -

2v:

Ref: Dana's System of Mineralogy, 7th Ed.

Color: Yellow and brown

Specimen from Oldham, Lancashire, England. Analysis (wt.%): SiO₂ 0.15, Al₂O₃ 0.28, Fe₂O₃ 0.10, FeO 12.06, MnO 0.77, MgO 12.85, CaO 29.23, Na₂O 0.06, K₂O 0.01, CO₂ 44.70, H₂O 0.02. Intensities affected by preferred orientation. Rhombohedral parameters: a=6.045, α =47.0. PSC: hR10. To replace 12-88.

d A	Int	h	k	l	d A	Int	h	k	l
3.7	4	0	1	2	1.300	<1	2	1	7
2.899	100	1	0	4	1.273	<1	0	2	10
2.685	4	0	0	6	1.241	<1	1	2	8
2.552	1	0	1	5	1.205	<1	2	2	0
2.411	4	1	1	0	1.171	<1	1	1	12
2.199	6	1	1	3	1.144	<1	3	1	2
2.067	<1	0	2	1	1.126	<1	2	1	10
2.020	4	2	0	2	1.112	<1	1	3	4
1.852	<1	0	2	4	1.099	<1	2	2	6
1.812	6	0	1	8	1.066	<1	[0	2	13]
1.792	6	1	1	6	1.010	<1	4	0	4
1.569	<1	2	1	1	1.003	<1	3	1	8
1.548	1	1	2	2	0.976	<1	1	0	16
1.501	<1	1	0	10	0.966	<1	3	0	12
1.468	1	2	1	4	0.952	<1	2	3	2
1.449	4	[2	0	8]					
1.436	<1	1	1	9					
1.416	<1	1	2	5					
1.391	<1	0	3	0					
1.341	<1	0	0	12					

33-1161

JCPDS-ICDD Copyright 1988

Quality: *

SiO₂

Silicon Oxide

Rad: CuK α 1 wl: 1.540598 Filter: Mono. d-sp: Diffractometer
 Cutoff: Int: Diffractometer I/Icor: 3.6
 Ref: Natl. Bur. Stand. (U.S.) Monogr. 25, 18 61 (1981)

Sys: Hexagonal Space Group: P3221 (154)
 a: 4.9133(2) b: c: 5.4053(4) A: C: 1.1001
 α : β : v: Z: 3
 Ref: Ibid.
 mp: Dx: 2.65 Dm: 2.66 SS/FOM: F(30)=76.6(.0126,31)

ex: nw β : 1.544 ev:1.553 Sign: + 2v:
 Ref: Swanson, Fuyat, Natl. Bur. Stand. (U.S.), Circ. 539, 3 24 (1954)

Color: Colorless

Pattern at 25 C. Sample from the Glass Section at NBS, Gaithersburg, Maryland, USA, ground single-crystals of optical quality. Pattern reviewed by J. Holzer and G. McCarthy, North Dakota State University, Fargo, North Dakota, USA, JCPDS Grant-in-Aid ReportRG(1990). Agrees well with experimental and calculated patterns. 02Si. Also called silica. Silicon used as internal standard. PSC: hp9. To replace 5-490. Plus 6 reflections to 0.9089.

d. A	Int	h k l	d A	Int	h k l
4.257	22	1 0 0	1.2285	1	2 2 0
3.342	100	1 0 1	1.1999	2	2 1 3
2.457	8	1 1 0	1.1978	1	2 2 1
2.282	8	1 0 2	1.1843	3	1 1 4
2.237	4	1 1 1	1.1804	3	3 1 0
2.127	6	2 0 0	1.1532	1	3 1 1
1.9792	4	2 0 1	1.1405	<1	2 0 4
1.8179	14	1 1 2	1.1143	<1	3 0 3
1.8021	<1	0 0 3	1.0813	2	3 1 2
1.6719	4	2 0 2	1.0635	<1	4 0 0
1.6591	2	1 0 3	1.0476	1	1 0 5
1.6082	<1	2 1 0	1.0438	<1	4 0 1
1.5418	9	2 1 1	1.0347	<1	2 1 4
1.4536	1	1 1 3	1.0150	1	2 2 3
1.4189	<1	3 0 0	0.9898	1	4 0 2
1.3820	6	2 1 2	0.9873	1	3 1 3
1.3752	7	2 0 3	0.9783	<1	3 0 4
1.3718	8	3 0 1	0.9762	1	3 2 0
1.2880	2	1 0 4	0.9636	<1	2 0 5
1.2558	2	3 0 2			

6-0710 JCPDS-ICDD Copyright 1988 Quality: i
 FeS₂ Pyrite, syn
 Iron sulfide

Rad: CuKα1 wl: 1.5405 Filter: Ni d-sp:
 Cutoff: Int: Diffractometer I/Icor:
 Ref: Swanson et al, Natl. Bur. Stand. (U.S.), Circ. 539, 5 29 (1955)

Sys: Cubic Space Group: Pa3 (205)
 a: 5.417 b: c: A: C:
 α: β: v: Z: 4
 Ref: Ibid.
 mp: 642 C Dx: 5.01 Dm: 5.02 SS/FOM: F(24)=22.4(0.029,37)

Color: Black (in powder), brass-yellow (in crystals)
 X-ray pattern at 26 C. CAS RN: 1309-36-0. Sample prepared as a fine precipitate and heated in a closed tube in S₂ atmosphere for 4 hours at 700 C.
 Spectroscopic analysis: <0.1% Al, Ca, Mg, Si; <0.01% Co, Cu, Mo, Ni, Pb; <0.001% Cr, Ge, Mn; <0.0001% Ag. Validated by calculated pattern 24-76.
 Opaque mineral optical data on specimen from Tavistock, Devon, England: RR2Re=51.7, Disp.=16, VHN100=1505-1620, Color values=.327, .335, 51.8, Ref.: IMA Commission on Ore Microscopy QDF. Measured density and melting point by Dana's System of Mineralogy, 7th Ed. RG, 1RG 238. FeS₂. Also called pyrites; fools gold. PSC: cP12. To be deleted by Z-506, lower Fn, Bayliss, 11/90.

d A	Int	h k l	d A	Int	h k l
3.128	35	1 1 1	1.0060	8	2 5 0
2.709	85	2 0 0	0.9892	6	5 2 1
2.423	65	2 1 0	0.9577	12	4 4 0
2.2118	50	2 1 1	0.9030	16	6 0 0
1.9155	40	2 2 0	0.8788	8	6 1 1
1.6332	100	3 1 1	0.8565	8	6 2 0
1.5640	14	2 2 2	0.8261	4	5 3 3
1.5025	20	2 3 0	0.8166	4	6 2 2
1.4448	25	3 2 1	0.7981	6	6 3 1
1.2427	12	3 3 1			
1.2113	14	4 2 0			
1.1823	8	4 2 1			
1.1548	6	3 3 2			
1.1057	6	4 2 2			
1.0427	25	5 1 1			

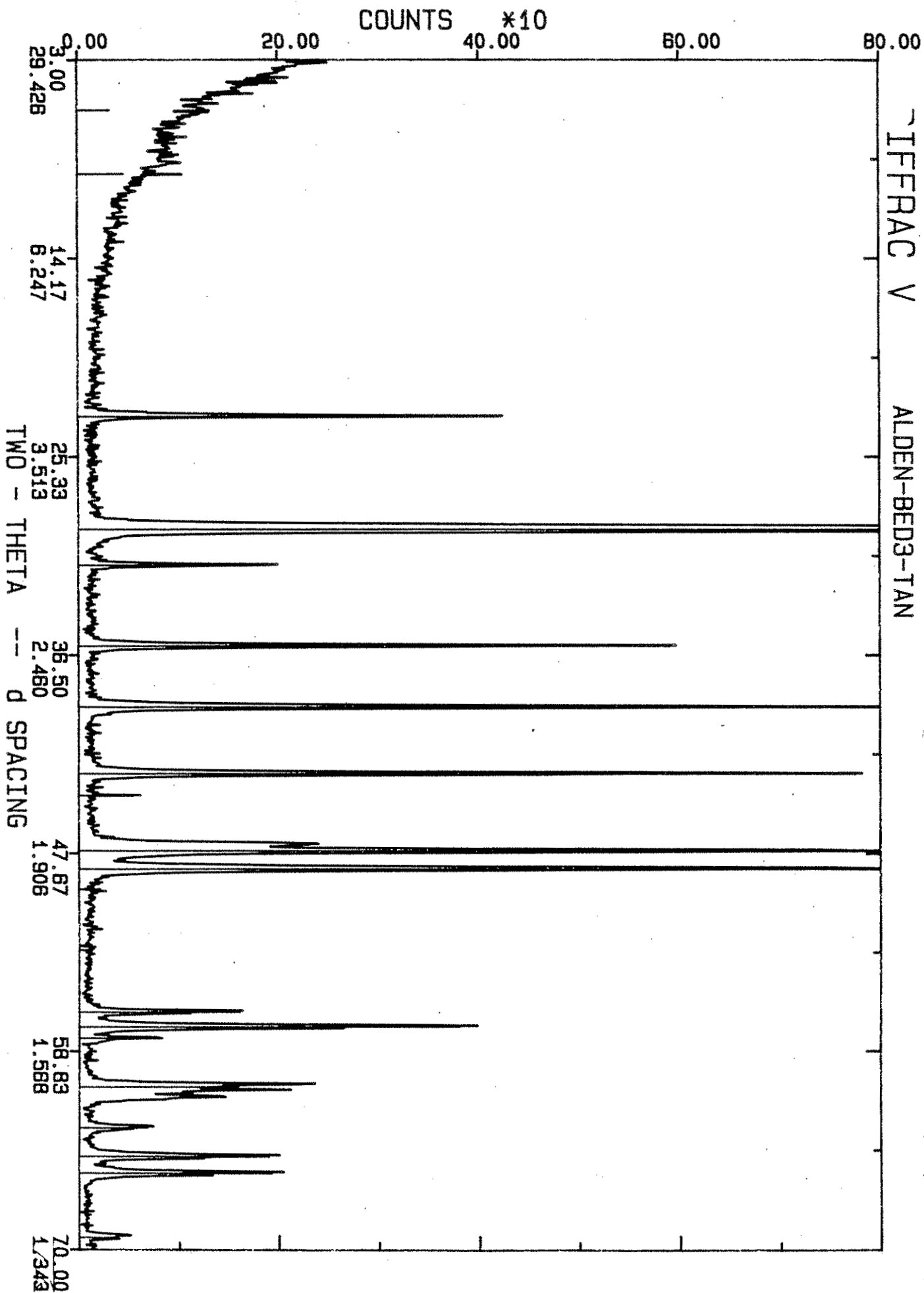


Figure 1, Appendix 1. X-ray diffractogram for Alden aggregate.

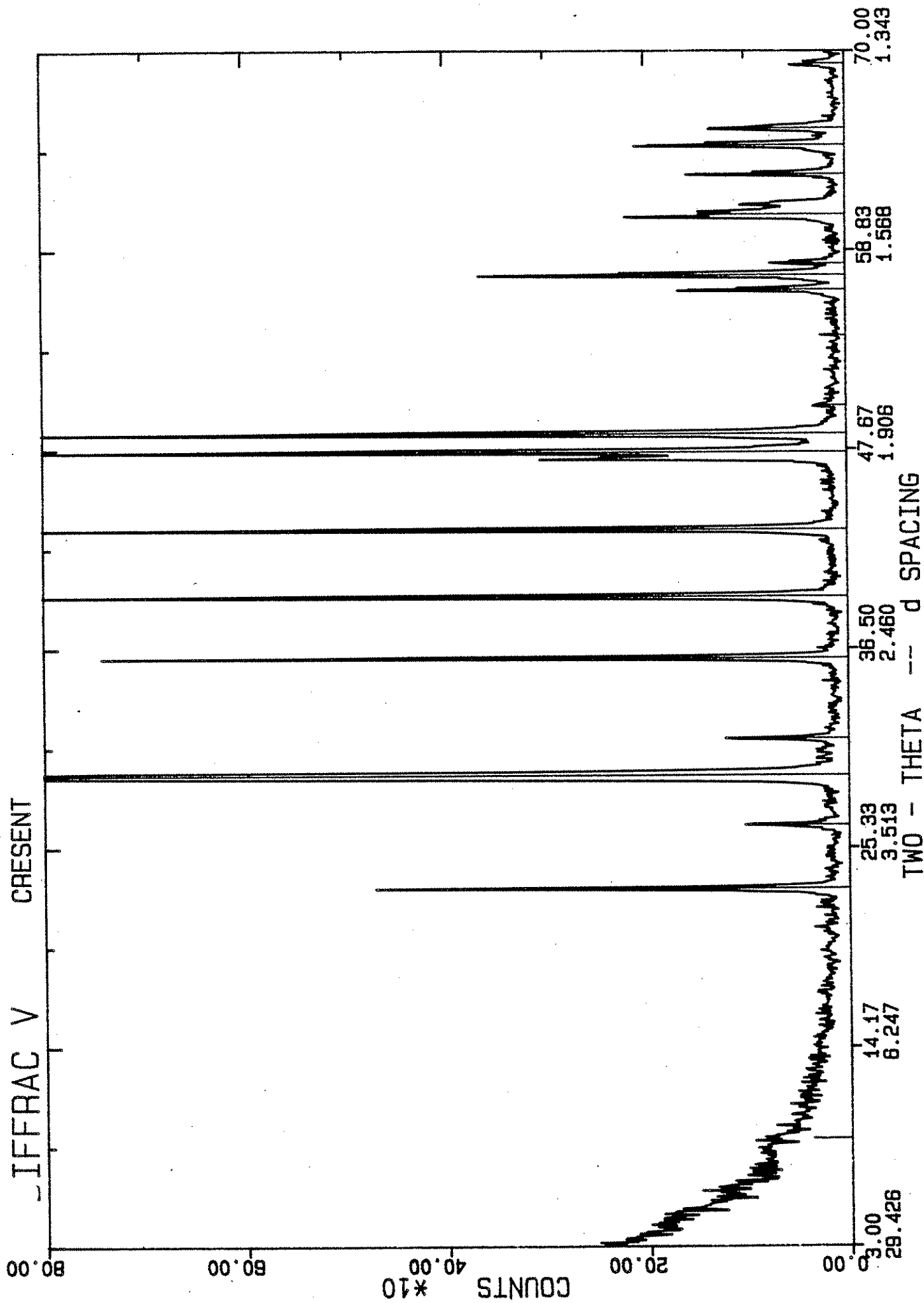


Figure 2, Appendix 1. X-ray diffractogram for Crescent aggregate.

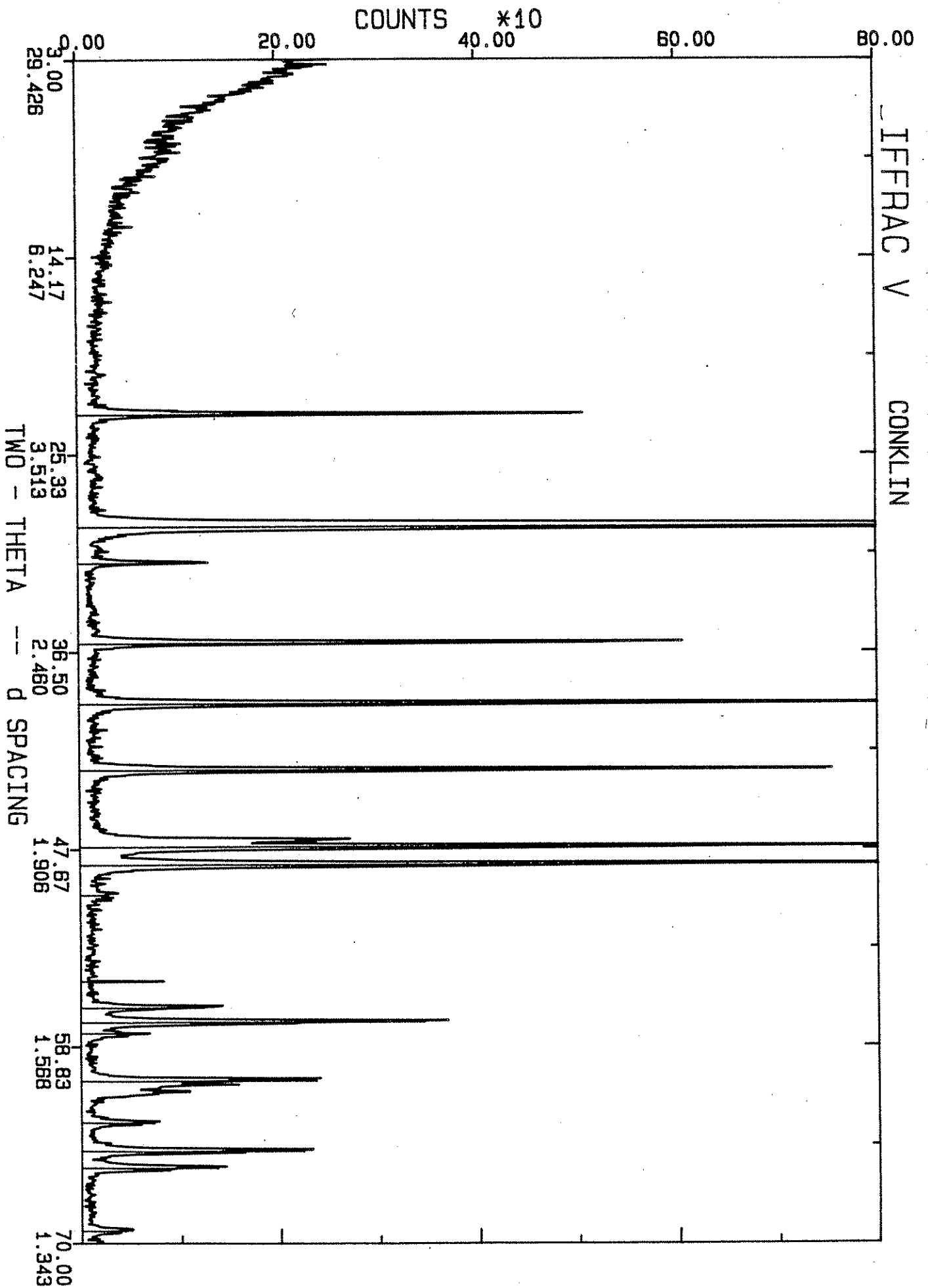


Figure 3, Appendix 1. X-ray diffractogram for Conklin aggregate.

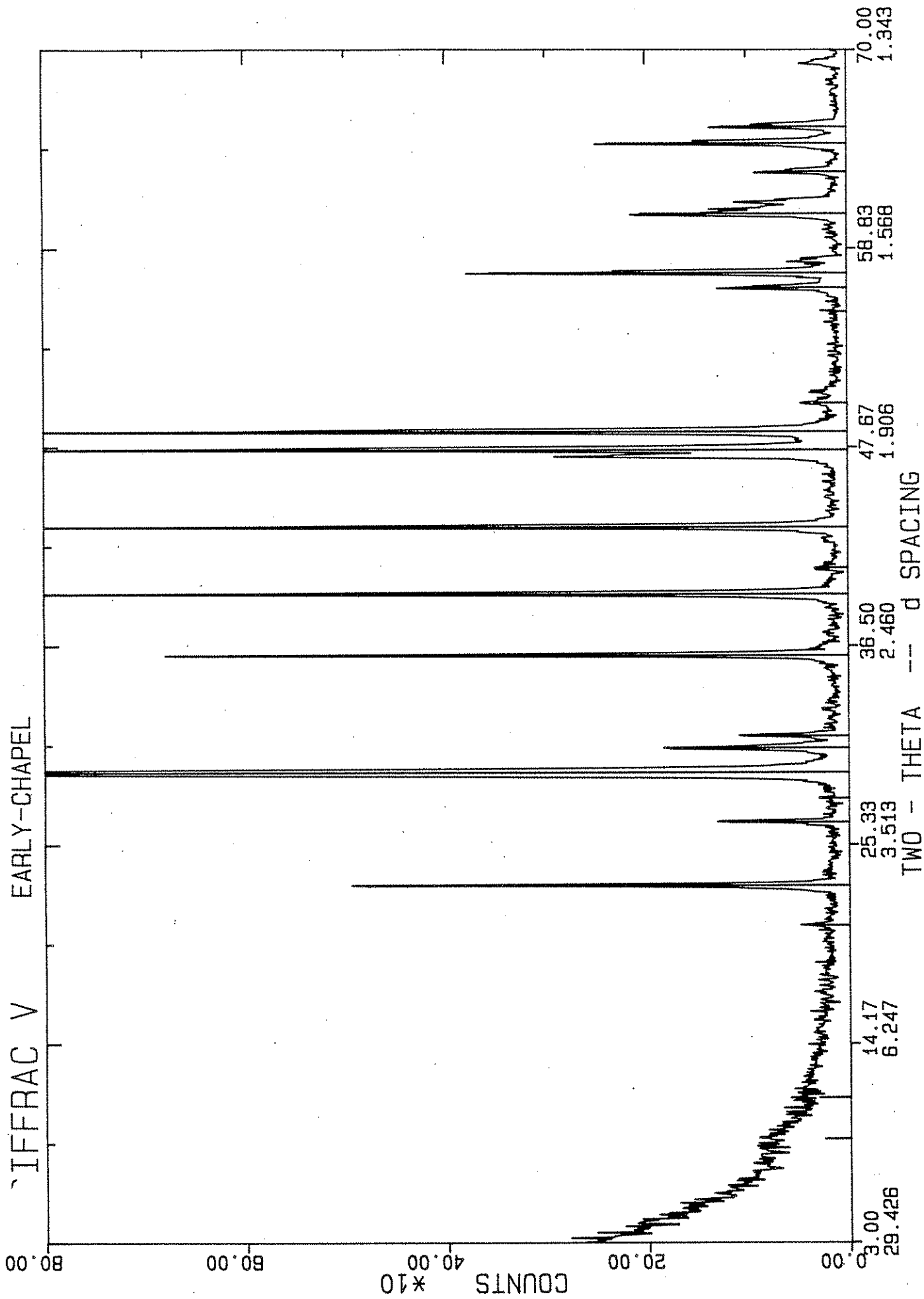


Figure 4, Appendix 1. X-ray diffractogram for Early Chapel aggregate.

IFFRAC V ELDORADO

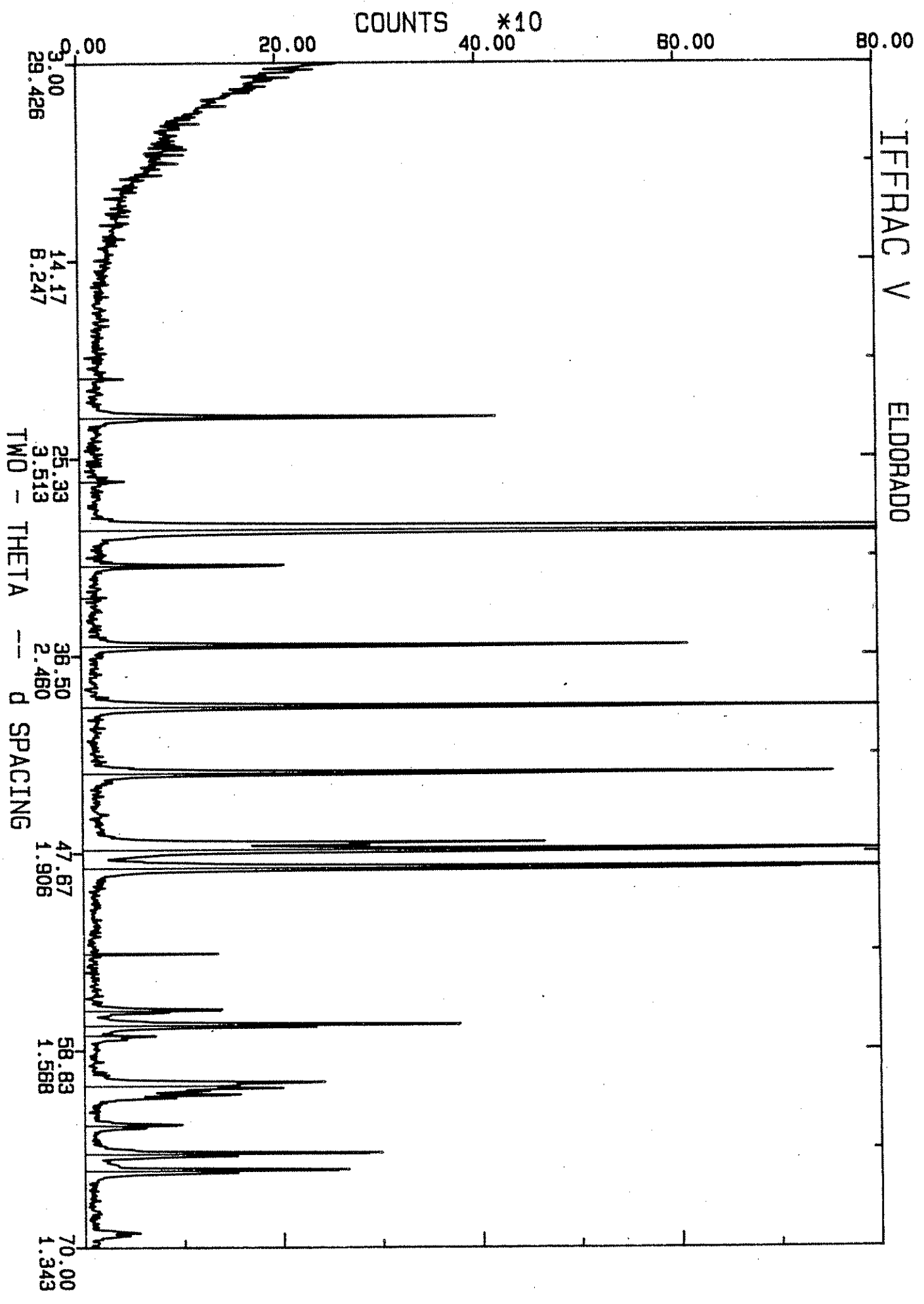


Figure 5, Appendix 1. X-ray diffractogram for Eldorado aggregate.

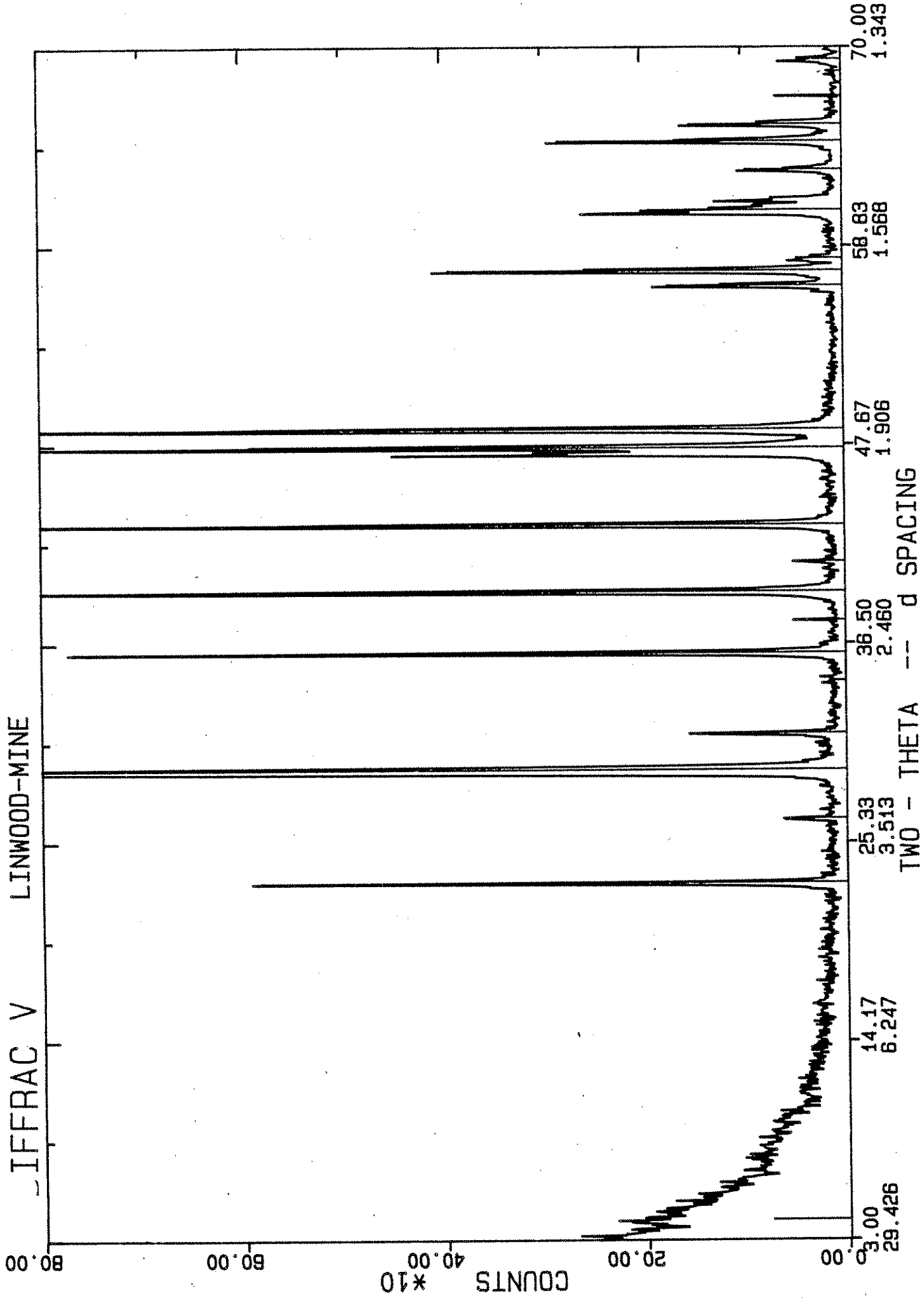


Figure 6, Appendix 1. X-ray diffractogram for Linwood aggregate.

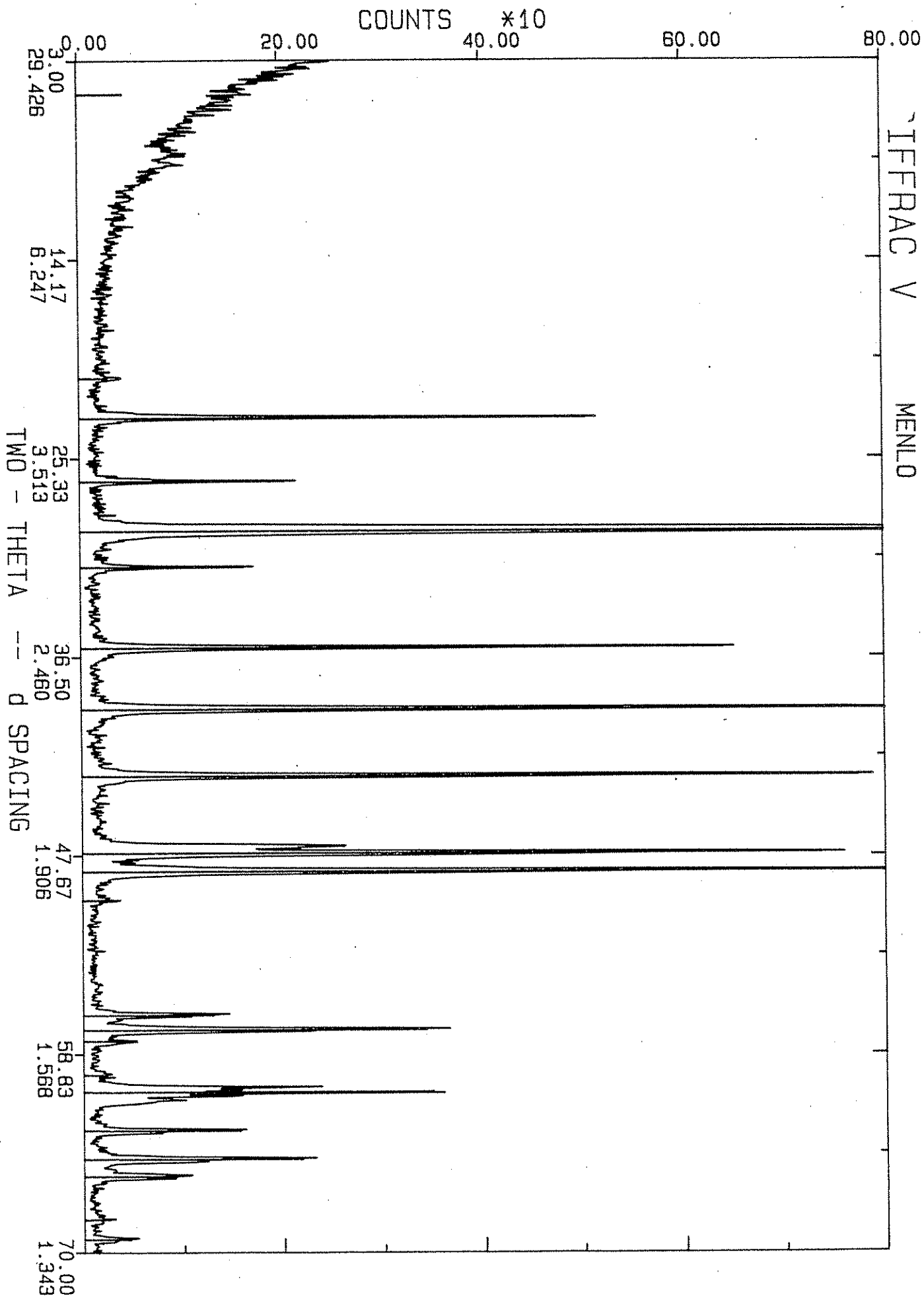


Figure 7, Appendix 1. X-ray diffractogram for Menlo aggregate.

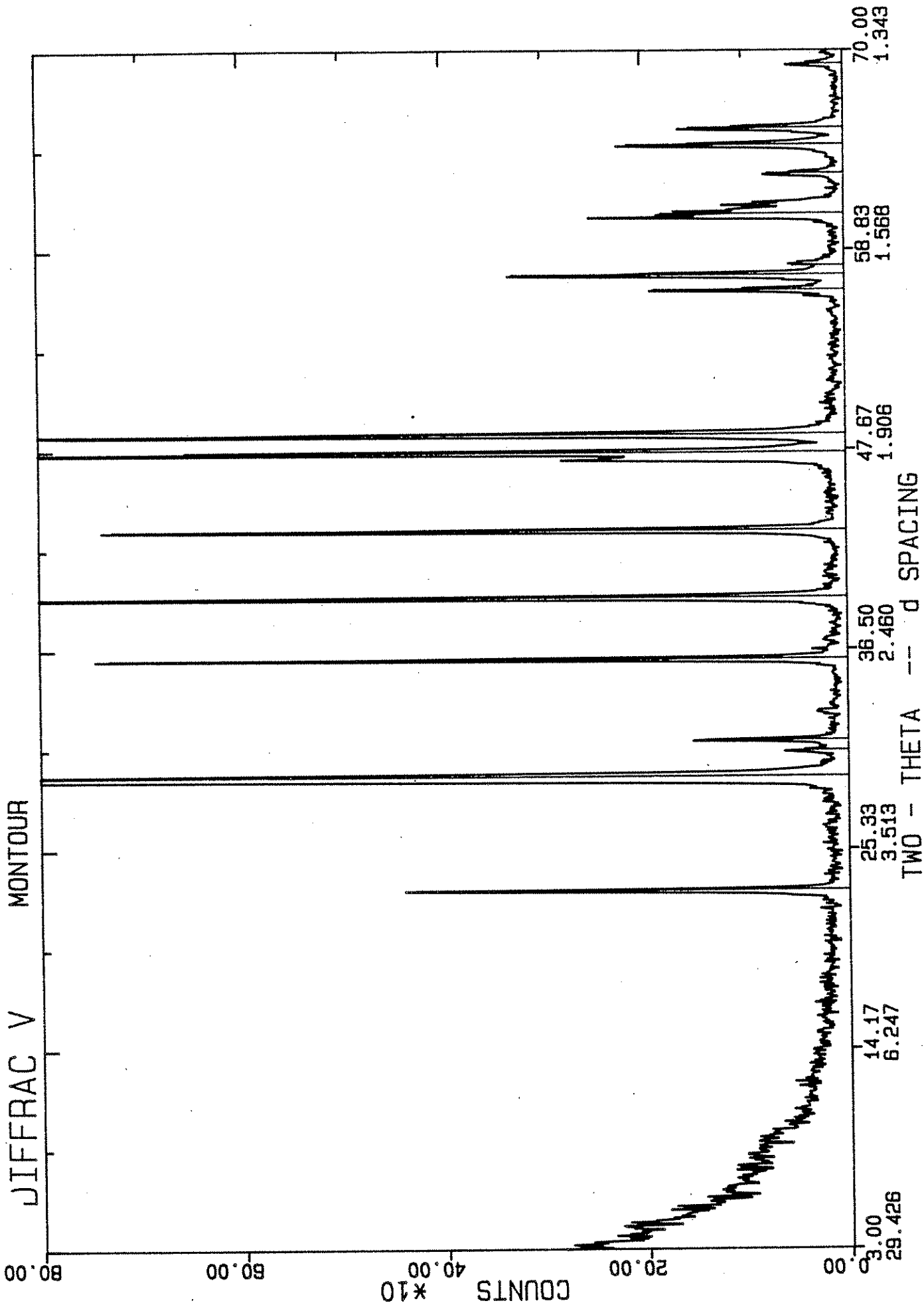


Figure 8, Appendix 1. X-ray diffractogram for Montour aggregate.

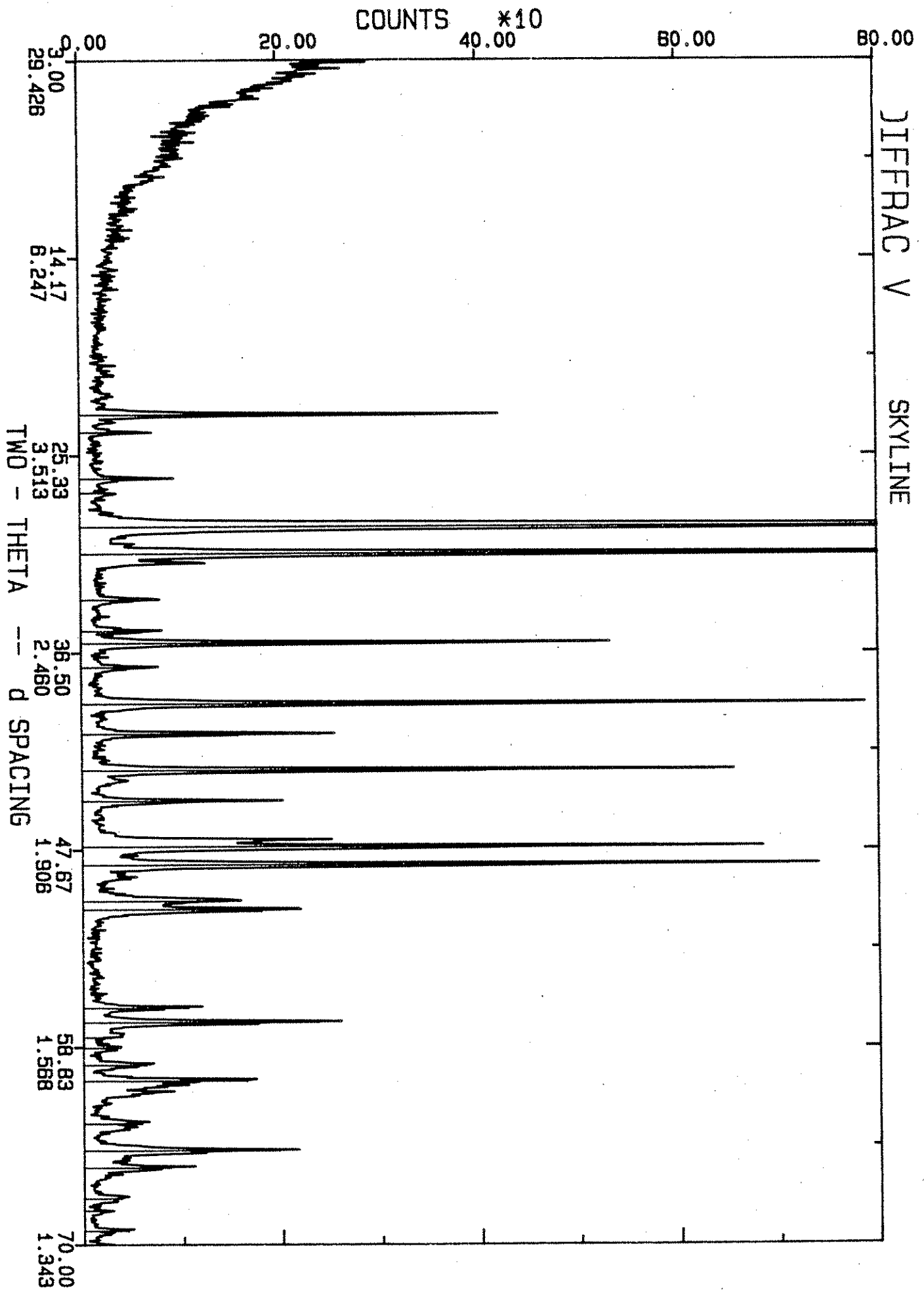


Figure 9, Appendix 1. X-ray diffractogram for Skyline aggregate.

DIFFRACTOGRAM HUNTINGTON

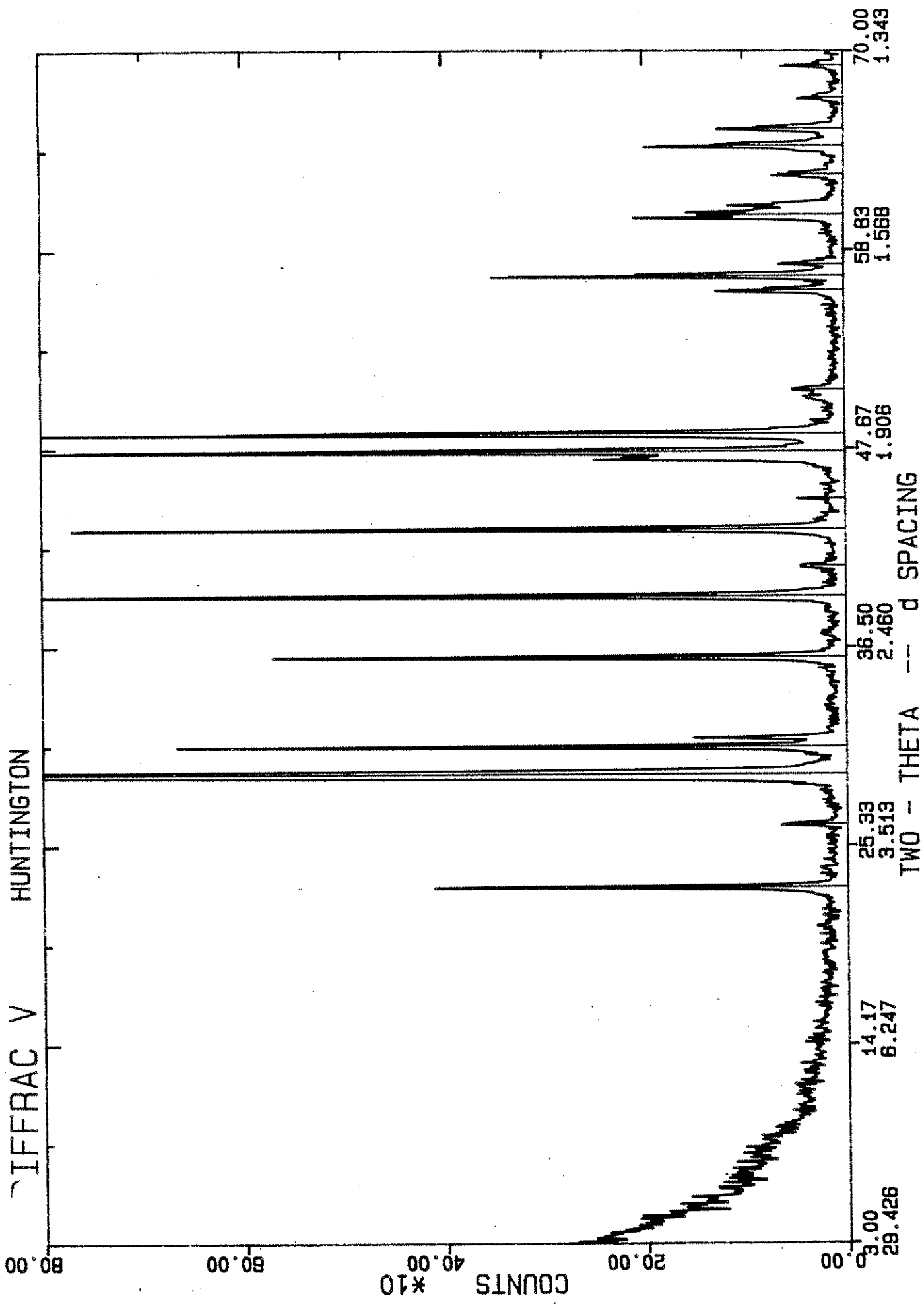


Figure 10, Appendix 1. X-ray diffractogram for Huntington aggregate.

JFFRAC V FISHER-CALCITE

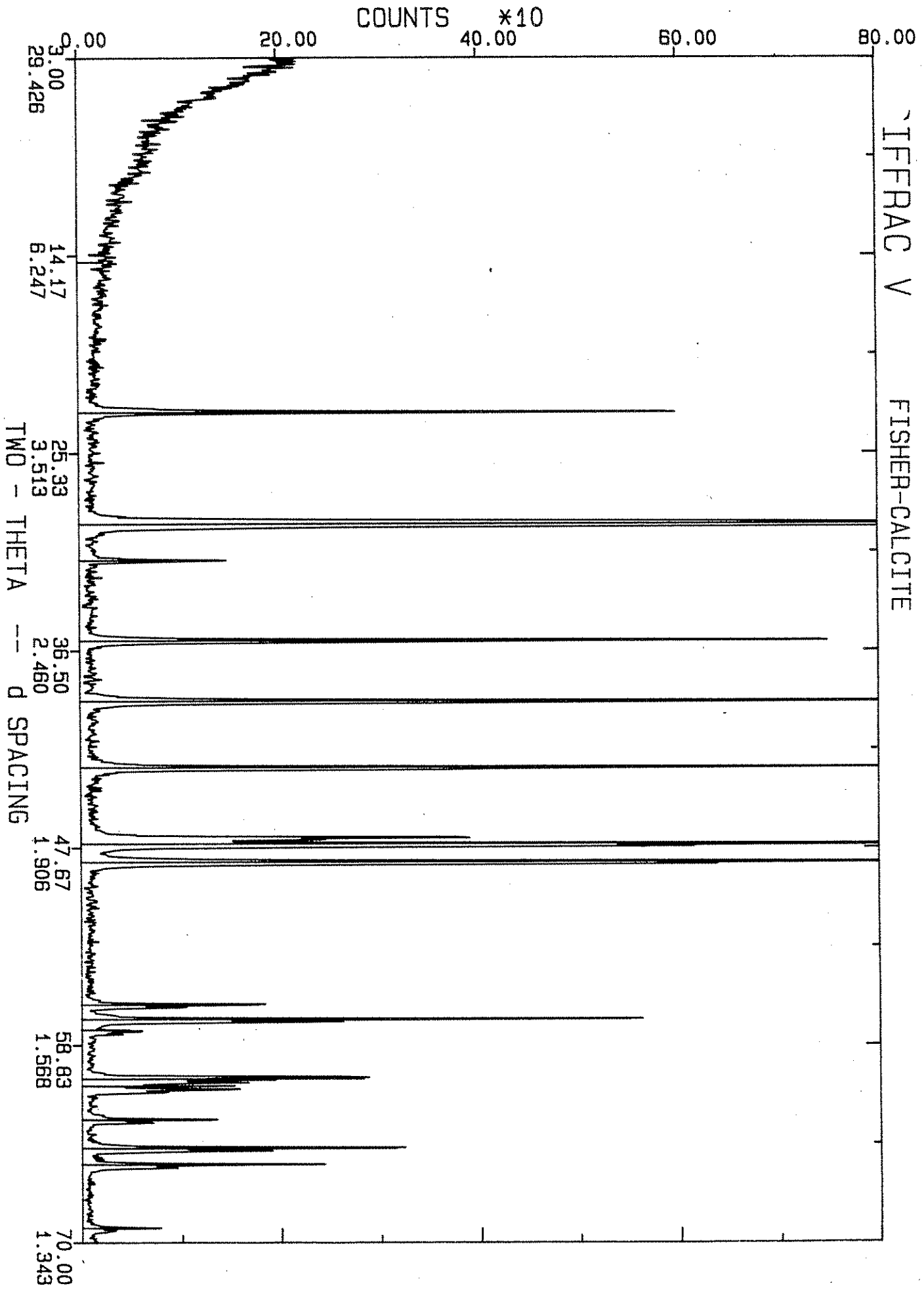


Figure 11, Appendix 1. X-ray diffractogram for Fisher Calcite.

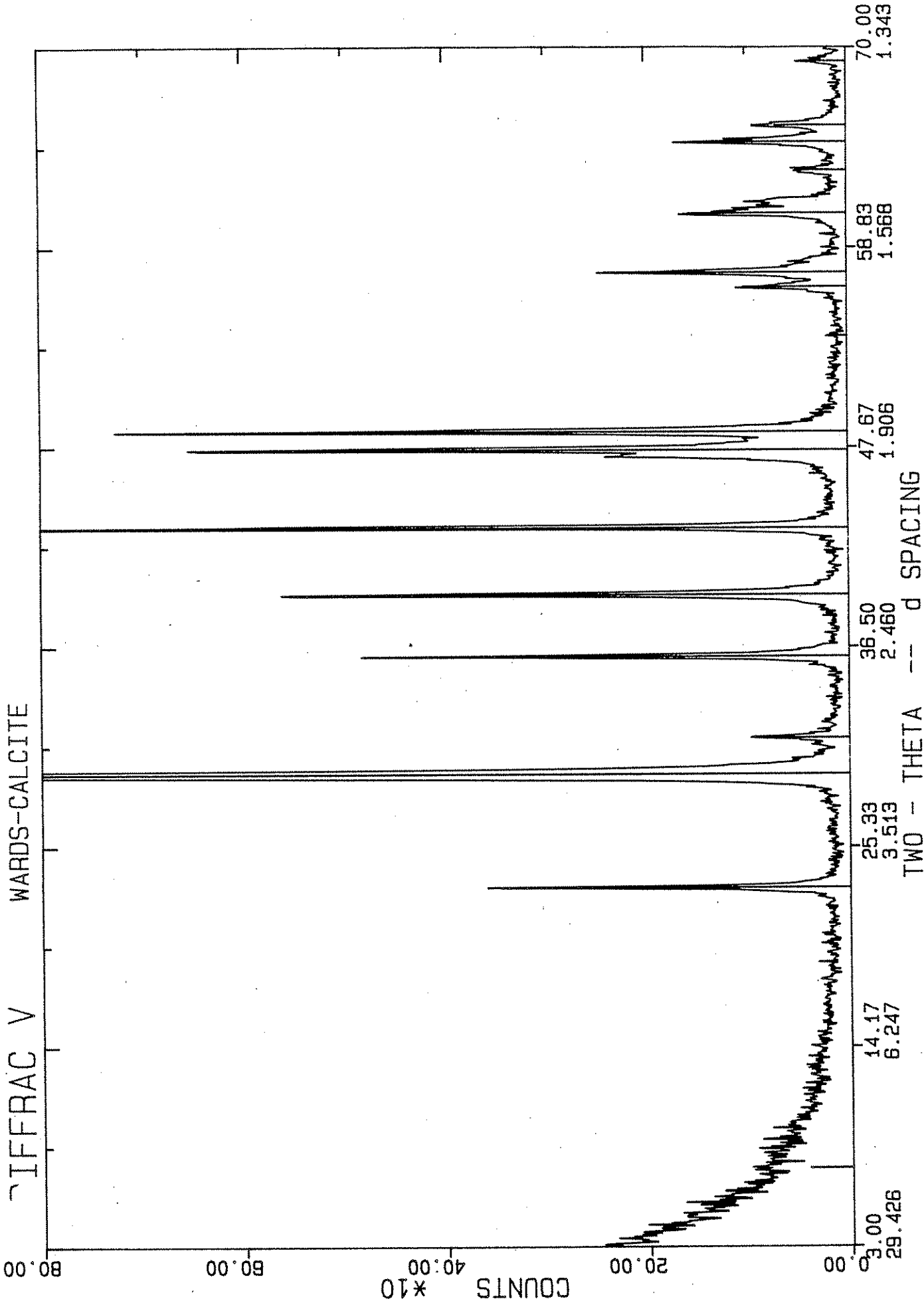


Figure 12, Appendix 1. X-ray diffractogram for Ward's Calcite.

DIFFRAC V
MARYVILLE

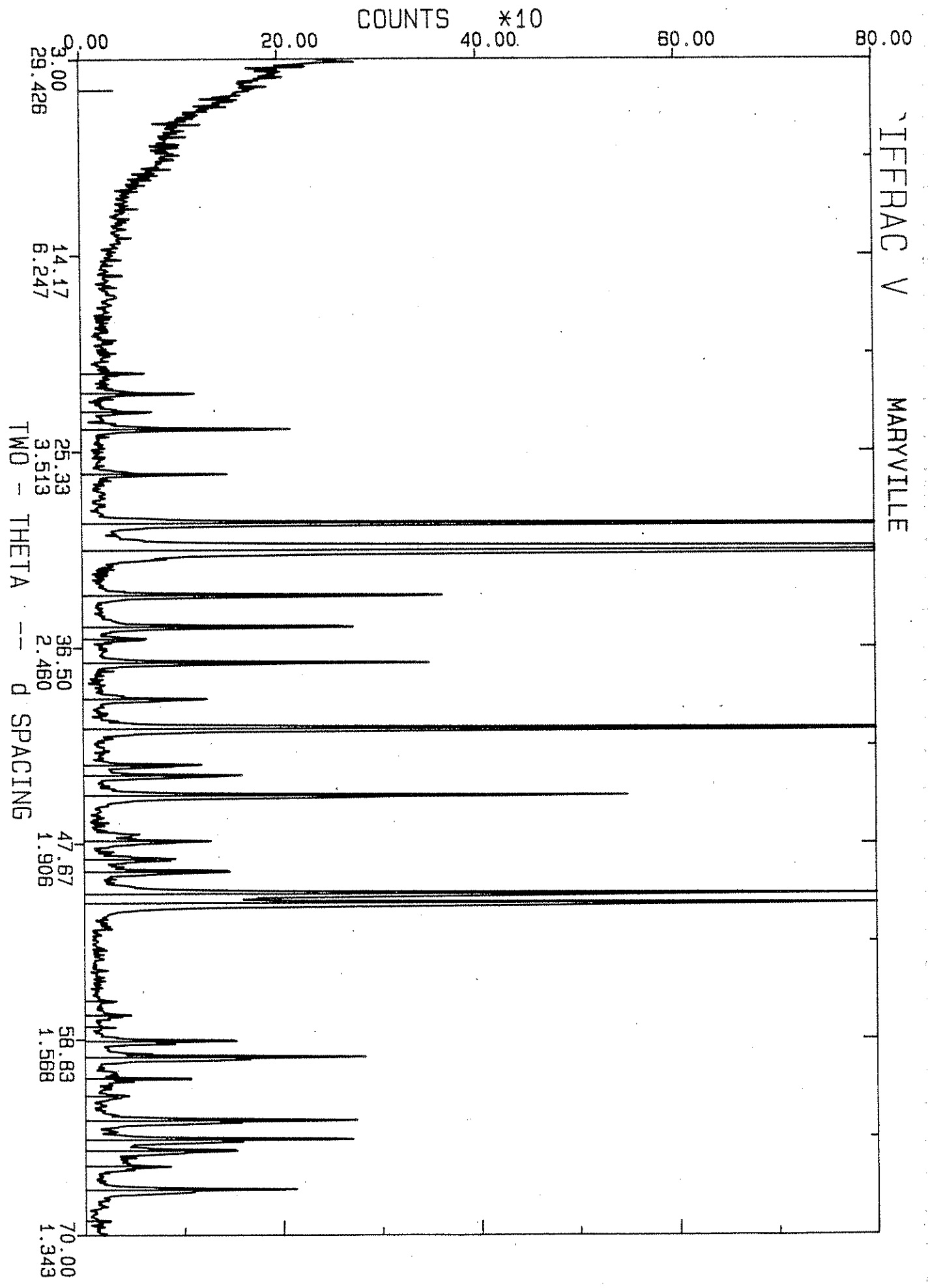


Figure 13, Appendix 1. X-ray diffractogram for Maryville aggregate.

DIFFRAC V BRYAN

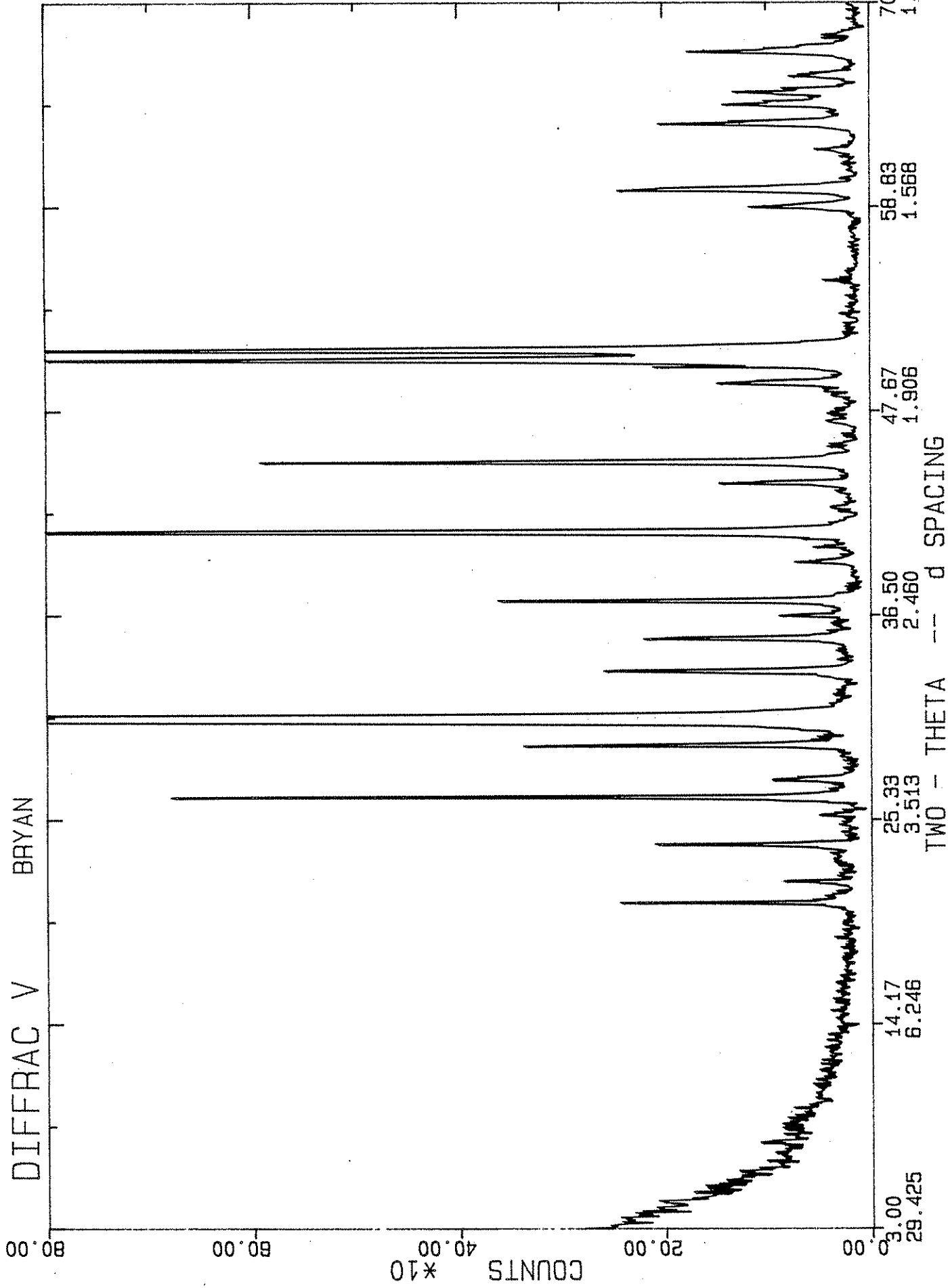


Figure 14, Appendix 1. X-ray diffractogram for Bryan aggregate.

XIFFRAC V GRY-S.CED.RAPIC

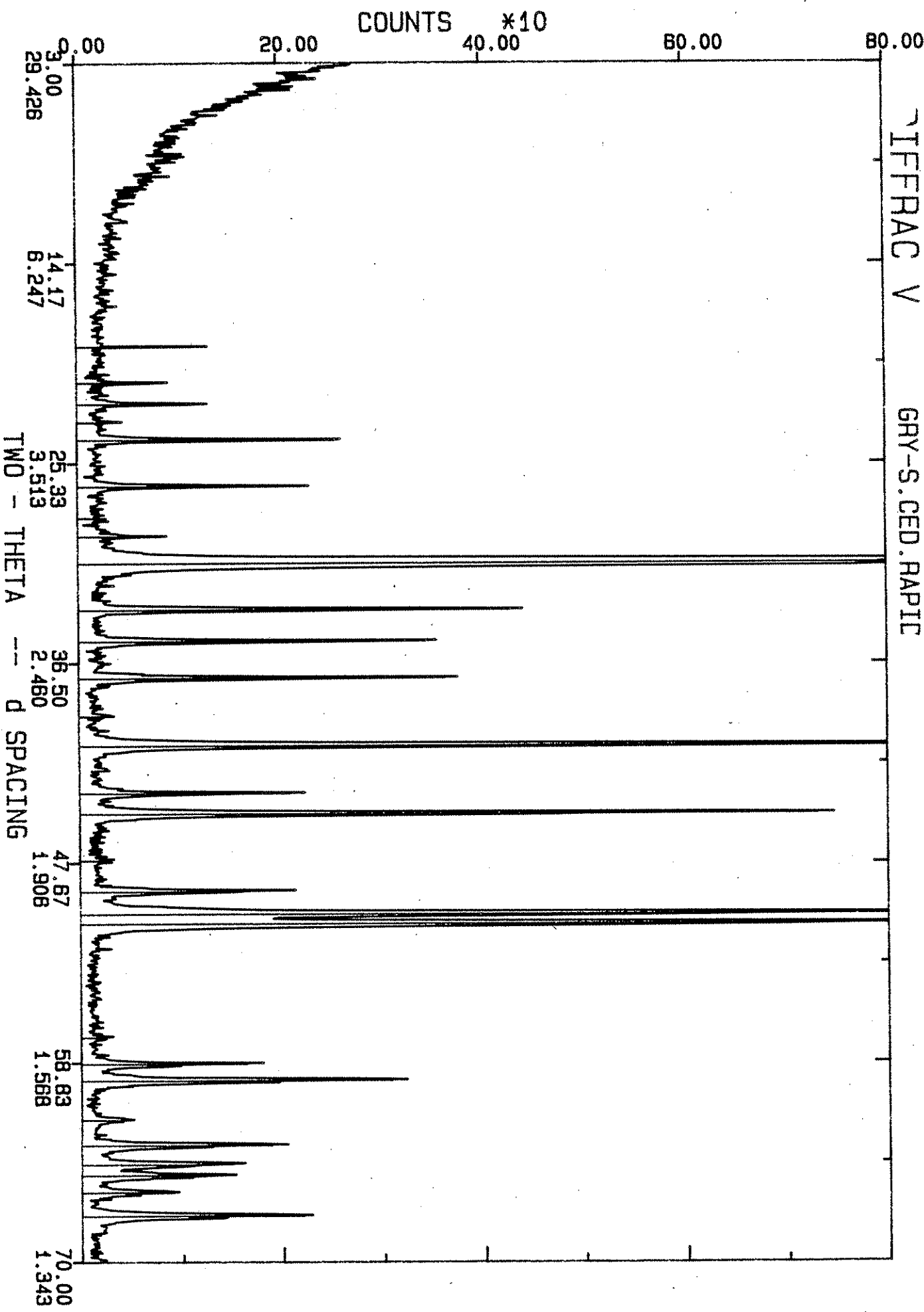


Figure 15, Appendix 1. X-ray diffractogram for Ced. Rap. Gray aggregate.

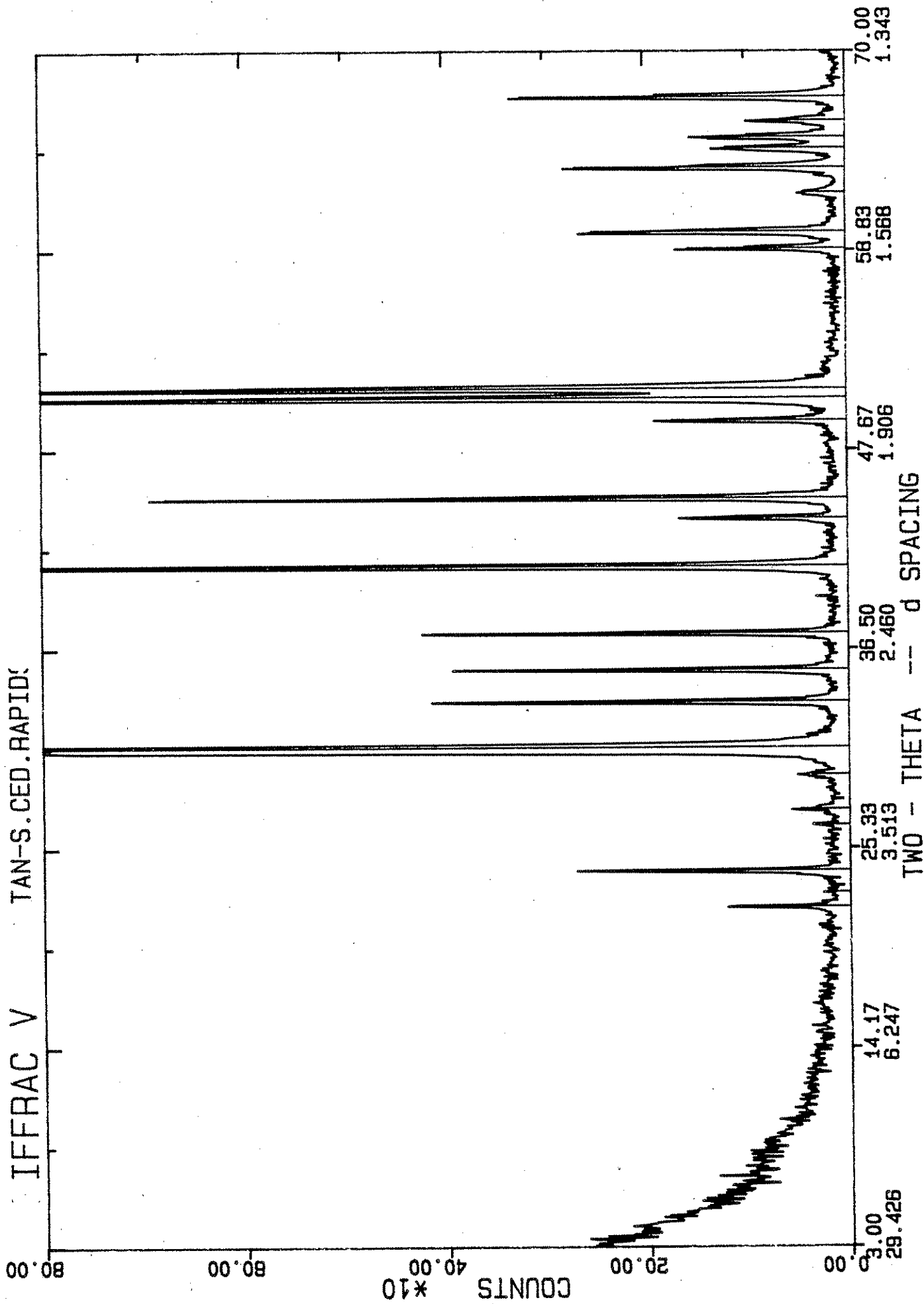


Figure 16, Appendix 1. X-ray diffractogram for Ced. Rap. Tan aggregate.

JIFFRAC V GARRISON

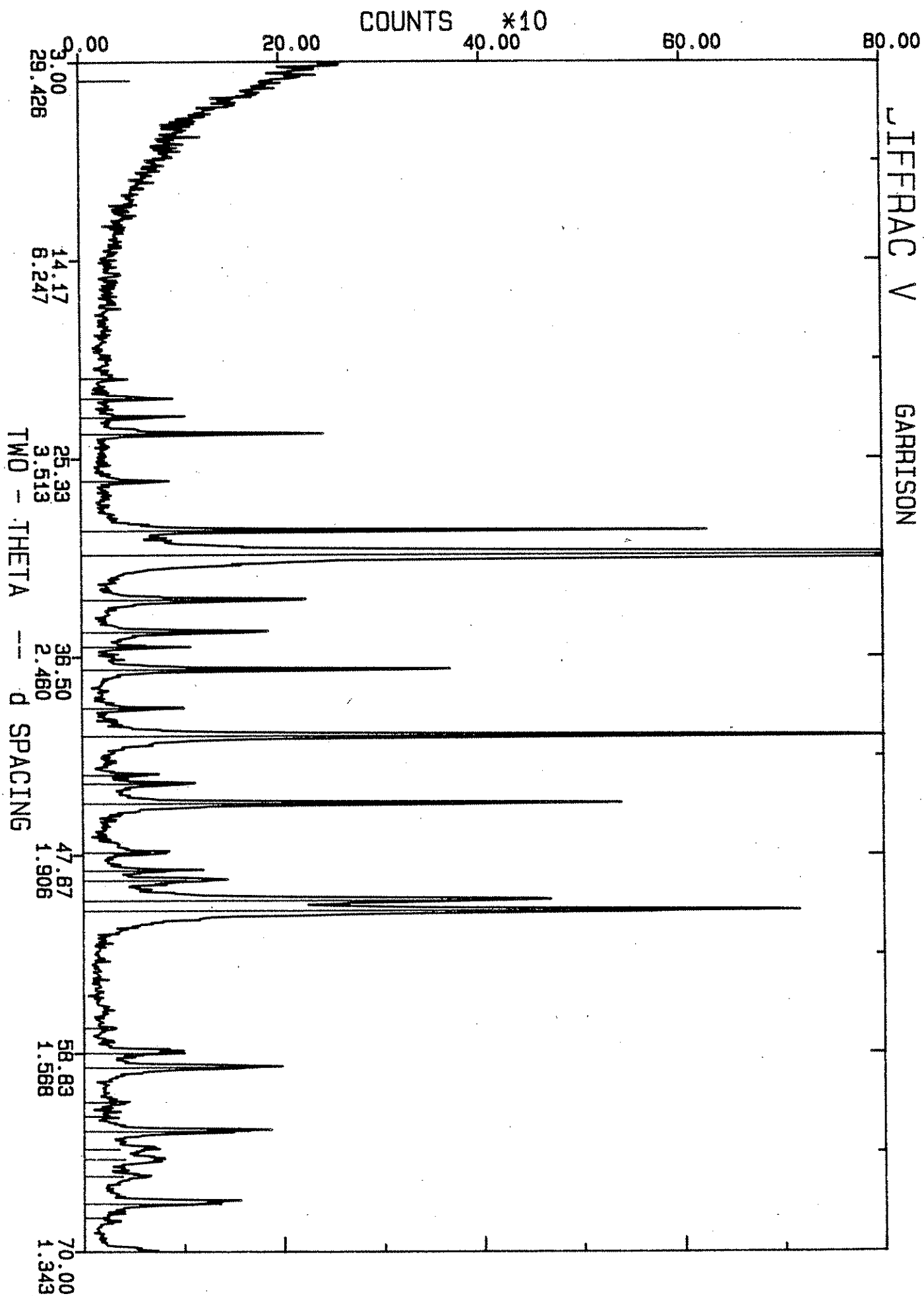


Figure 17, Appendix 1. X-ray diffractogram for Garrison aggregate.

JIFFRAC V GASSMAN

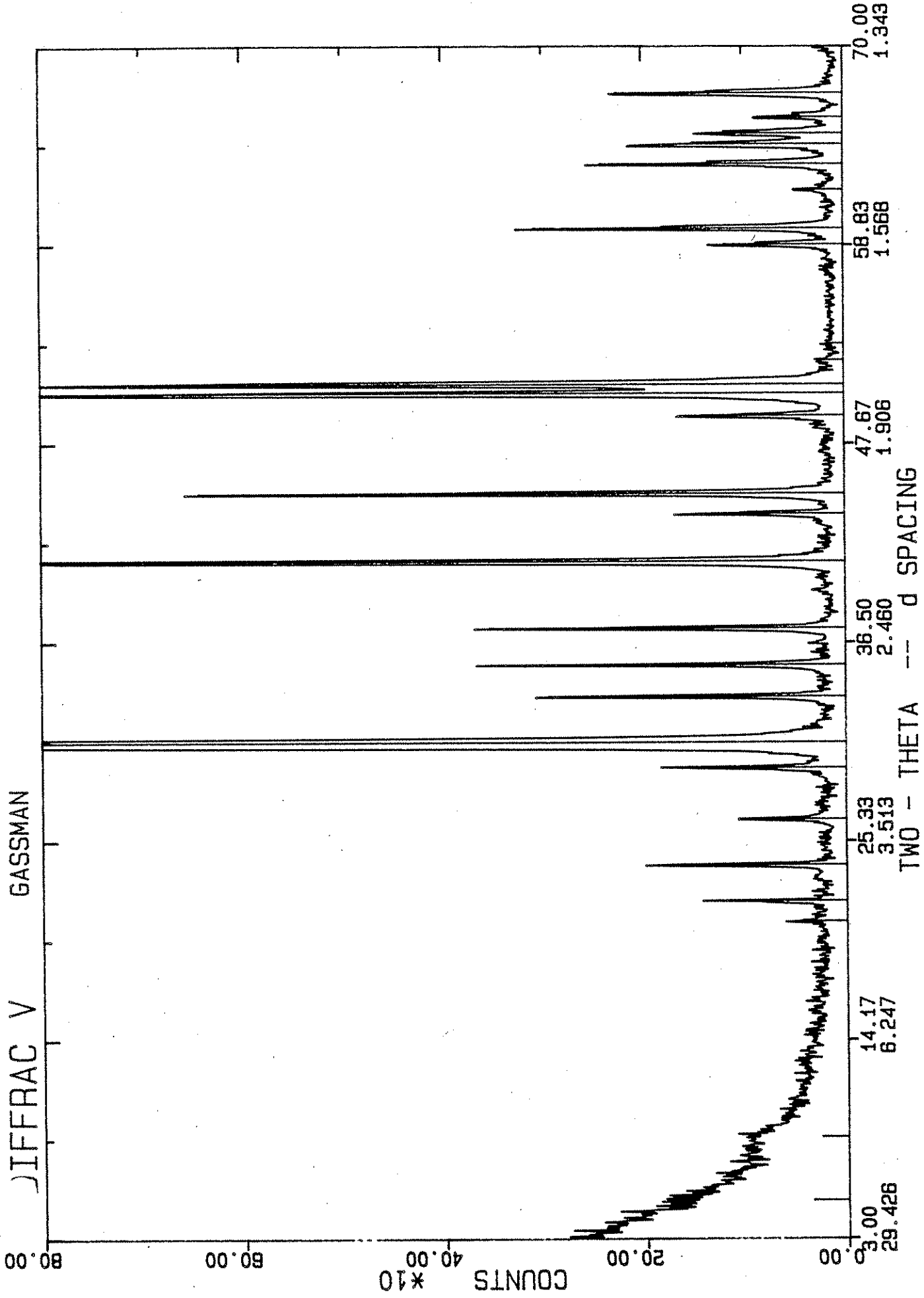


Figure 18, Appendix 1. X-ray diffractogram for Gassman aggregate.

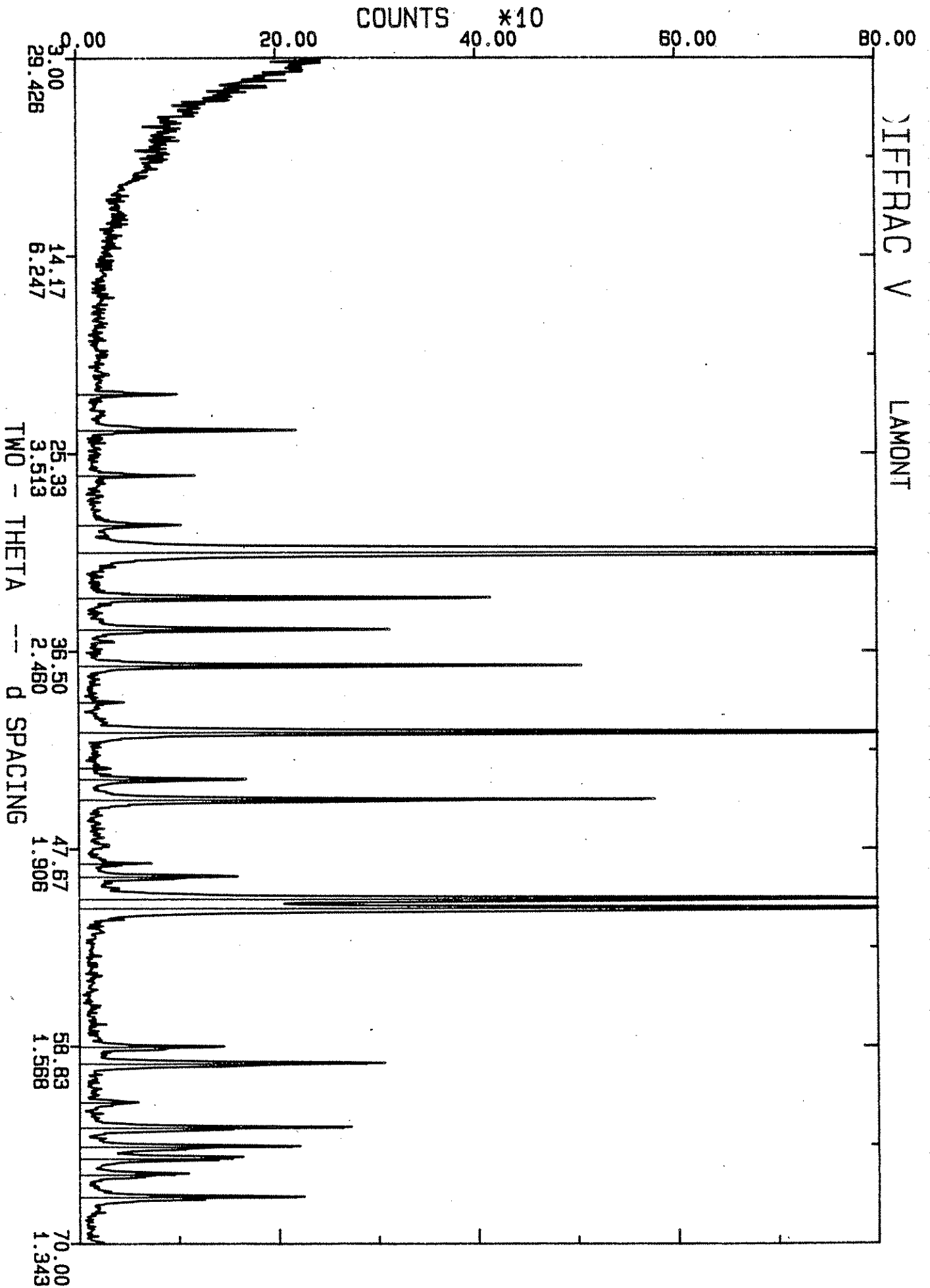


Figure 19, Appendix 1. X-ray diffractogram for Lamont aggregate.

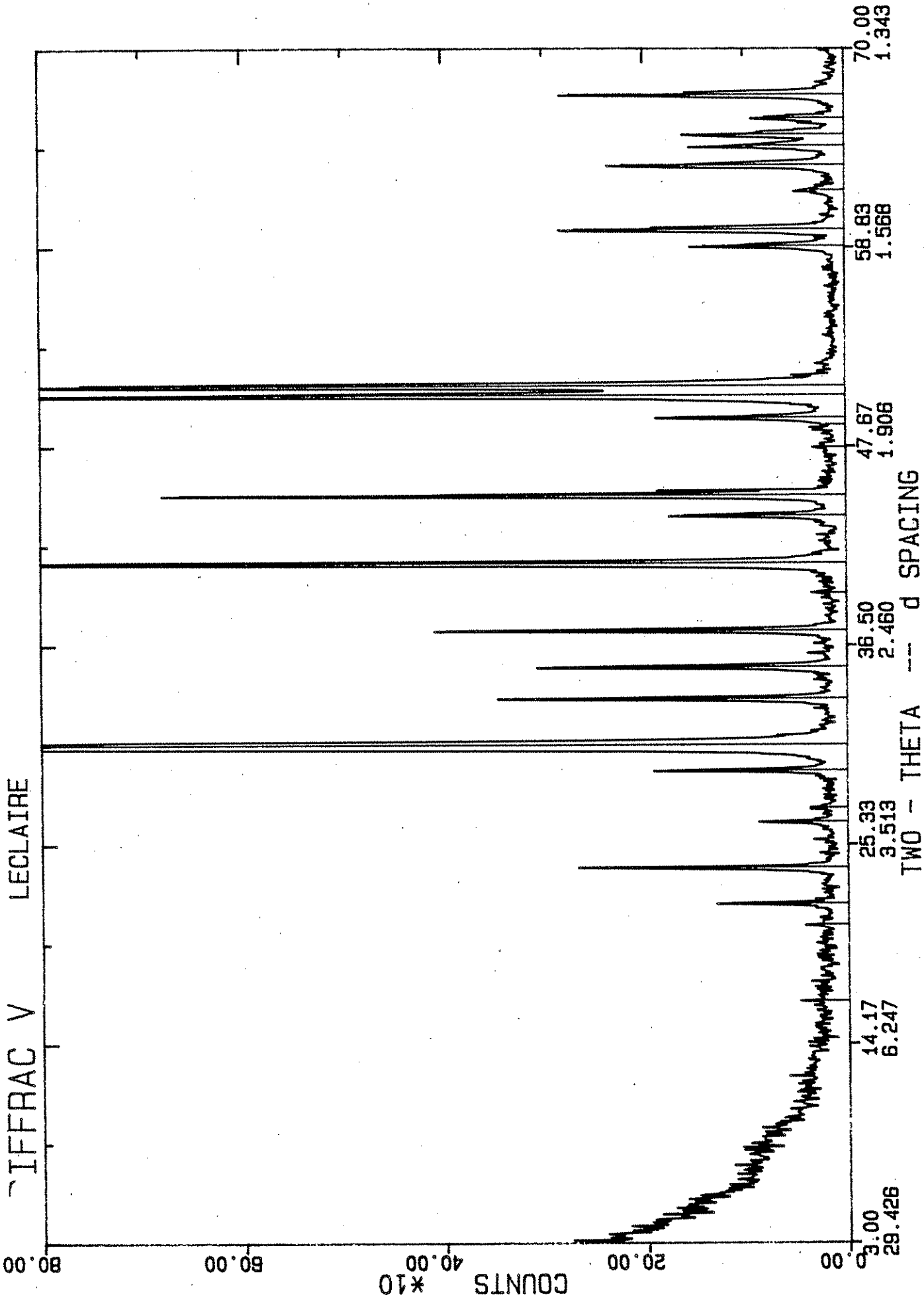


Figure 20, Appendix 1. X-ray diffractogram for LeClaire aggregate.

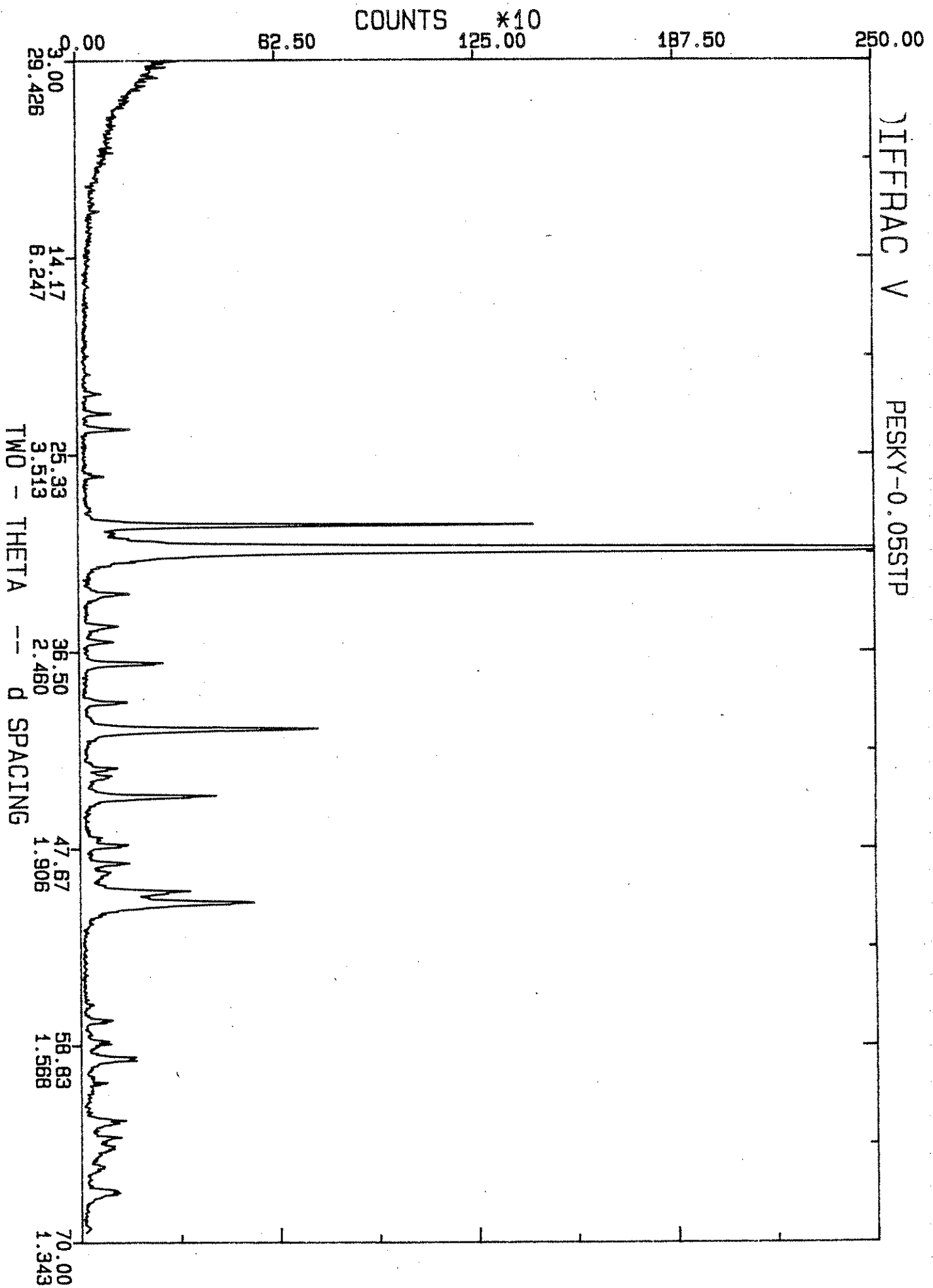


Figure 21, Appendix 1. X-ray diffractogram for Pesky aggregate.

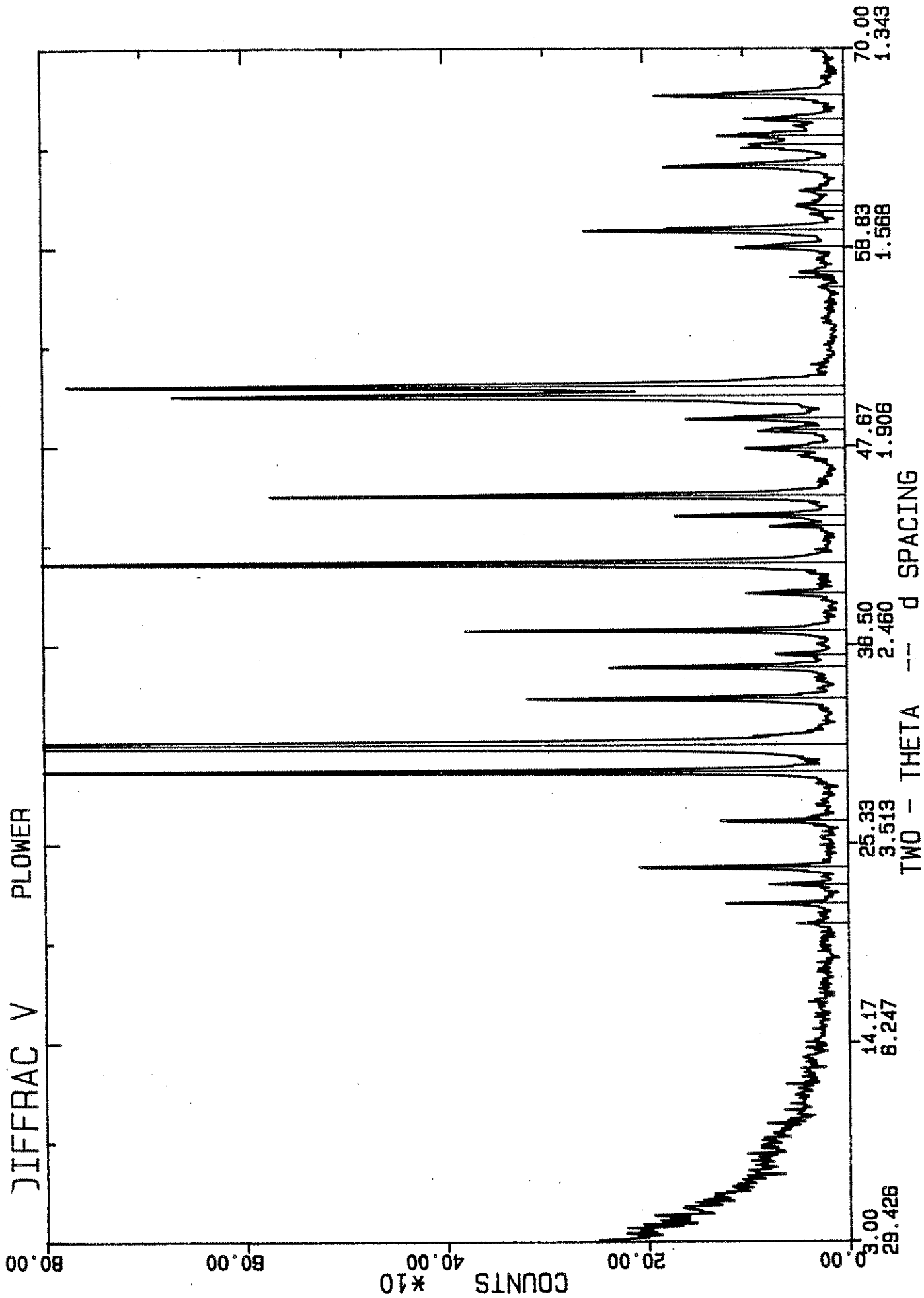


Figure 22, Appendix 1. X-ray diffractogram for Plover aggregate.

APPENDIX II

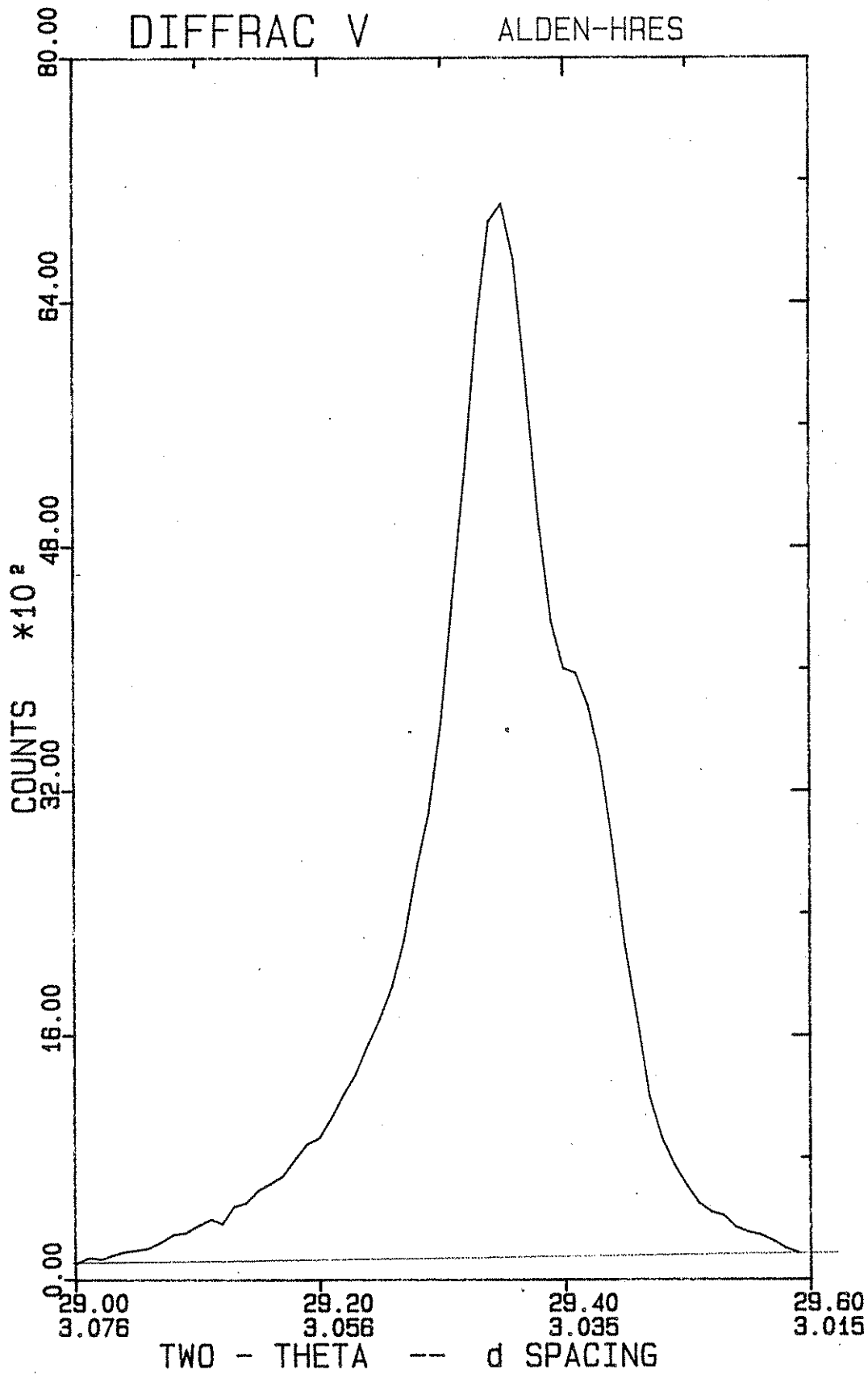


Figure 1, Appendix II. Crystallite size study for Alden aggregate.

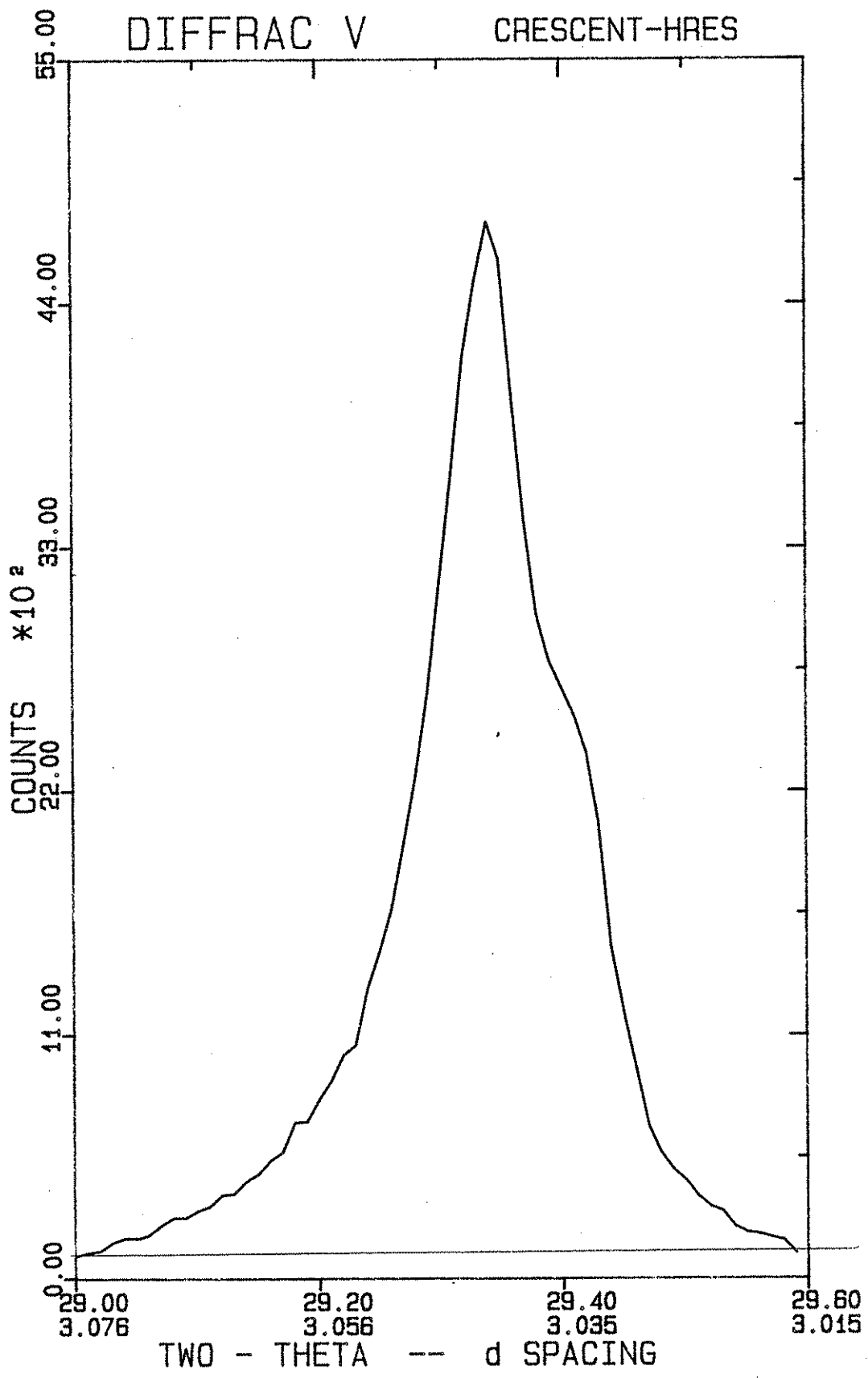


Figure 2, Appendix II. Crystallite size study for Crescent aggregate.

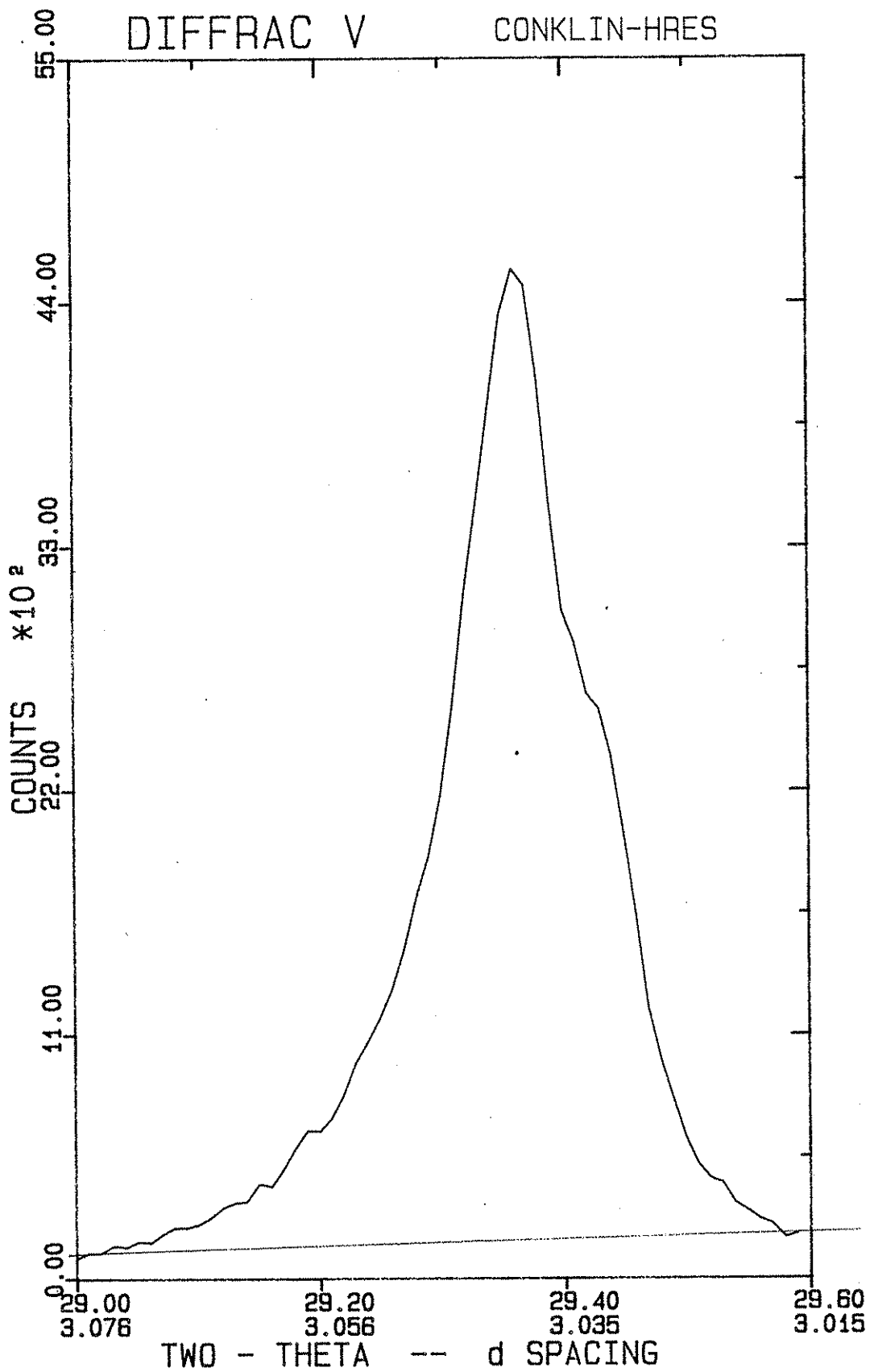


Figure 3, Appendix II. Crystallite size study for Conklin aggregate.

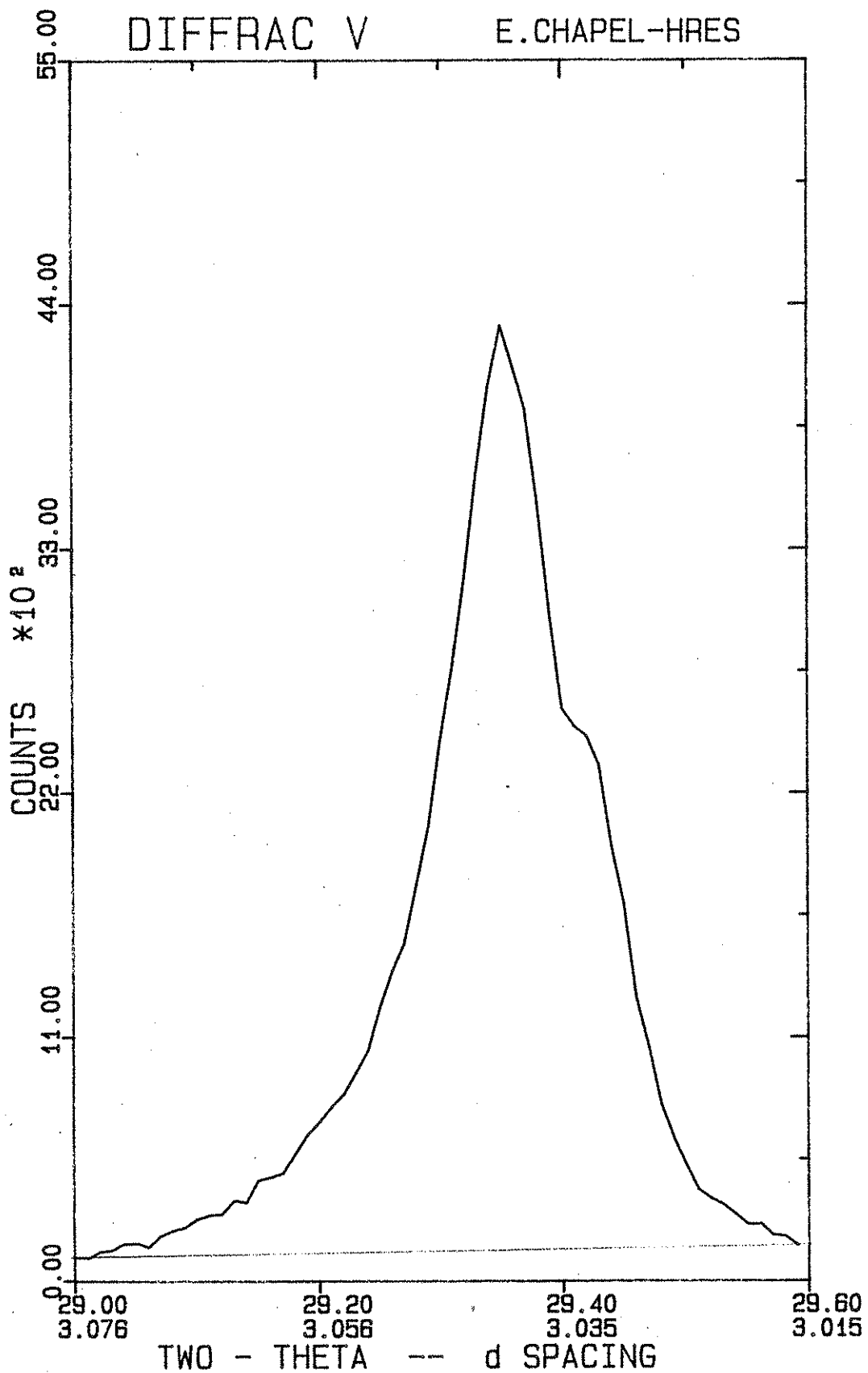


Figure 4, Appendix II. Crystallite size study for Early Chapel aggregate.

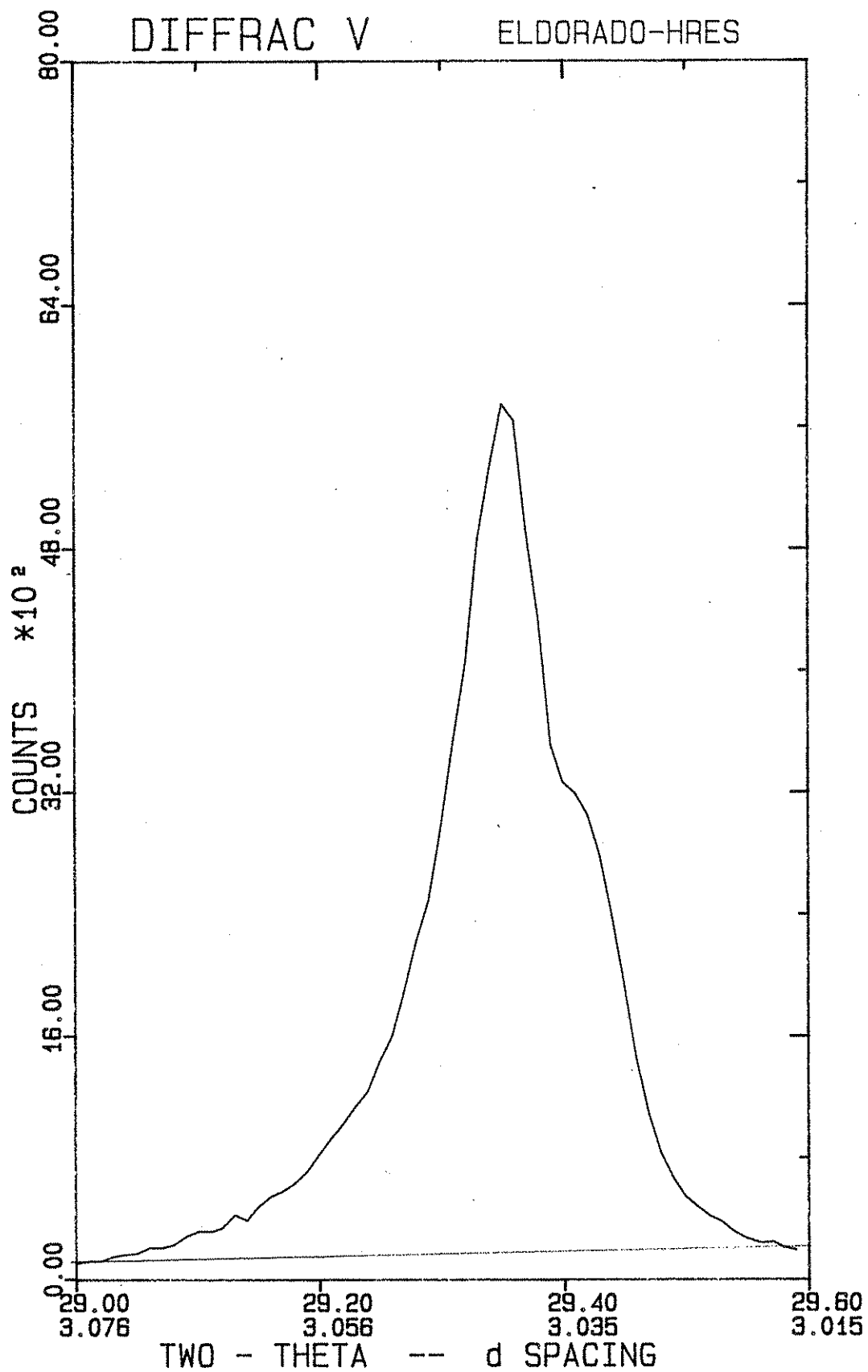


Figure 5, Appendix II. Crystallite size study for Eldorado aggregate.

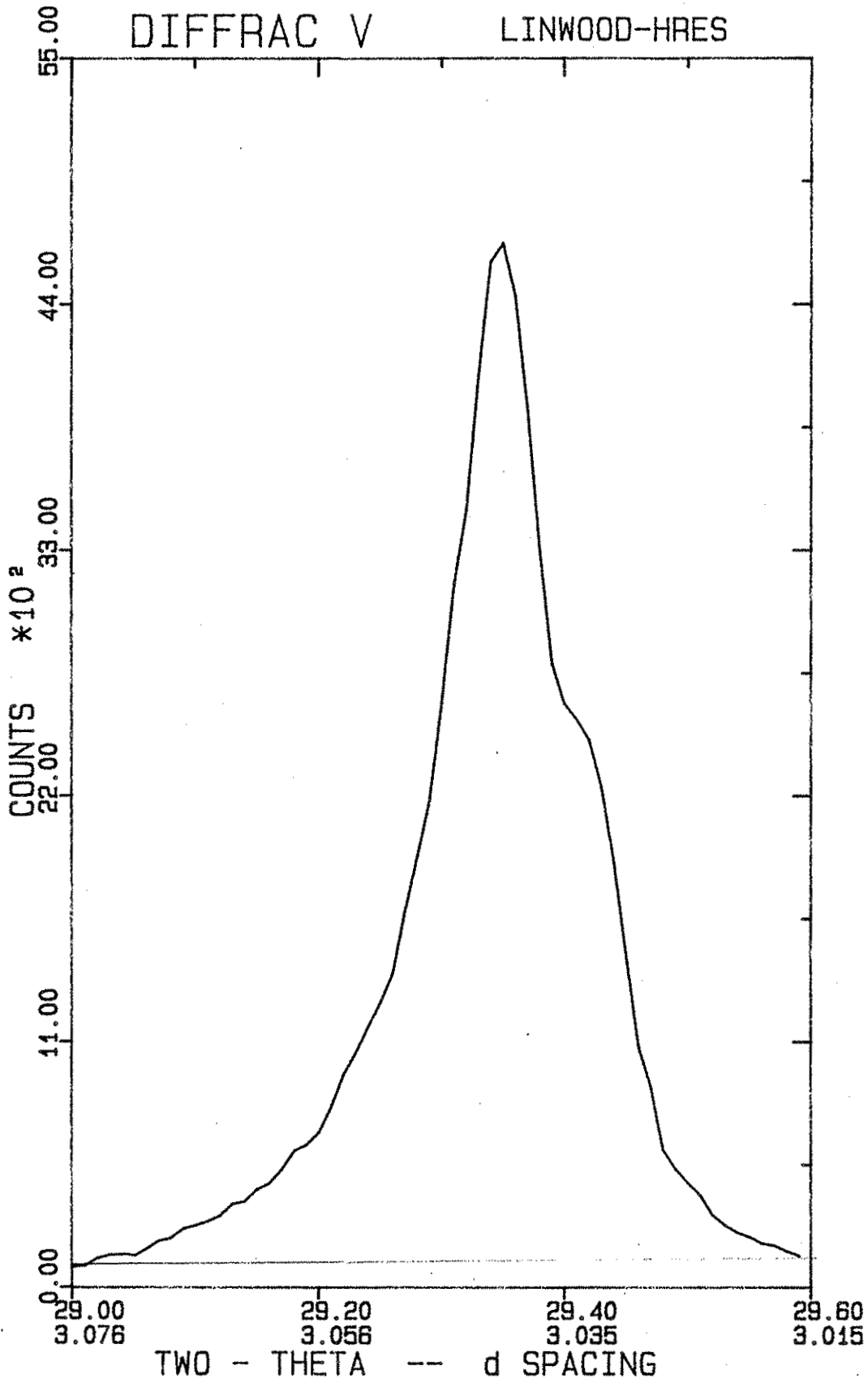


Figure 6, Appendix II. Crystallite size study for Linwood aggregate.

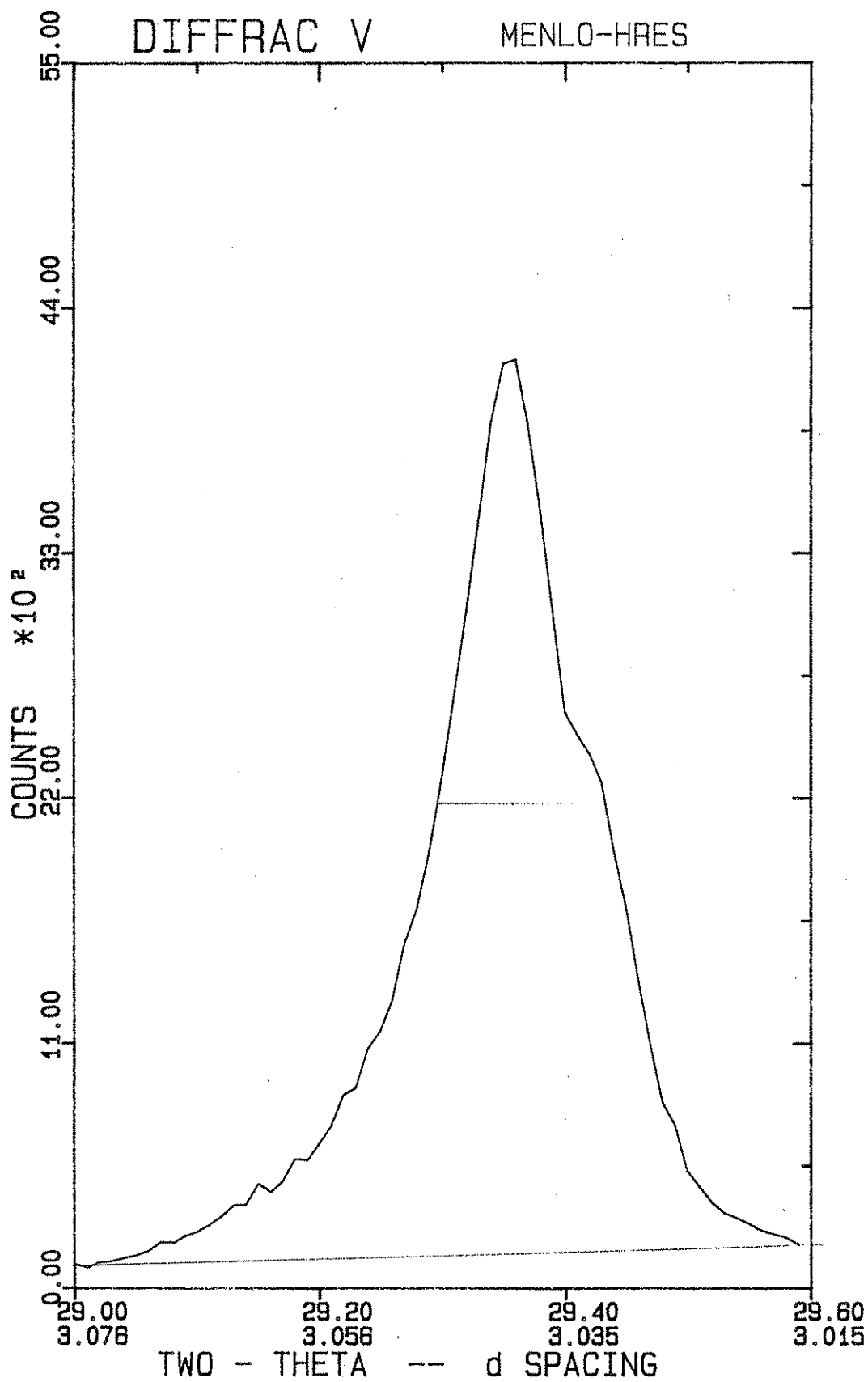


Figure 7, Appendix II. Crystallite size study for Menlo aggregate.

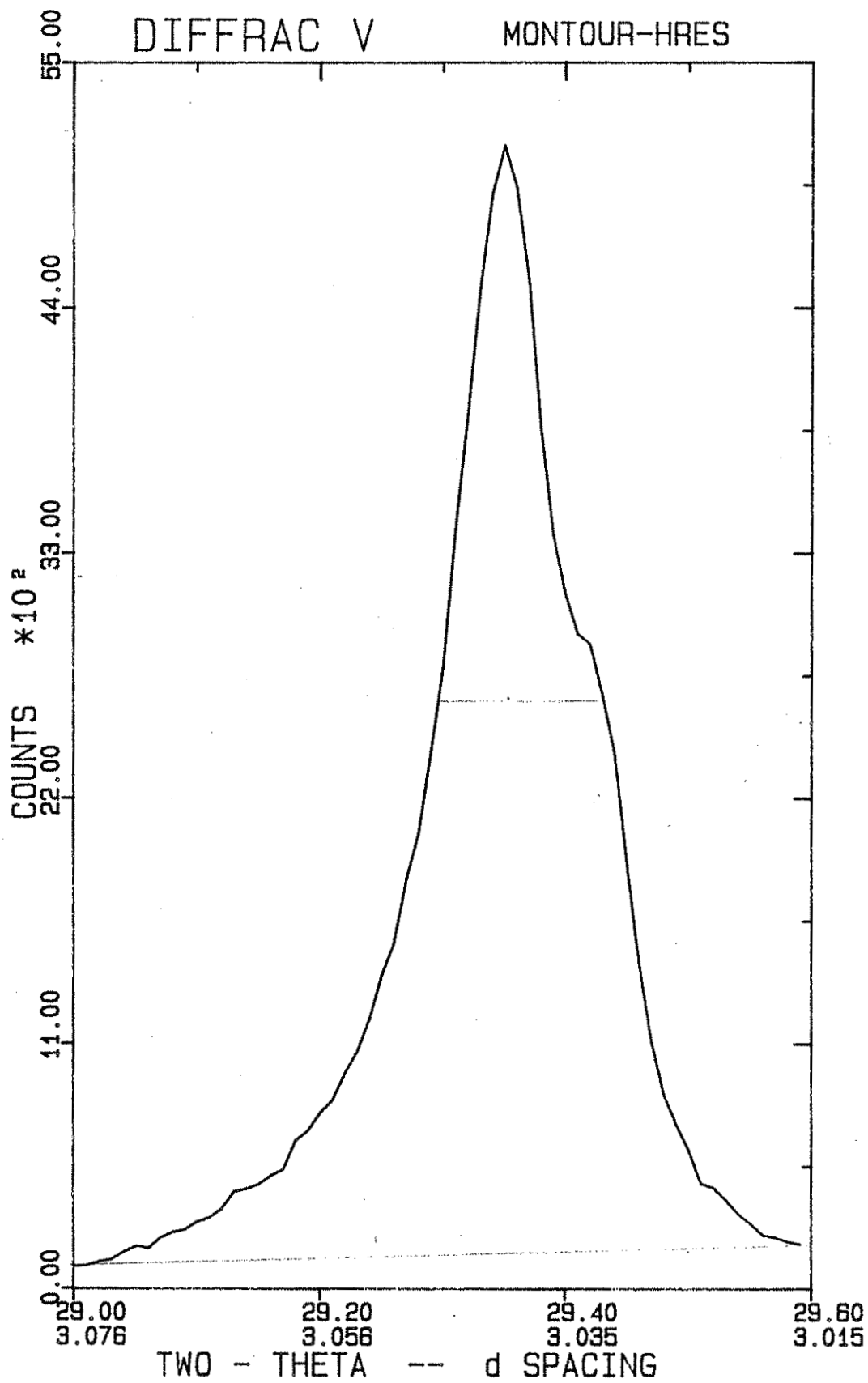


Figure 8, Appendix II. Crystallite size study for Montour aggregate.

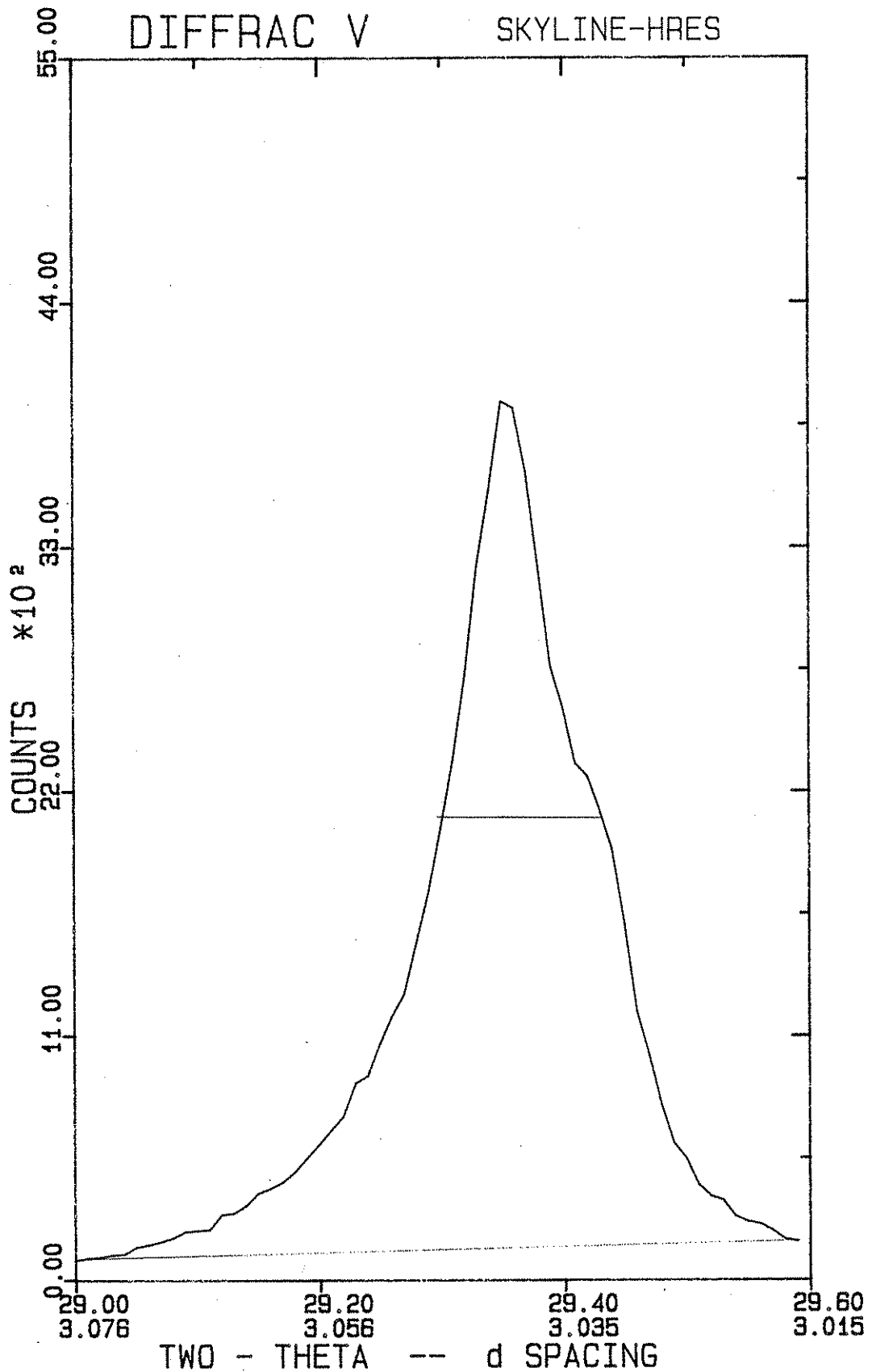


Figure 9, Appendix II. Crystallite size study for Skyline aggregate.

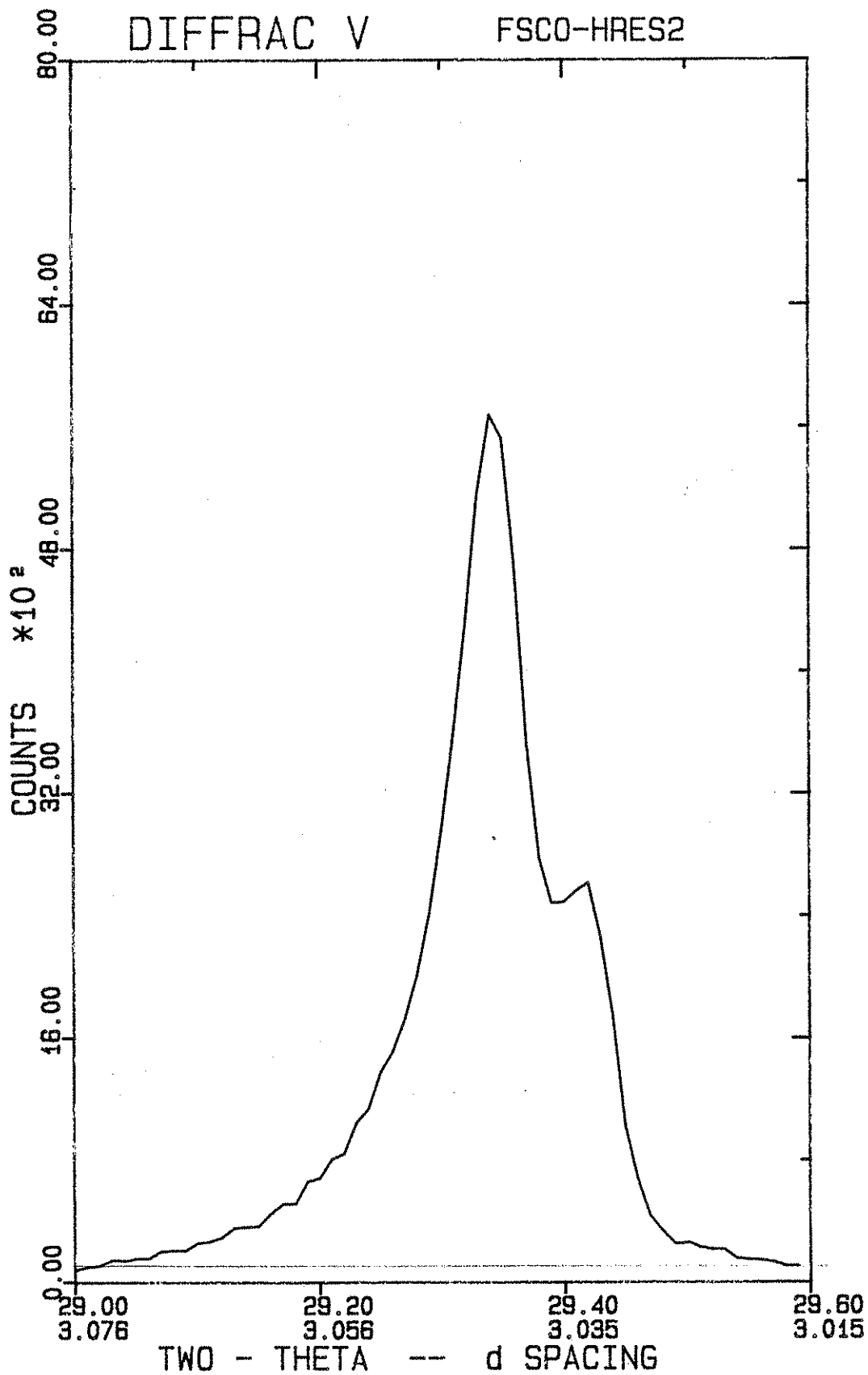


Figure 11, Appendix II. Crystallite size study for Fisher Calcite.

APPENDIX III

Sample: HR-337 ALDEN
Size: 55.5980 mg
Method: 40 deg/min, Res 5, Eq1 100
Comment: CO2 purge, 100 ml/min, sensit=1, deriv=1, Hi-Res TGA scan

TGA

File: C:\SCOTT\HR.011
Operator: J. AMENSON
Run Date: 26-Aug-91 09:01

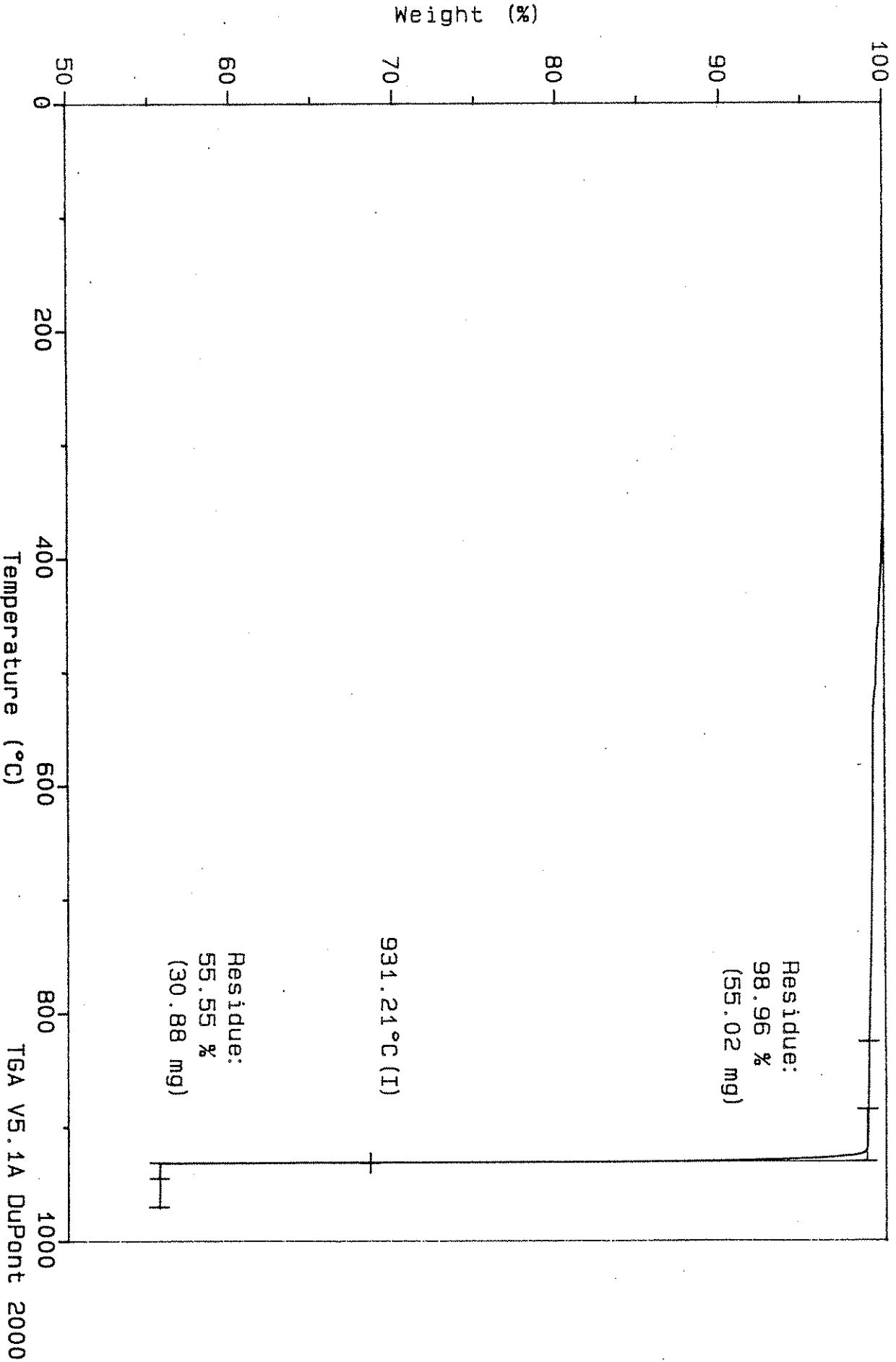


Figure 1, Appendix III. Thermal curve (CO2 atmosphere) for Alden aggregate.

Sample: HR-337 CRESCENT

Size: 55.6220 mg

Method: 40 deg/min, Res 5, Eq1 100

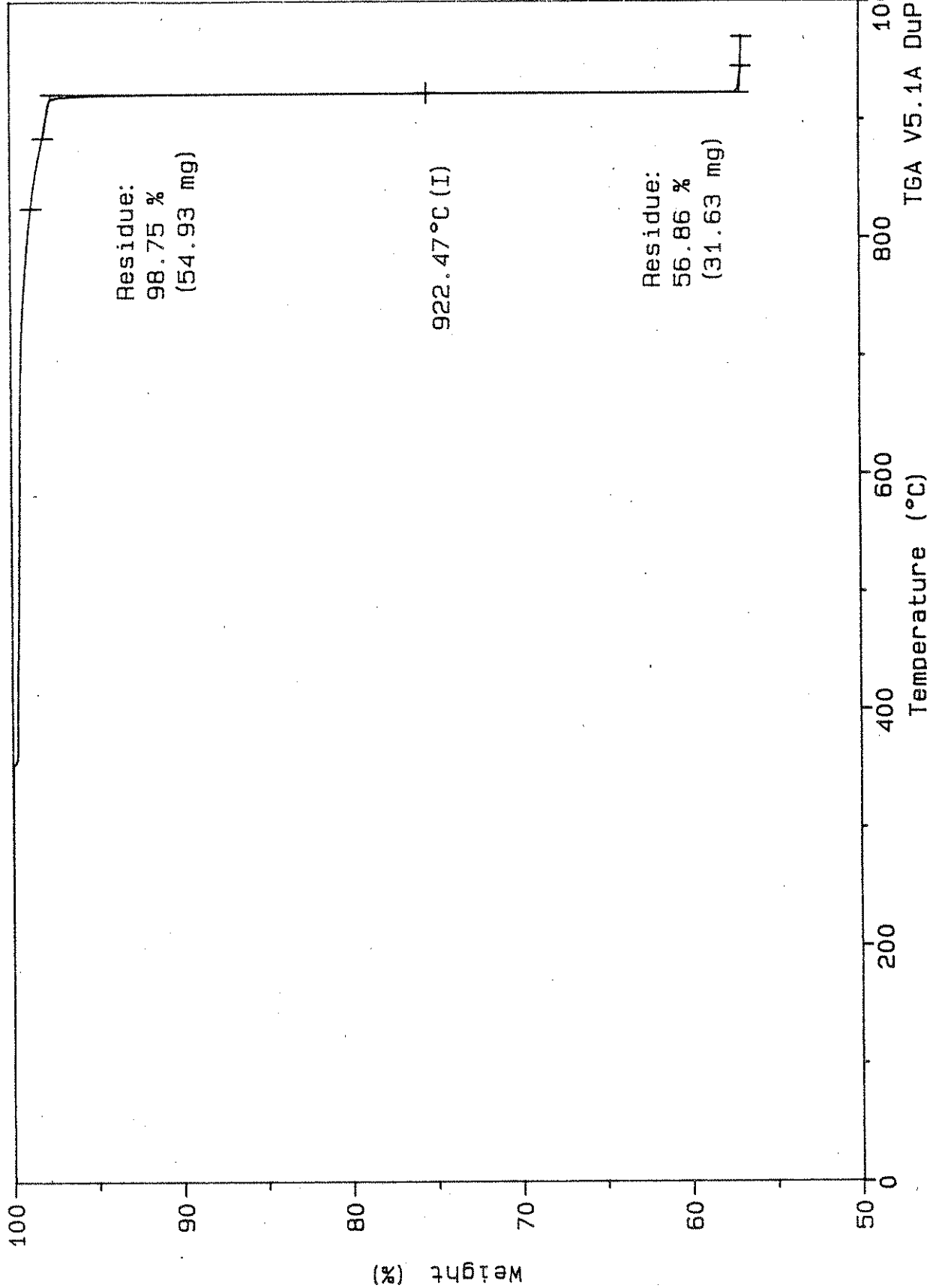
Comment: CO2 purge, 100 ml/min, sensit=1, deriv=1, Hi-Res TGA scan

TGA

File: C: SCOTTHR.002

Operator: J. AMENSON

Run Date: 23-Aug-91 11:30



TGA V5.1A DuPont 2000

Figure 2, Appendix III. Thermal curve (CO2 atmosphere) for Crescent aggregate.

Sample: HR-337 CONKLIN
Size: 55.4880 mg
Method: 40 deg/min, Res 5, Eq1 100
Comment: CO2 purge, 100 ml/min, sensit=1, deriv=1, Hi-Res TGA scan

TGA

File: C:SCOTTHR.007
Operator: J. AMENSON
Run Date: 24-Aug-91 16:10

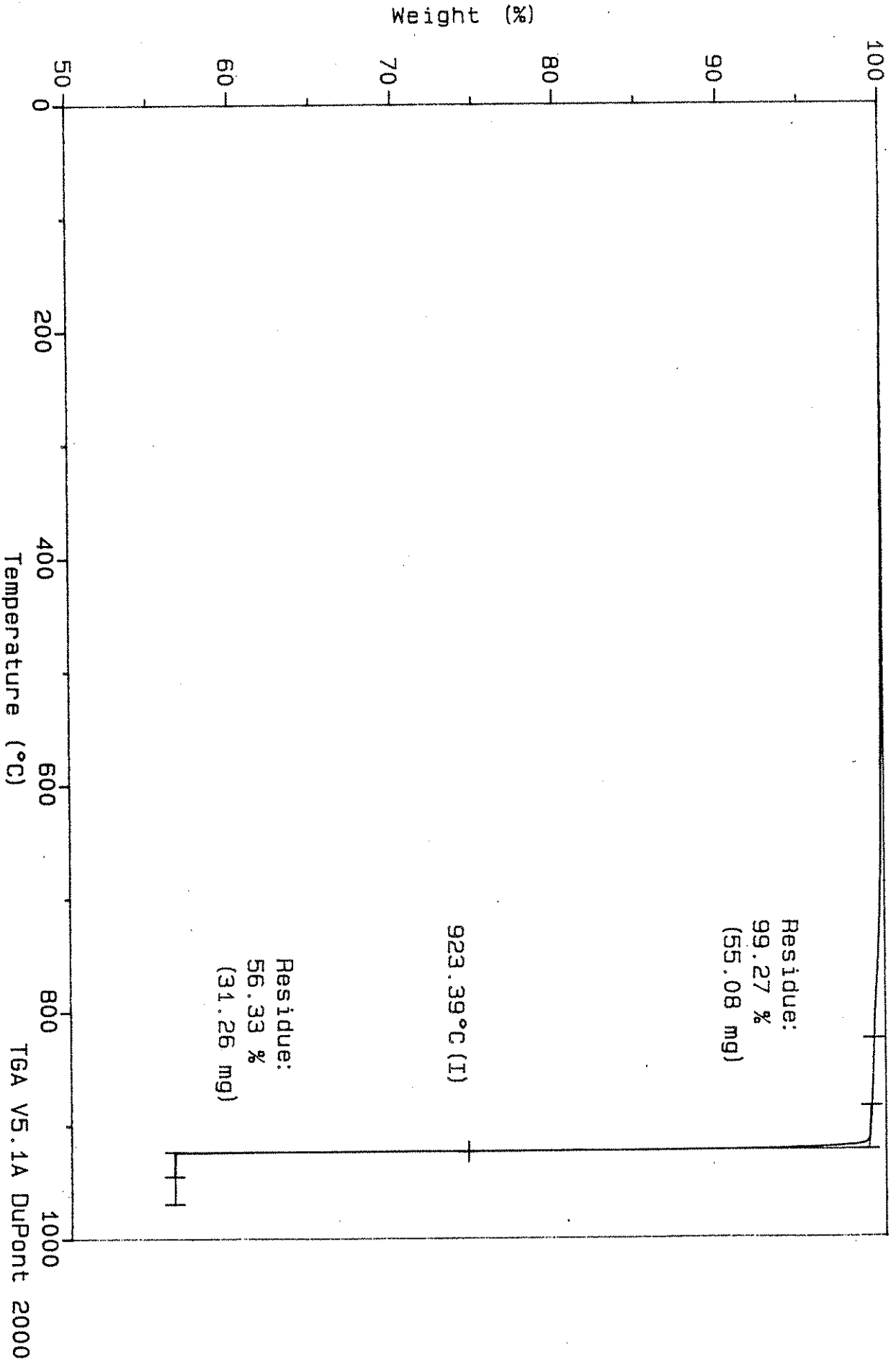


Figure 3, Appendix III. Thermal curve (CO2 atmosphere) for Conklin aggregate.

Sample: HR-337 EARLY CHAPEL
Size: 55.6030 mg
Method: 40 deg/min, Res 5, Eq1 100
Comment: CO2 purge, 100 ml/min, sensit=1, deriv=1, Hi-Res TGA scan

TGA

File: C: SCOTTHR.010
Operator: J. AMENSON
Run Date: 26-Aug-91 07:56

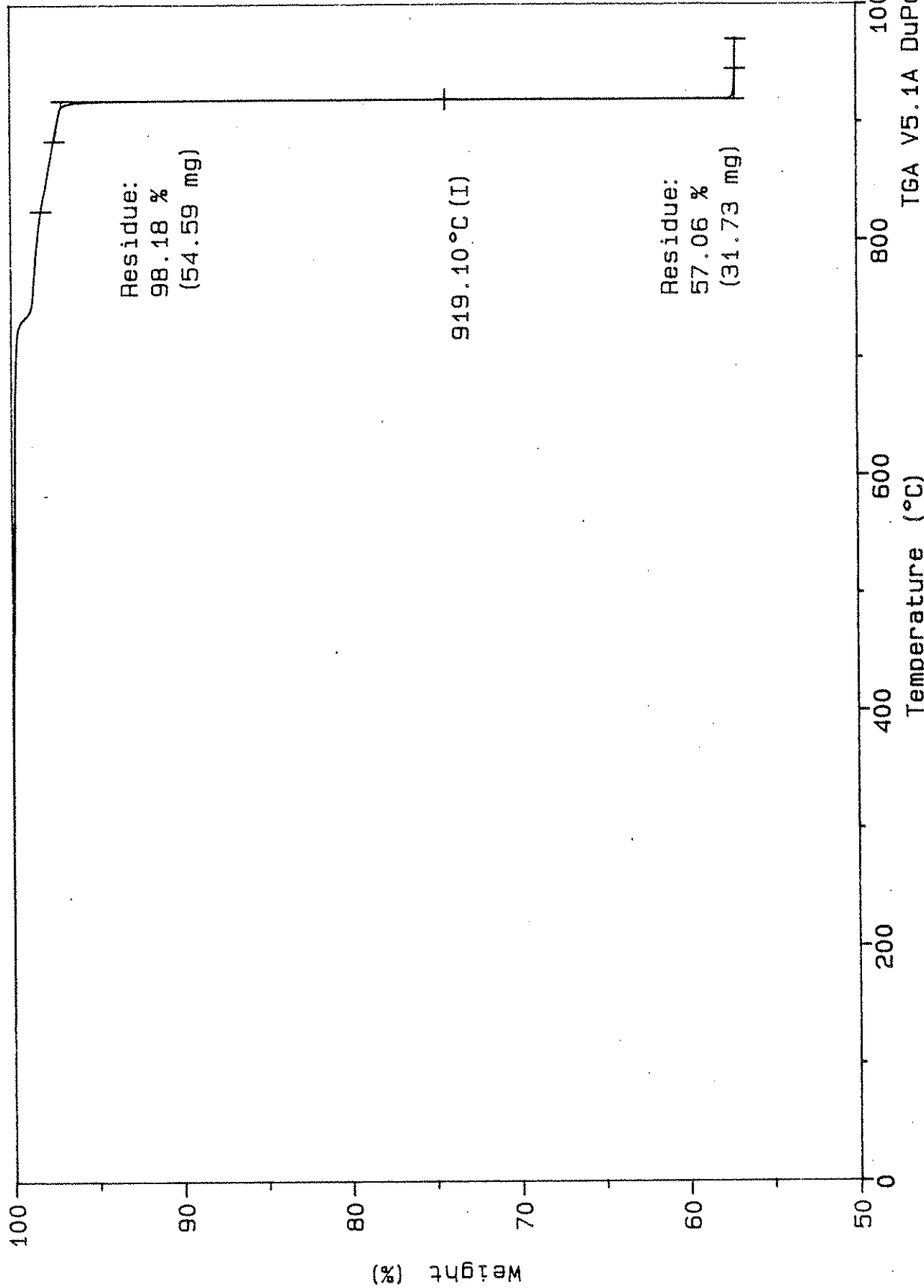


Figure 4, Appendix III. Thermal curve (CO2 atmosphere) for Early Chapel agg

Sample: HR-337 ELDORADO
Size: 55.6440 mg
Method: 40 deg/min, Res 5, Eq1 100
Comment: CO2 purge, 100 ml/min, sensit=1, deriv=1, Hi-Res TGA scan

TGA

File: C:SCOTT\HR.008
Operator: J. AMENSON
Run Date: 24-Aug-91 17:09

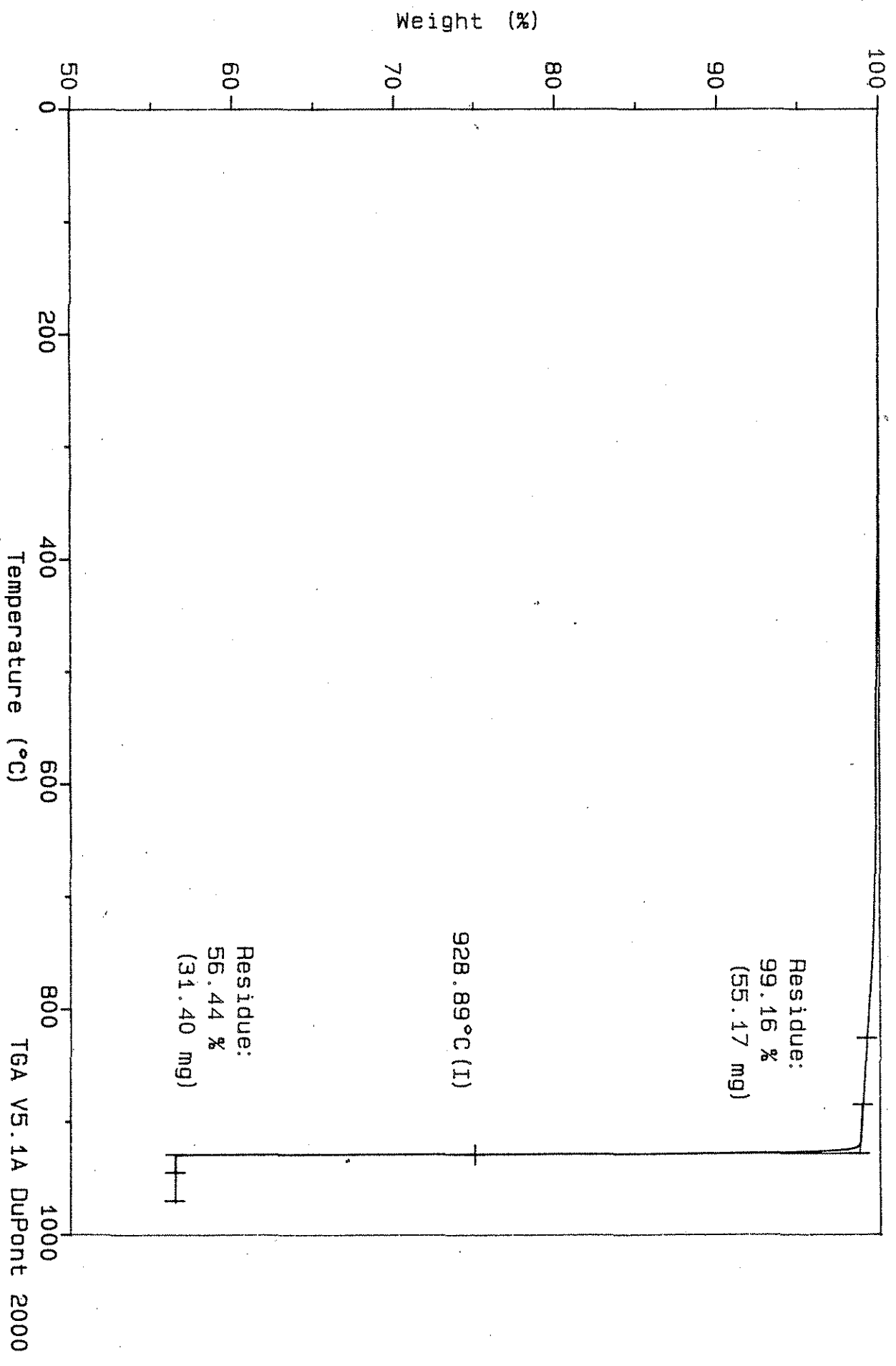


Figure 5, Appendix III. Thermal curve (CO2 atmosphere) for Eldorado aggregate. TGA V5.1A Dupont 2000

Sample: HR-337 LINWOOD
Size: 55.6240 mg
Method: 40 deg/min, Res 5, Eq1 100
Comment: CO2 purge, 100 ml/min, sensit=1, deriv=1, Hi-Res TGA scan

TGA

File: C: SCOTTHR.012
Operator: J. AMENSON
Run Date: 26-Aug-91 10:00

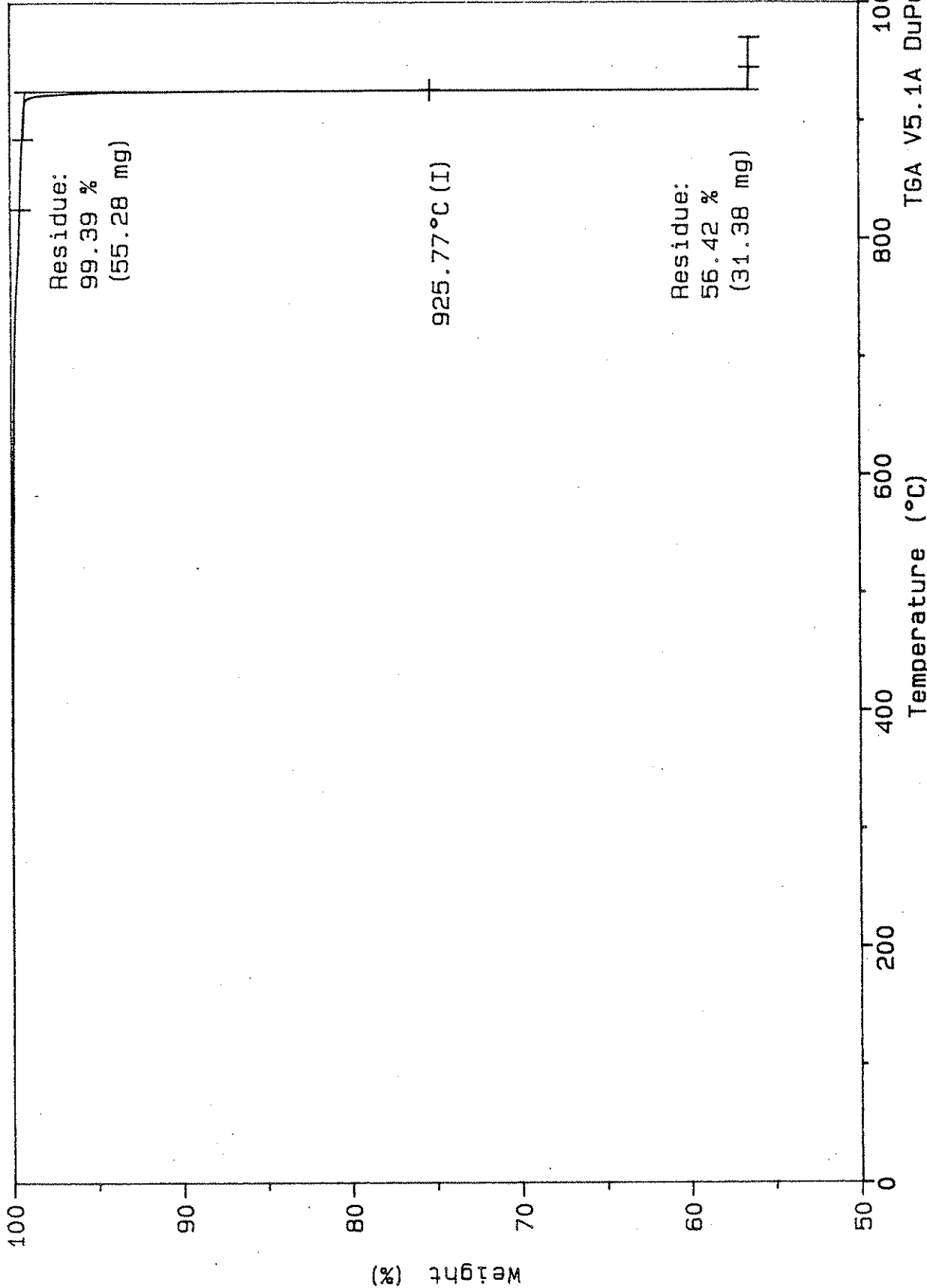


Figure 6, Appendix III. Thermal curve (CO2 atmosphere) for Linwood aggregate. TGA V5.1A DuPont 2000

Sample: HR-337 MENLO
Size: 55.6060 mg
Method: 40 deg/min, Res 5, Eq1 100
Comment: CO2 purge, 100 ml/min, sensit=1, deriv=1, Hi-Res TGA scan

TGA

File: C:SCOTT\HR.003
Operator: J. AMENSON
Run Date: 23-Aug-91 12:36

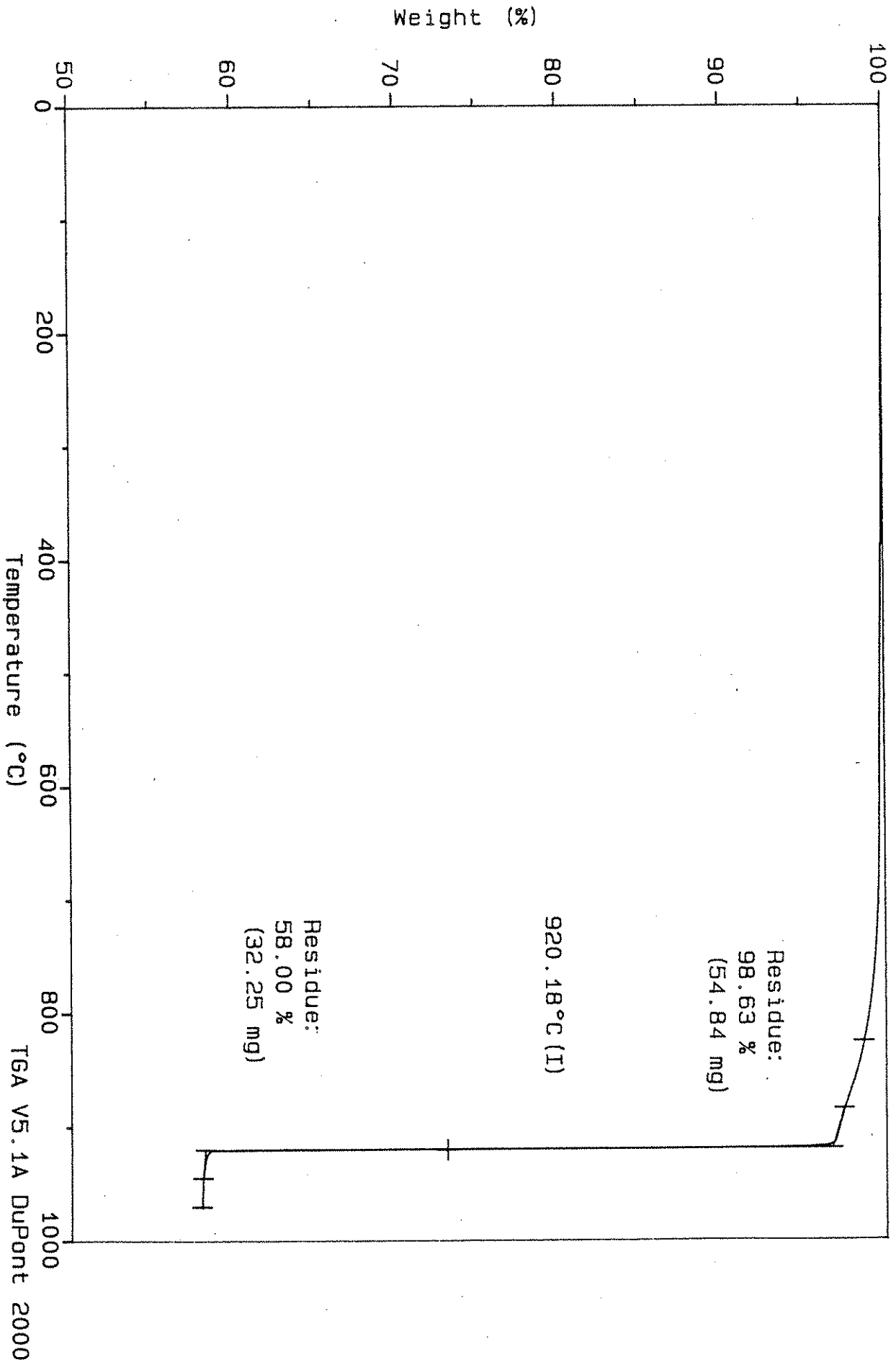


Figure 7, Appendix III. Thermal curve (CO2 atmosphere) for Menlo aggregate.

Sample: HR-337 MONTOUR
Size: 55.8680 mg
Method: 40 deg/min, Res 5, Eq1 100
Comment: CO2 purge, 100 ml/min, sensit=1, deriv=1, Hi-Res TGA scan

TGA

File: C:SCOTT\HR.006
Operator: J. AMENSON
Run Date: 24-Aug-91 15:11

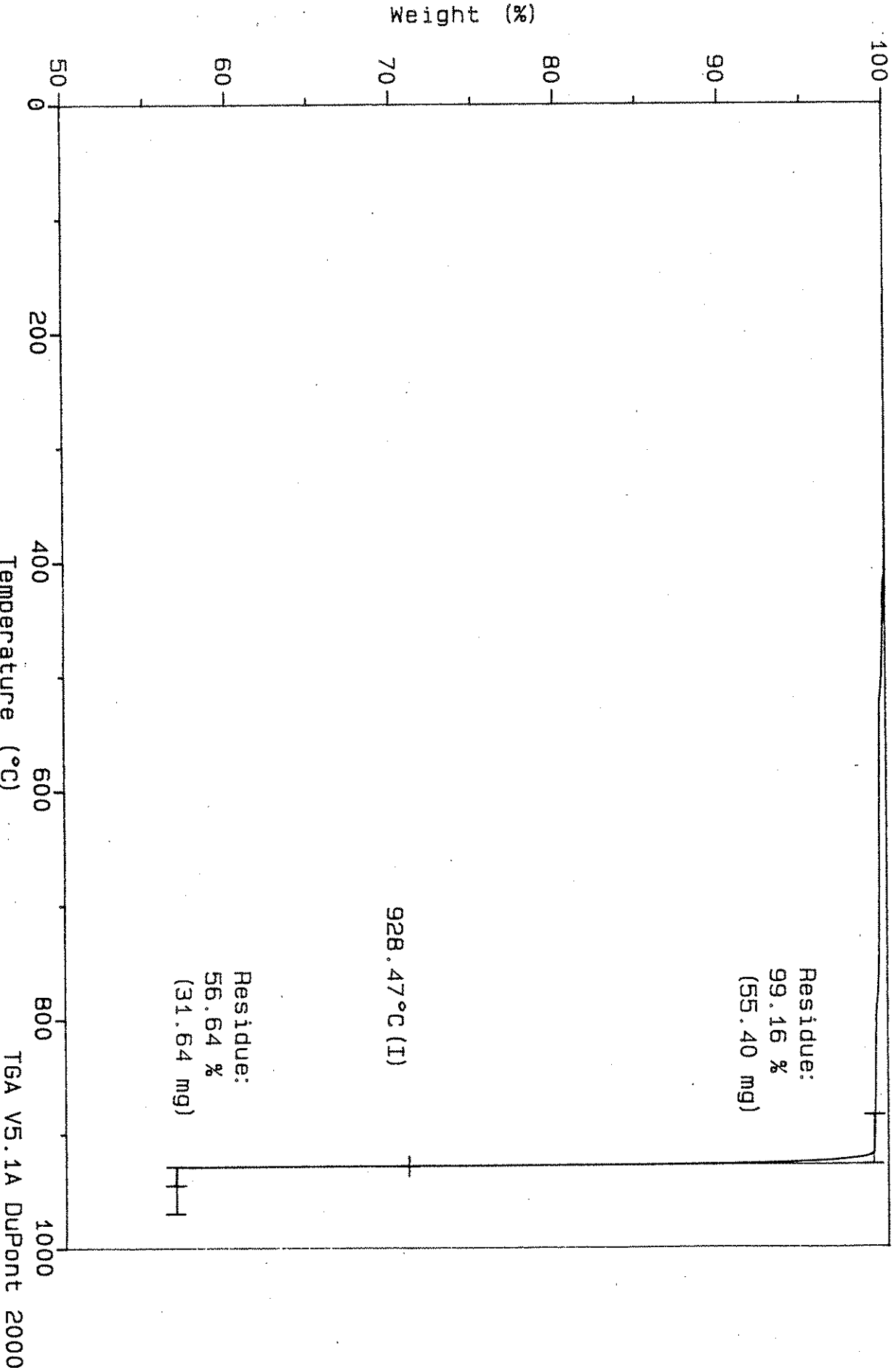


Figure 8, Appendix III. Thermal curve (CO2 atmosphere) for Montour aggregate.

TGA V5.1A DuPont 2000

Sample: HR-337 SKYLINE
Size: 55.6290 mg
Method: 40 deg/min, Res 5, Eq1 100
Comment: CO2 purge, 100 ml/min, sensit=1, deriv=1, Hi-Res TGA scan

TGA

File: C:SCOTTHR.013
Operator: J. AMENSON
Run Date: 26-Aug-91 10:55

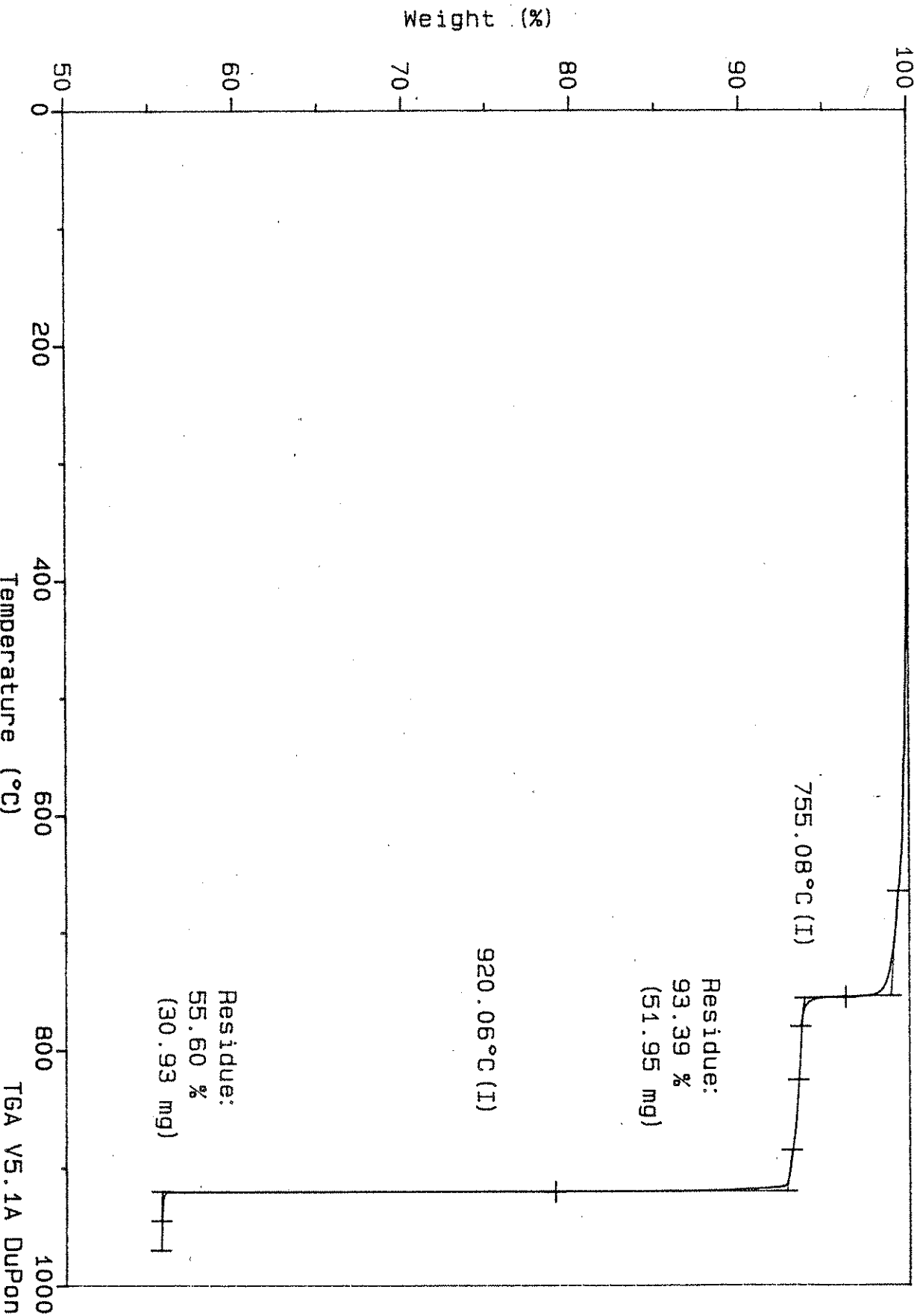


Figure 9, Appendix III.

Thermal curve (CO2 atmosphere) for Skyline aggregate.

Sample: HR-337 HUNTINGTON
Size: 55.4900 mg
Method: 40 deg/min, Res 5, Eq1 300
Comment: CO2 purge, 100 ml/min, sensit=1, deriv=1, Hi-Res TGA scan

TGA

File: C:SCOTT\HR.018
Operator: J. AMENSON
Run Date: 27-Sep-91 10:29

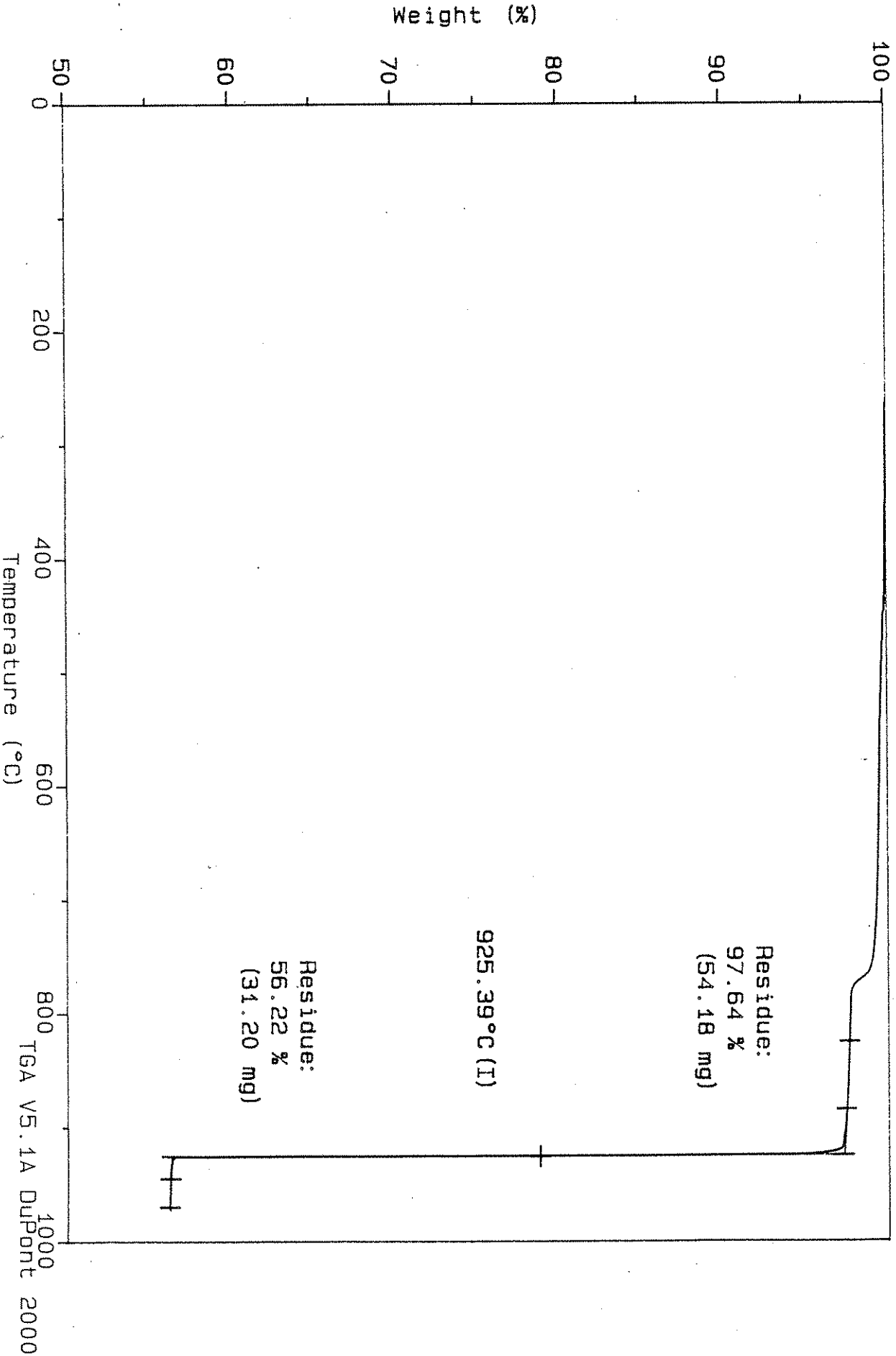


Figure 10, Appendix III. Thermal curve (CO2 atmosphere) for Huntington aq.

Sample: HR-337 F5CO CALCITE
Size: 55.5370 mg
Method: 40 deg/min, Res 5, Eq1 100
Comment: CO2 purge, 100 ml/min, sensit=1, deriv=1, Hi-Res TGA scan

TGA

File: C:SCOTTHR.024
Operator: J. AMENSON
Run Date: 22-Nov-91 09:34

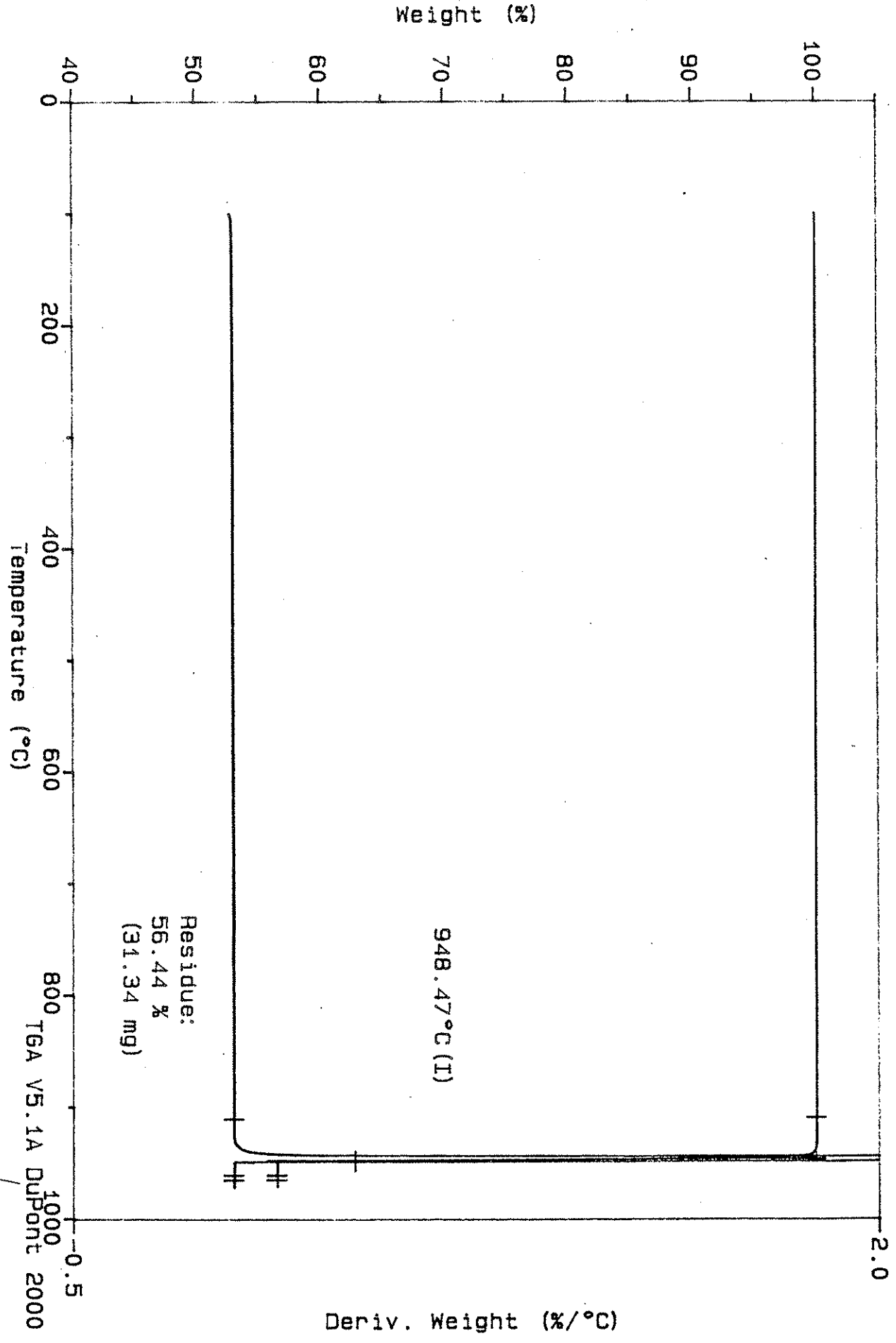


Figure 11, Appendix III. Thermal curve (CO2 atmosphere) for Fisher Calcite.

Sample: HR-337 WARDS CALCITE (GROUND)
Size: 55.5370 mg
Method: 40 deg/min, Res 5, Eq1 300
Comment: CO2 purge, 100 ml/min, sensit=1, deriv=1.

TGA

File: C:SCOTT\HR.036
Operator: J. AMENSON
Run Date: 4-Dec-91 11:46
HI-Res TGA scan

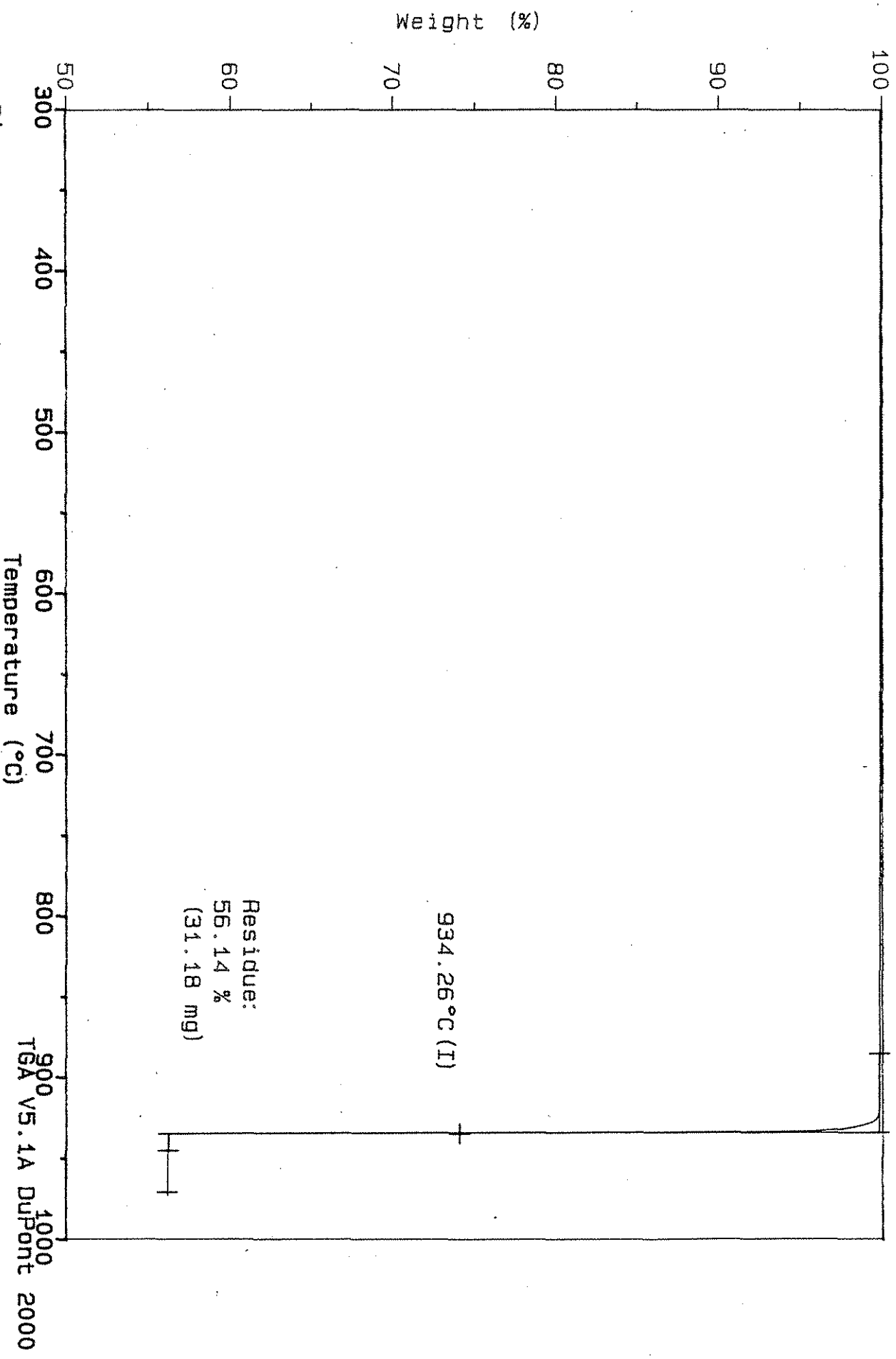


Figure 12, Appendix III. Thermal curve (CO2 atmosphere) for Ward's Calcite.

Sample: HR-337 MARYVILLE
Size: 55.4710 mg
Method: 40 deg/min, Res 5, Eq1 100
Comment: CO2 purge, 100 ml/min, sensit=1, deriv=1, Hi-Res TGA scan

TGA

File: C:SCOTTHR.004
Operator: J. AMENSON
Run Date: 23-Aug-91 13:40

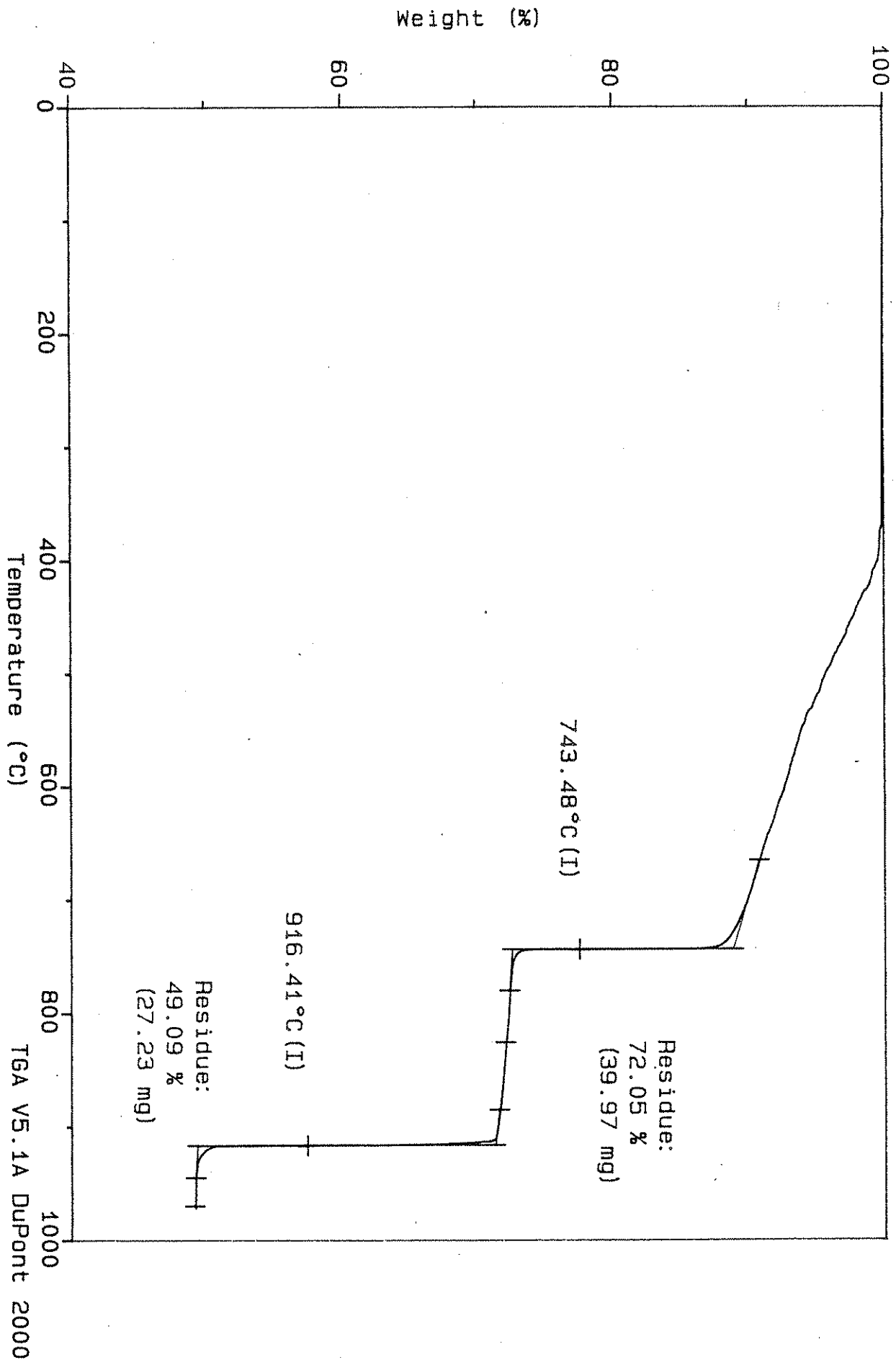
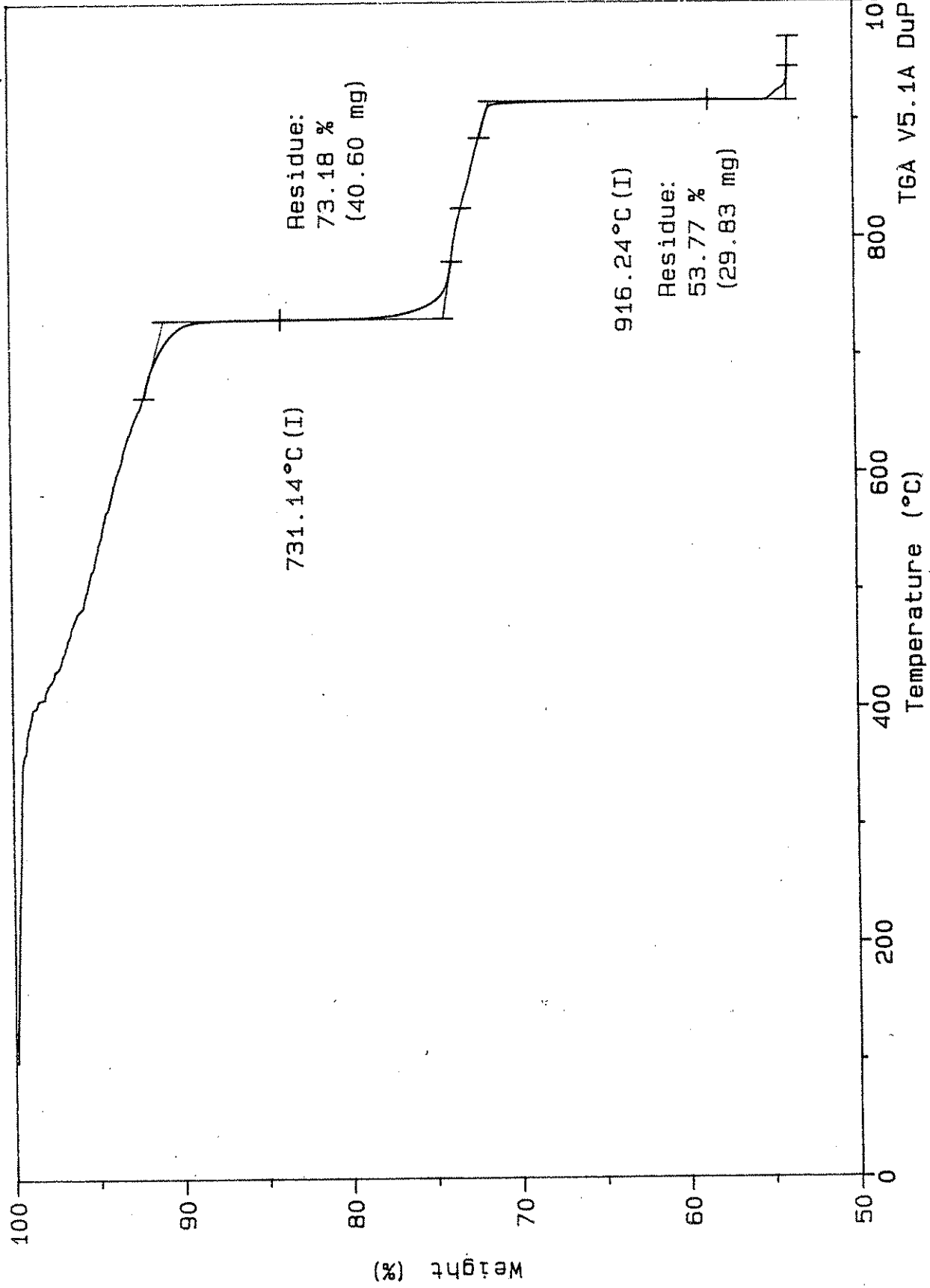


Figure 13, Appendix III. Thermal curve (CO2 atmosphere) for Maryville aggregate

Sample: HR-337 BRYAN
Size: 55.4810 mg
Method: 40 deg/min, Res 5, Eq1 100
Comment: CO2 purge, 100 ml/min, sensit=1, deriv=1, Hi-Res TGA scan

TGA

File: C: SCOTTHR.009
Operator: J. AMENSON
Run Date: 24-Aug-91 18:08



TGA V5.1A DuPont 2000

Figure 14, Appendix III. Thermal curve (CO2 atmosphere) for Bryan aggregate.

Sample: HR-337 CEDAR RAPIDS
Size: 55.4540 mg
Method: 40 deg/min, Res 5, Eq1 100
Comment: CO2 purge, 100 ml/min, sensit=1, deriv=1, Hi-Res TGA scan

TGA

File: C:SCOTT\HR.005
Operator: J. AMENSON
Run Date: 23-Aug-91 15:21

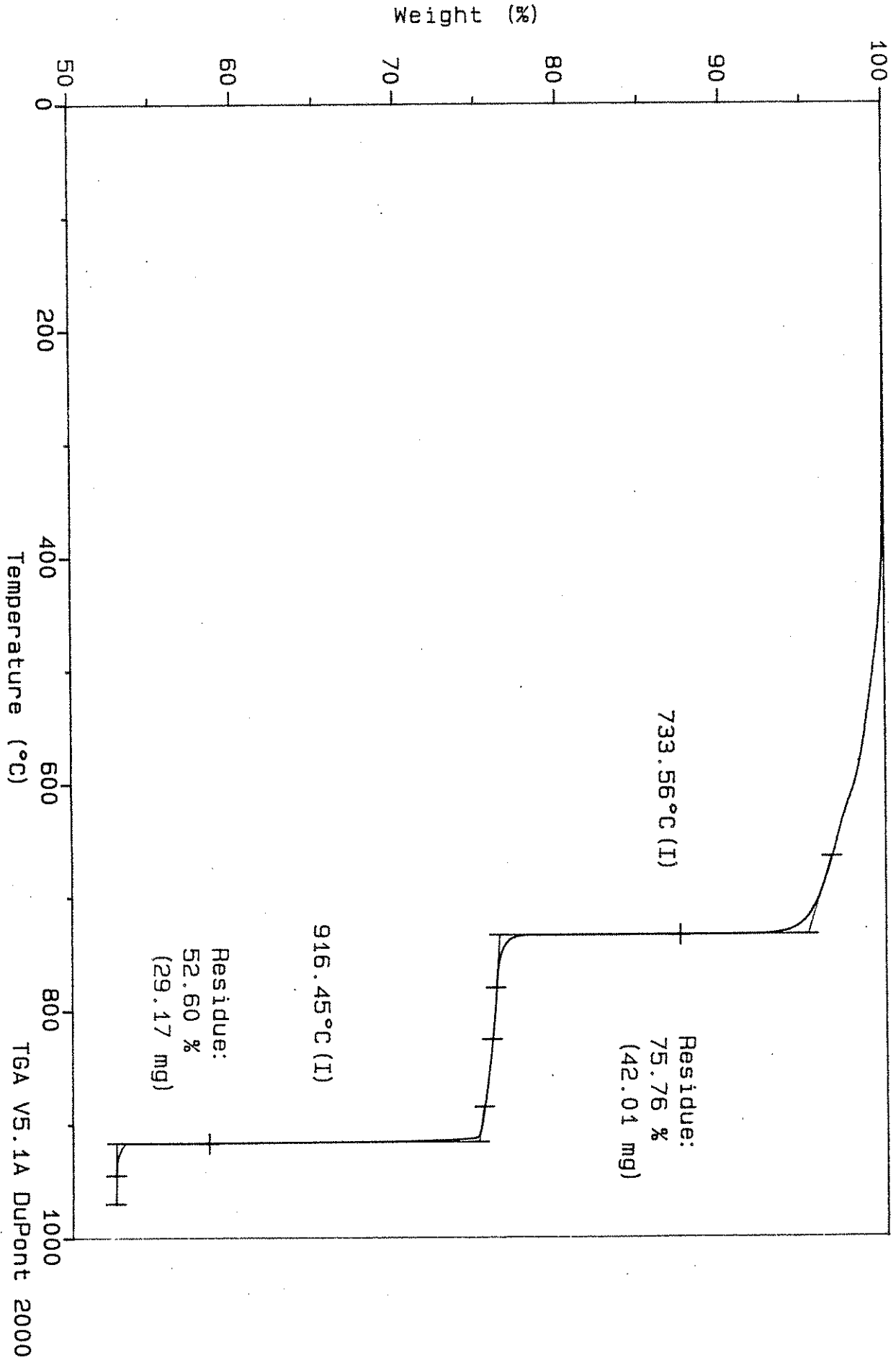


Figure 15, Appendix III. Thermal curve (CO2 atmosphere) for Ced. Rap. Gray aggr

Sample: HR-337 TAN-SOUTH CEDAR RAPIDS

Size: 55.5050 mg

Method: 40 deg/min, Res 5, Eq1 300

Comment: CO2 purge, 100 ml/min, sensit=1, deriv=1, Hi-Res TGA scan

TGA

File: C: SCOTTHR.019

Operator: J. AMENSON

Run Date: 27-Sep-91 13:27

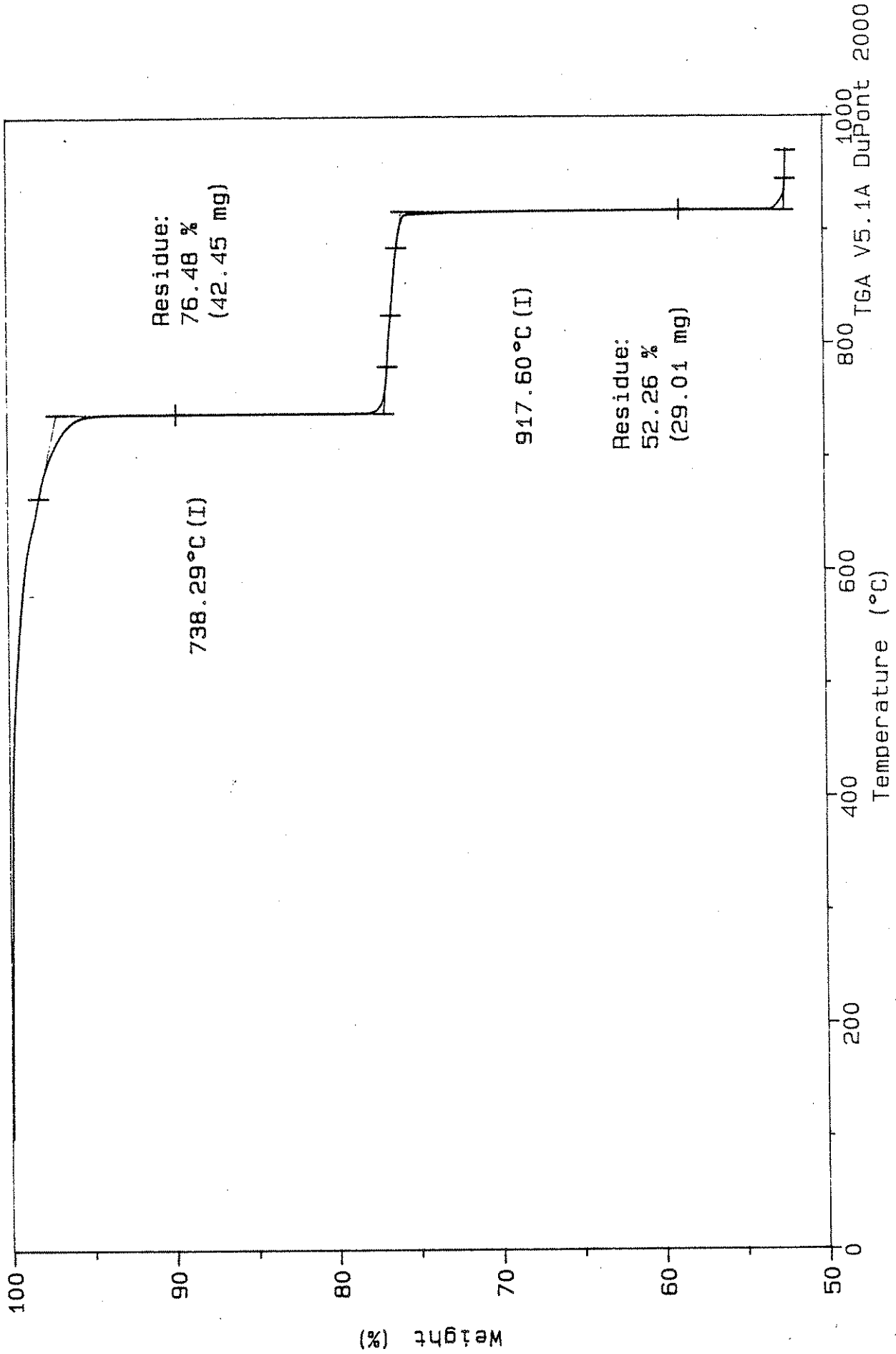


Figure 16, Appendix III. Thermal curve (CO2 atmosphere) for Ced. Rap. Tan aggr

Sample: HR-337 GARRISON
Size: 55.5250 mg
Method: 40 deg/min, Res 5, Eq1 100
Comment: CO2 purge, 100 ml/min, sensit=1, deriv=1, Hi-Res TGA scan

TGA

File: C:SCOTTHR.015
Operator: J. AMENSON
Run Date: 26-Aug-91 14:07

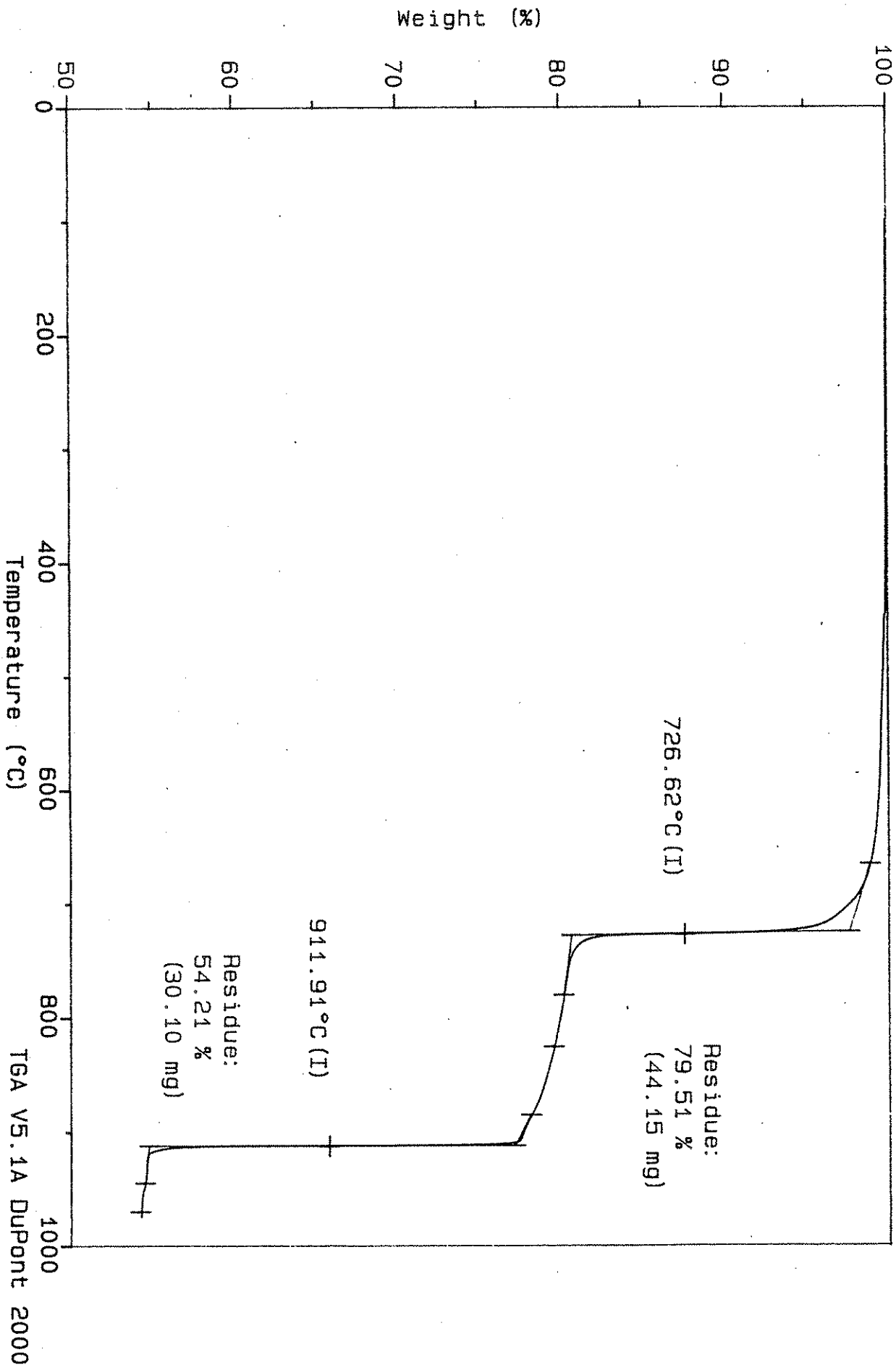


Figure 17, Appendix III. Thermal curve (CO2 atmosphere) for Garrison aggregate.

Sample: HR-337 GASSMAN

Size: 55.4990 mg

Method: 40 deg/min, Res 5, Eq1 300

Comment: CO2 purge, 100 ml/min, sensit=1, deriv=1, Hi-Res TGA scan

TGA

File: C:SCOTTHR.017

Operator: J. AMENSON

Run Date: 27-Sep-91 07:39

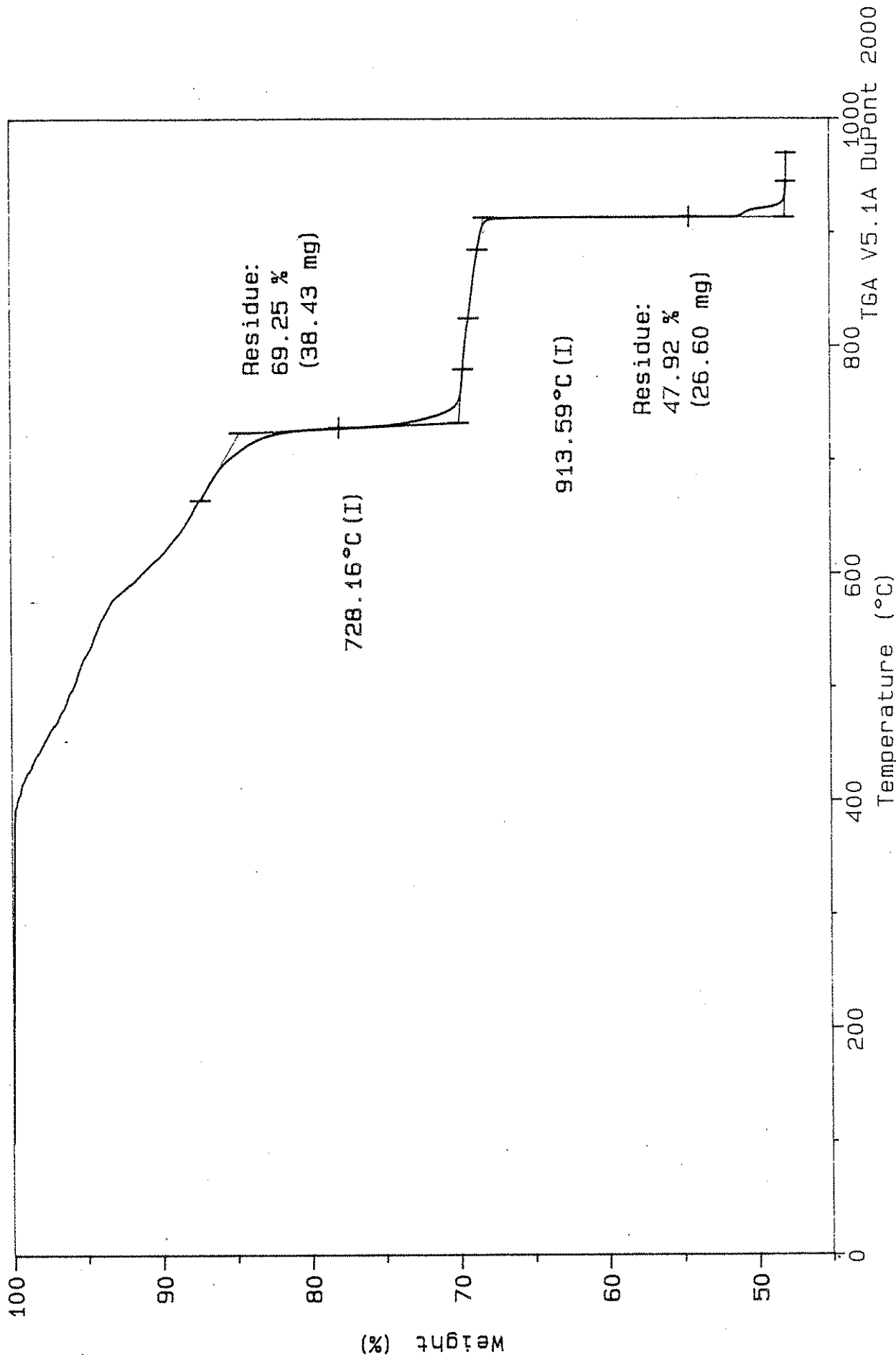


Figure 18, Appendix III. Thermal curve (CO2 atmosphere) for Gassman aggregate.

Sample: HR-337 LAMONT
Size: 55.6850 mg
Method: 40 deg/min, Res 5, Eq1 100
Comment: CO2 purge, 100 ml/min, sensit=1, deriv=1, Hi-Res TGA scan

TGA

File: C:SCOTTHR.014
Operator: J. AMENSON
Run Date: 26-Aug-91 12:21

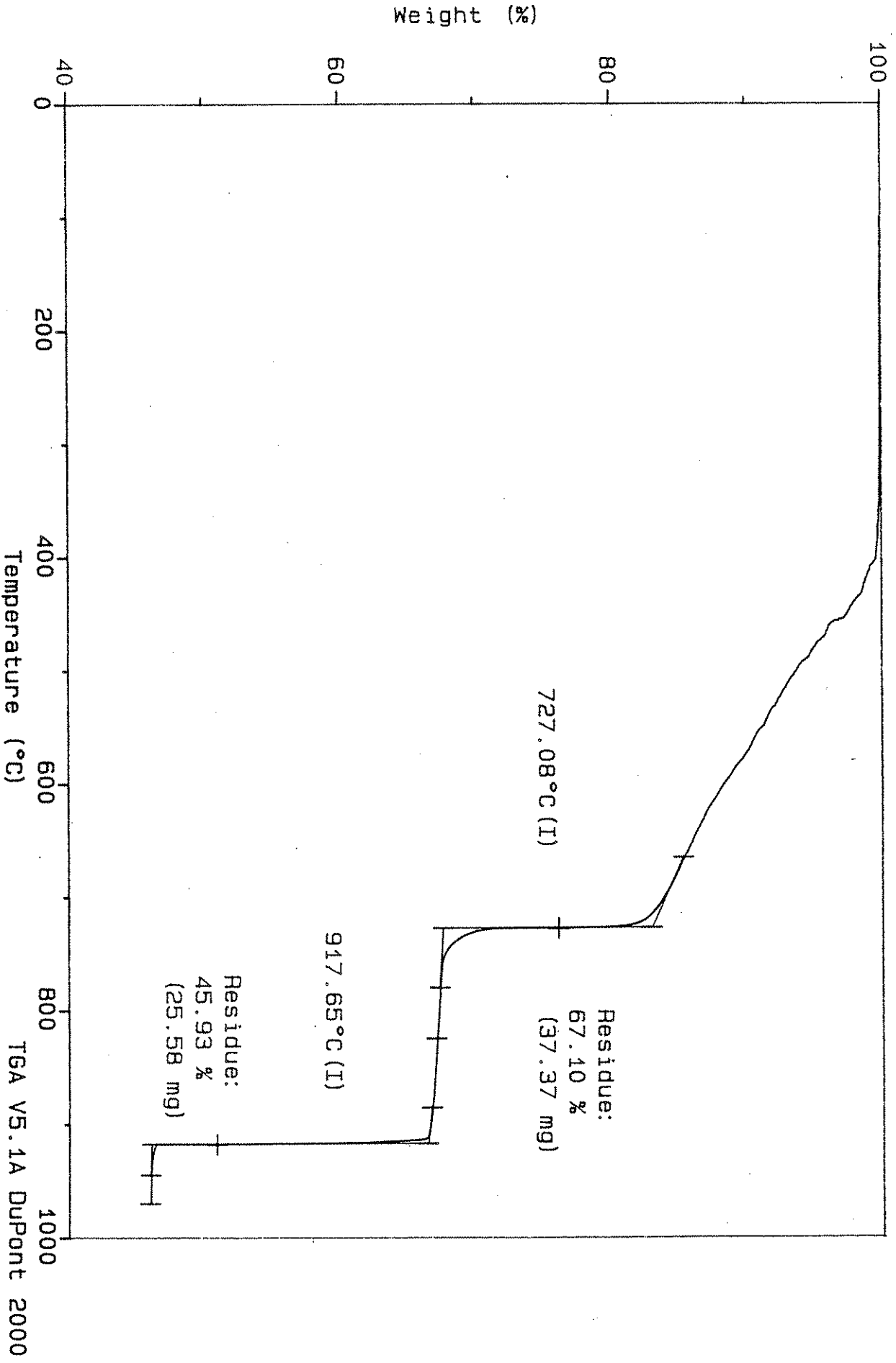


Figure 19, Appendix III. Thermal curve (CO2 atmosphere) for Lamont aggregate. TGA V5.1A DuPont 2000

Sample: HR-337 LE CLAIRE

Size: 55.4920 mg

Method: 40 deg/min, Res 5, Eq1 300

Comment: CO2 purge, 100 ml/min, sensit=1, deriv=1, Hi-Res TGA scan

TGA

File: C:SCOTTHR.020

Operator: J. AMENSON

Run Date: 27-Sep-91 15:05

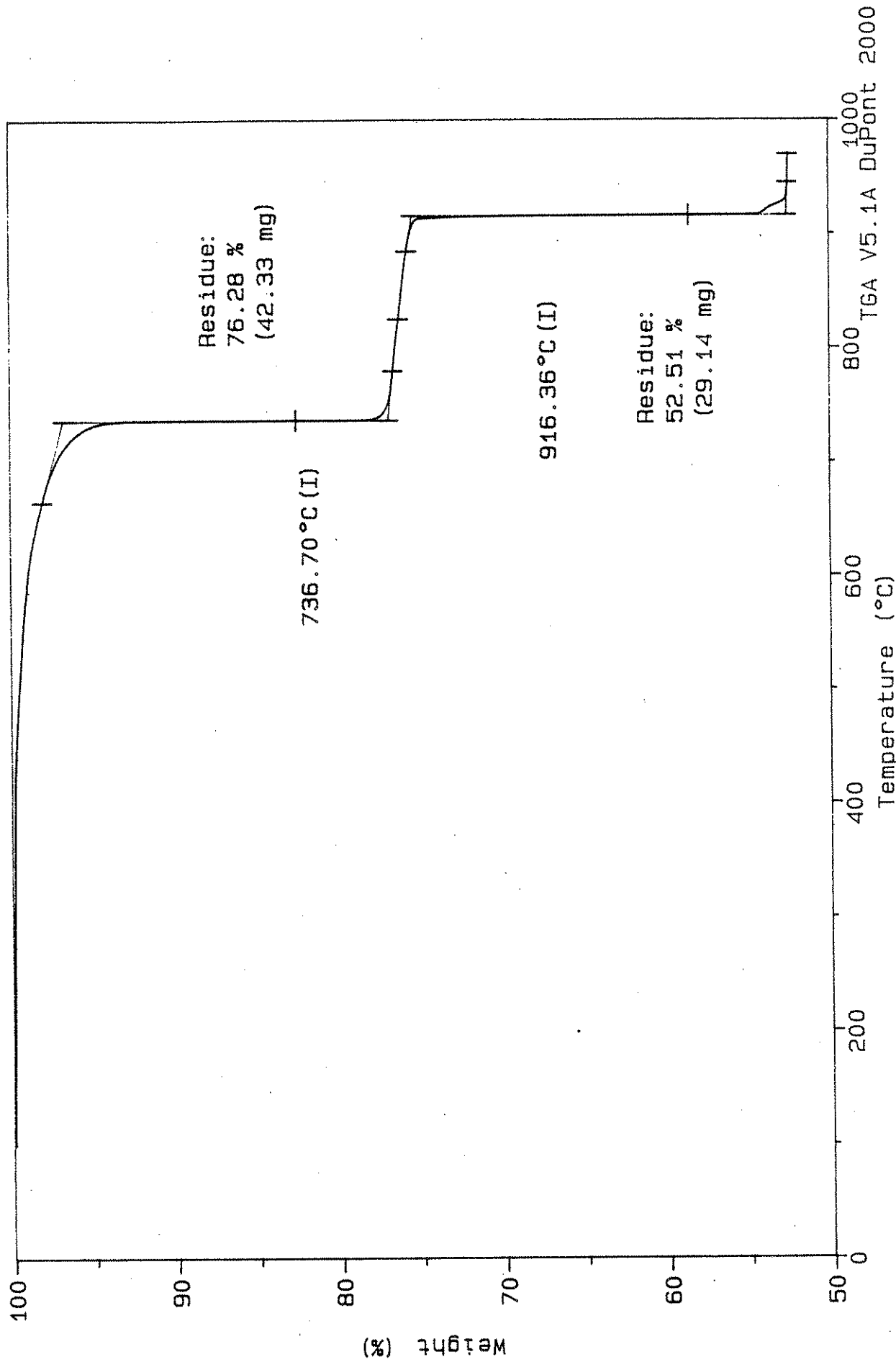


Figure 20, Appendix.III. Thermal curve (CO2 atmosphere) for LeClaire aggregate.

Sample: HR-337 PESKY
Size: 55.5450 mg
Method: 40 deg/min, Res 5, Eq1 100
Comment: CO2 purge, 100 ml/min, sensit=1, deriv=1, Hi-Res TGA scan

TGA

File: C:SCOTT\HR.016
Operator: J. AMENSON
Run Date: 26-Aug-91 15:42

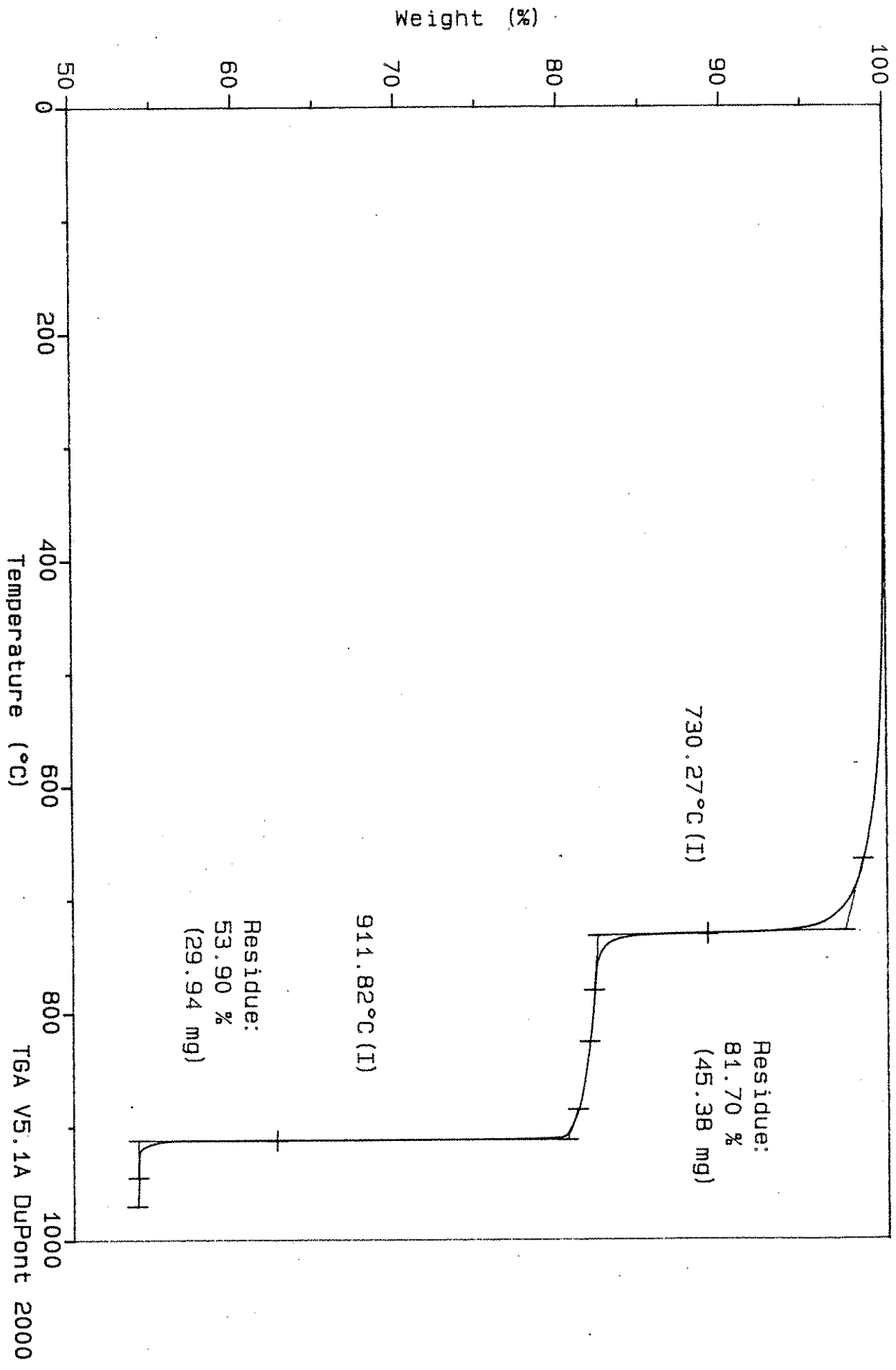


Figure 21, Appendix III. Thermal curve (CO2 atmosphere) for Pesky aggregate.

Sample: HR-337 PLOWER

Size: 55.5040 mg

Method: 40 deg/min, Res 5, Eq1 100

Comment: CO2 purge, 100 ml/min, sensit=1, deriv=1, Hi-Res TGA scan

TGA

File: C: SCOTTHR.001

Operator: J. AMENSON

Run Date: 23-AUG-91 09:40

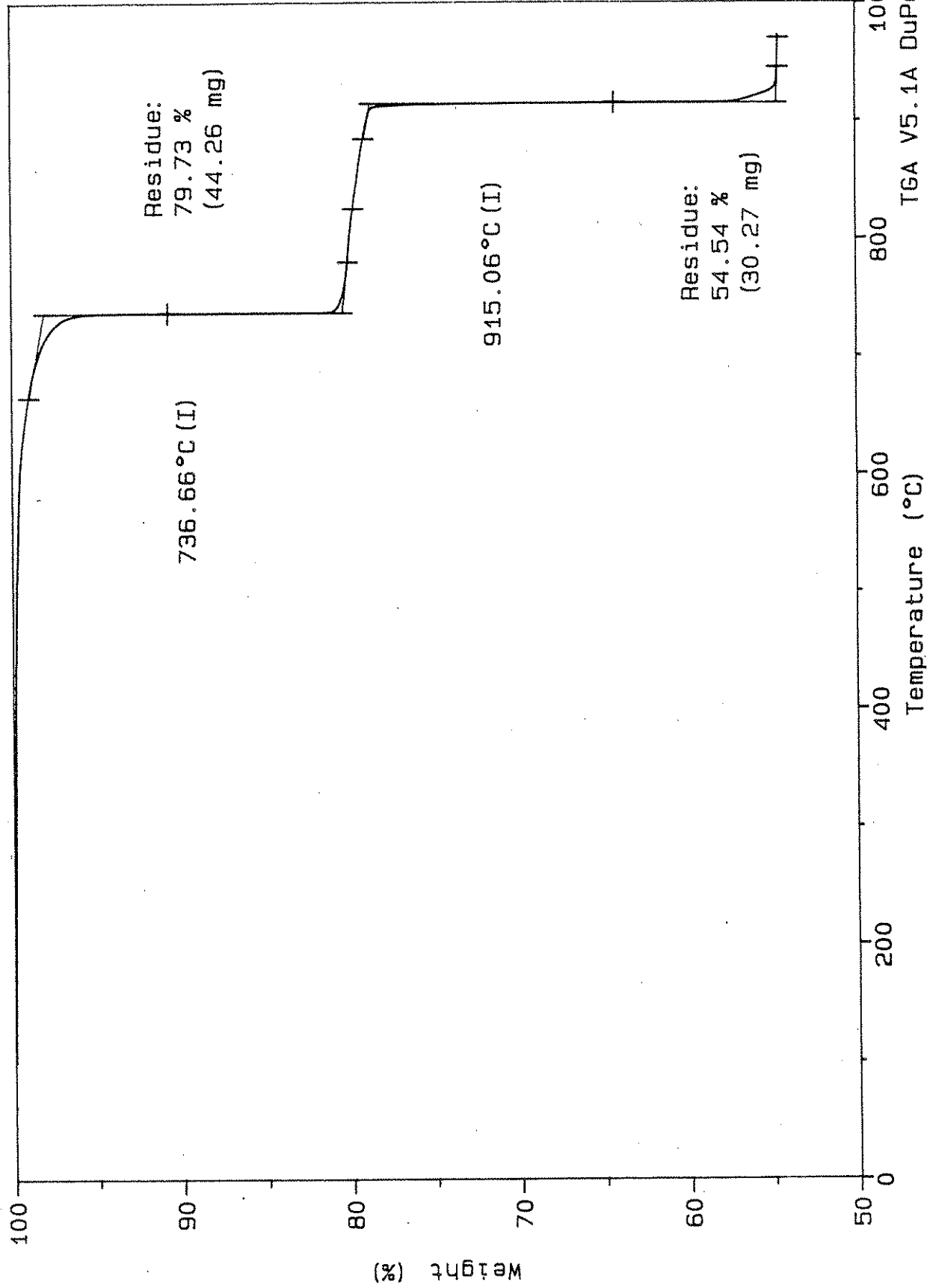


Figure 22, Appendix III. Thermal curve (CO2 atmosphere) for Plower aggregate.

Sample: HR-337 ALDEN (BED 3 TAN)
Size: 55.4980 mg
Method: 40°C/min, Res 5
Comment: N2 purge @ 100 ml/min

TGA

File: C:SCOTT.078
Operator: J. AMENSON
Run Date: 21-Feb-92 22:05

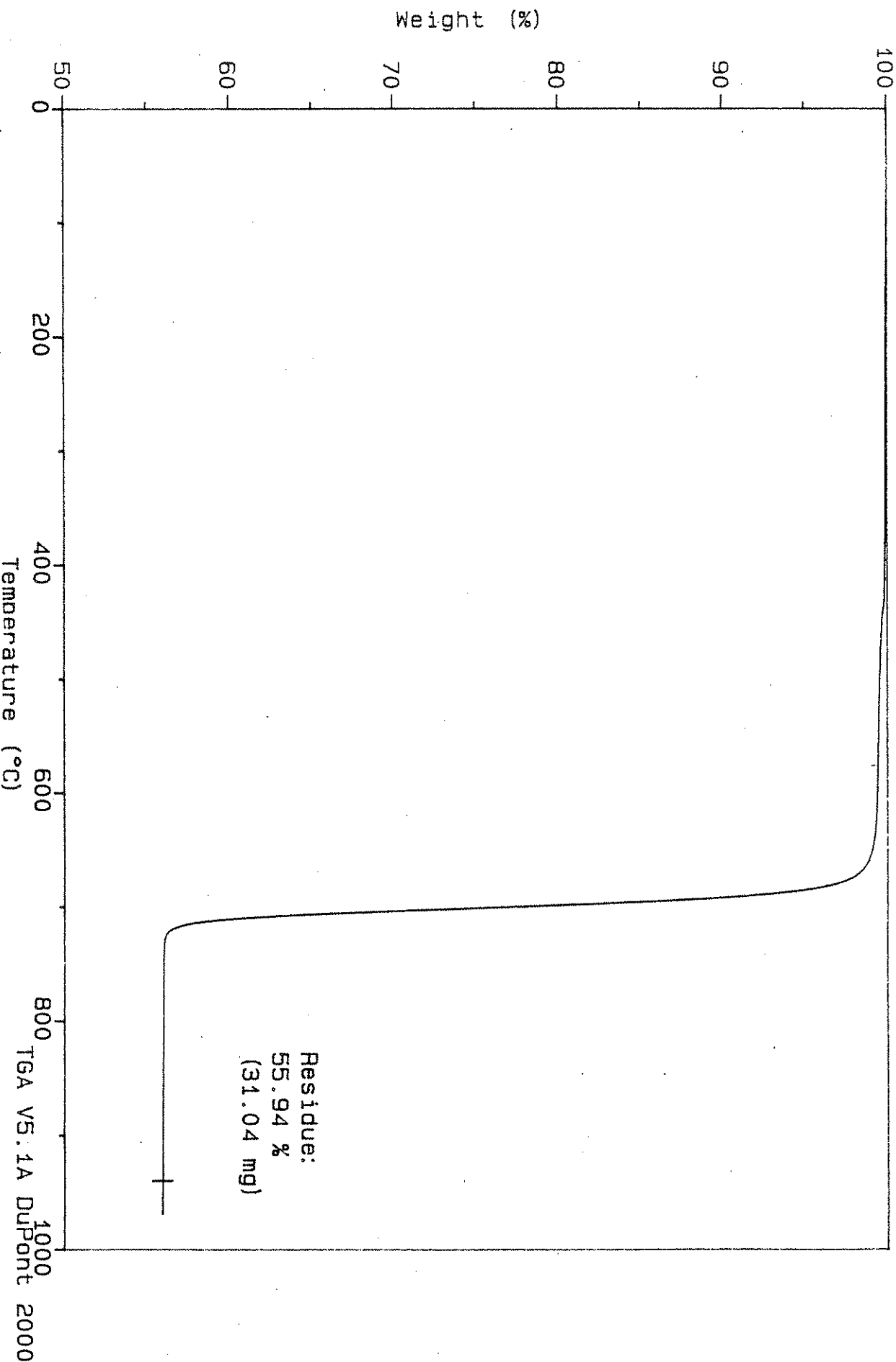


Figure 23, Appendix III. Thermal curve (N2 atmosphere) for Alden aggregate.

Sample: HR-337 CRESENT
Size: 55.6610 mg
Method: 40°C/min, Res 5
Comment: N2 purge @ 100 ml/min

TGA

File: C:SCOTT.088
Operator: J. AMENSON
Run Date: 22-Feb-92 15:10

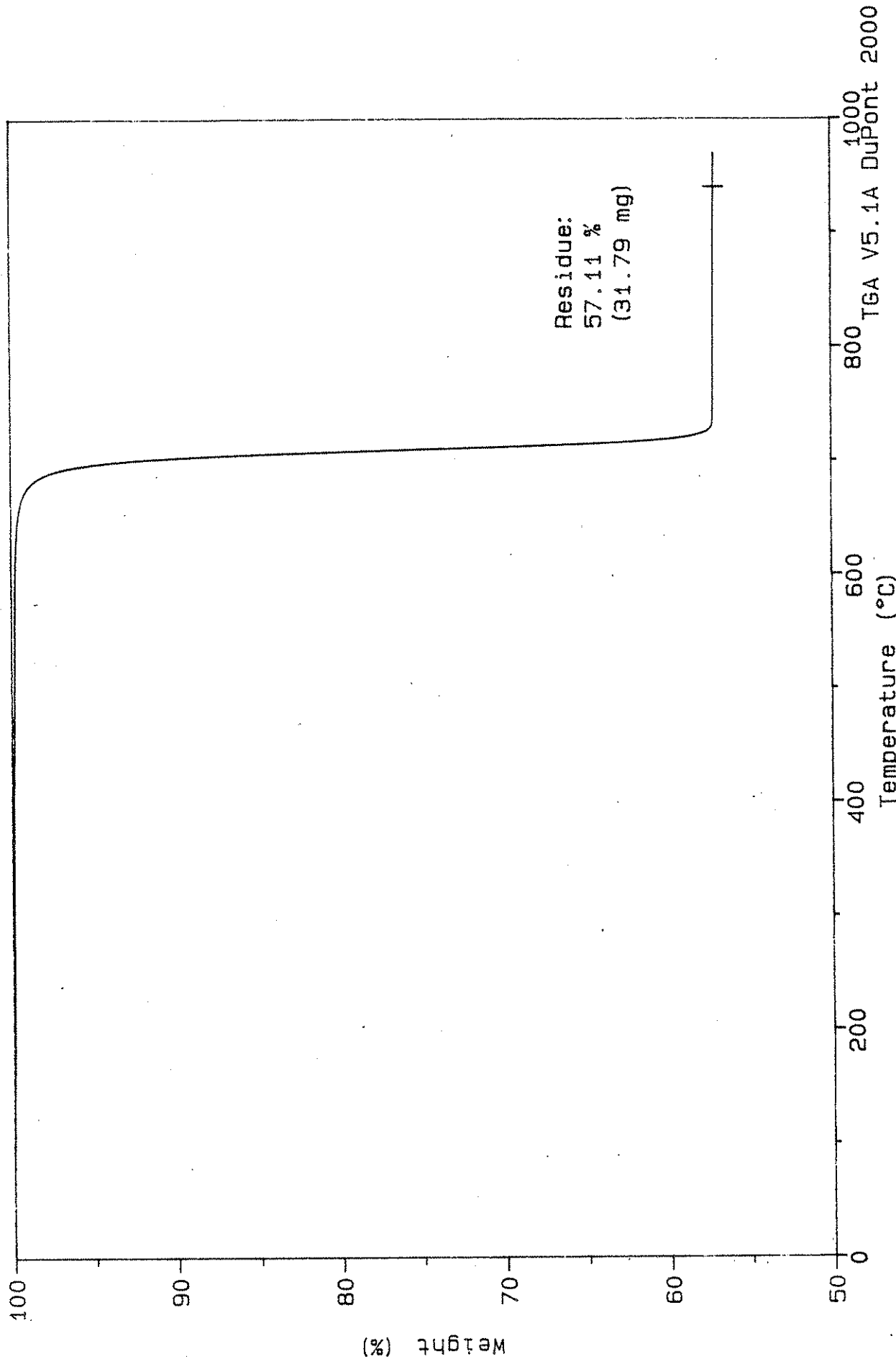


Figure 24, Appendix III. Thermal curve (N2 atmosphere) for Crescent aggregate.

Sample: HR-337 CONKLIN
Size: 55.5420 mg
Method: 40°C/min, Res 5
Comment: N2 purge @ 100 ml/min

TGA

File: C:SCOTT.080
Operator: J. AMENSON
Run Date: 22-Feb-92 01:23

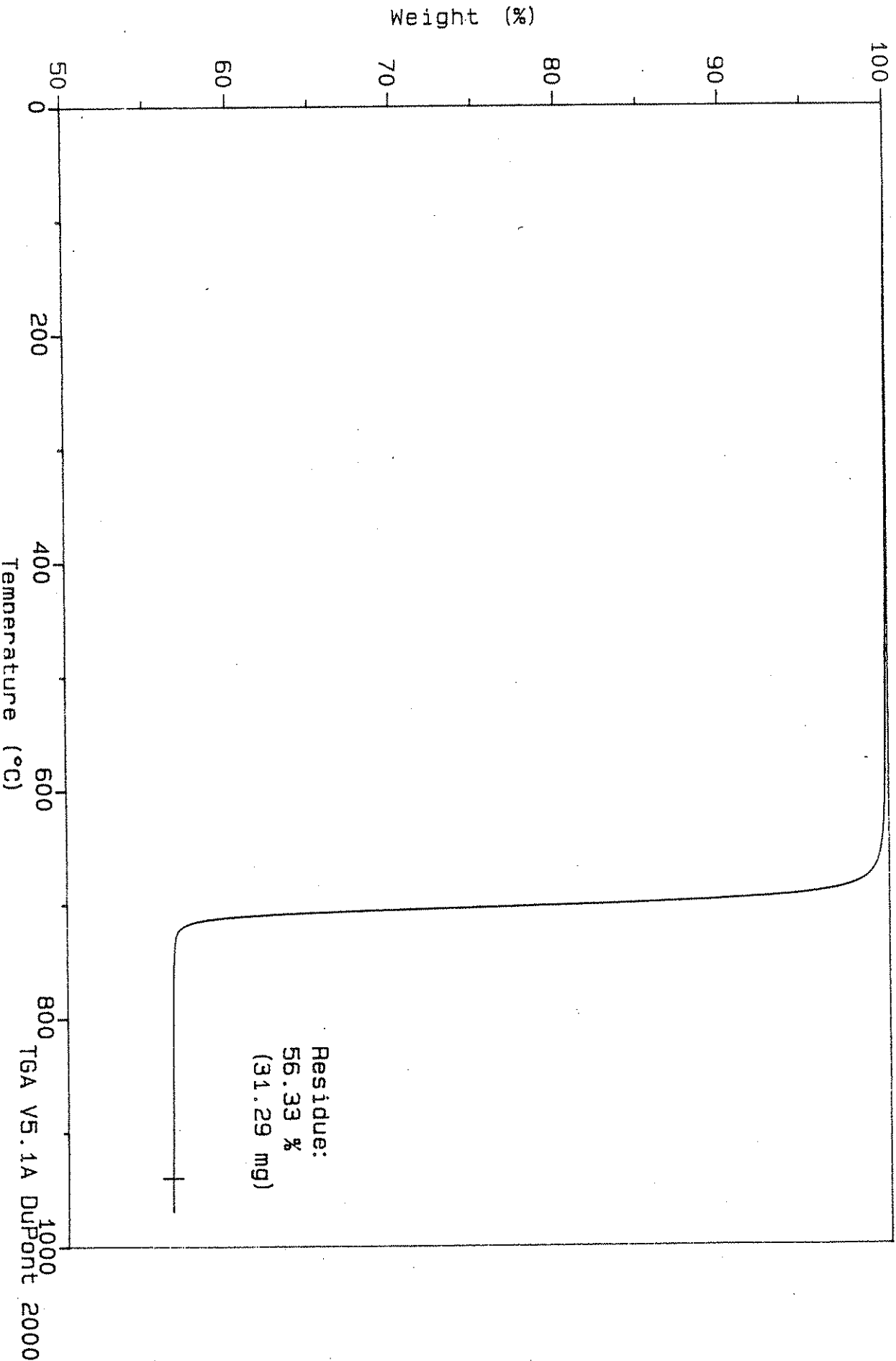


Figure 25, Appendix III. Thermal curve (N2 atmosphere) for Conklin aggregate.

Sample: HR-337 EARLY CHAPEL
Size: 55.5410 mg
Method: 40 °C/min. Res 5
Comment: N2 purge @ 100 ml/min

TGA

File: C:SCOTT.082
Operator: J. AMENSON
Run Date: 22-Feb-92 04:39

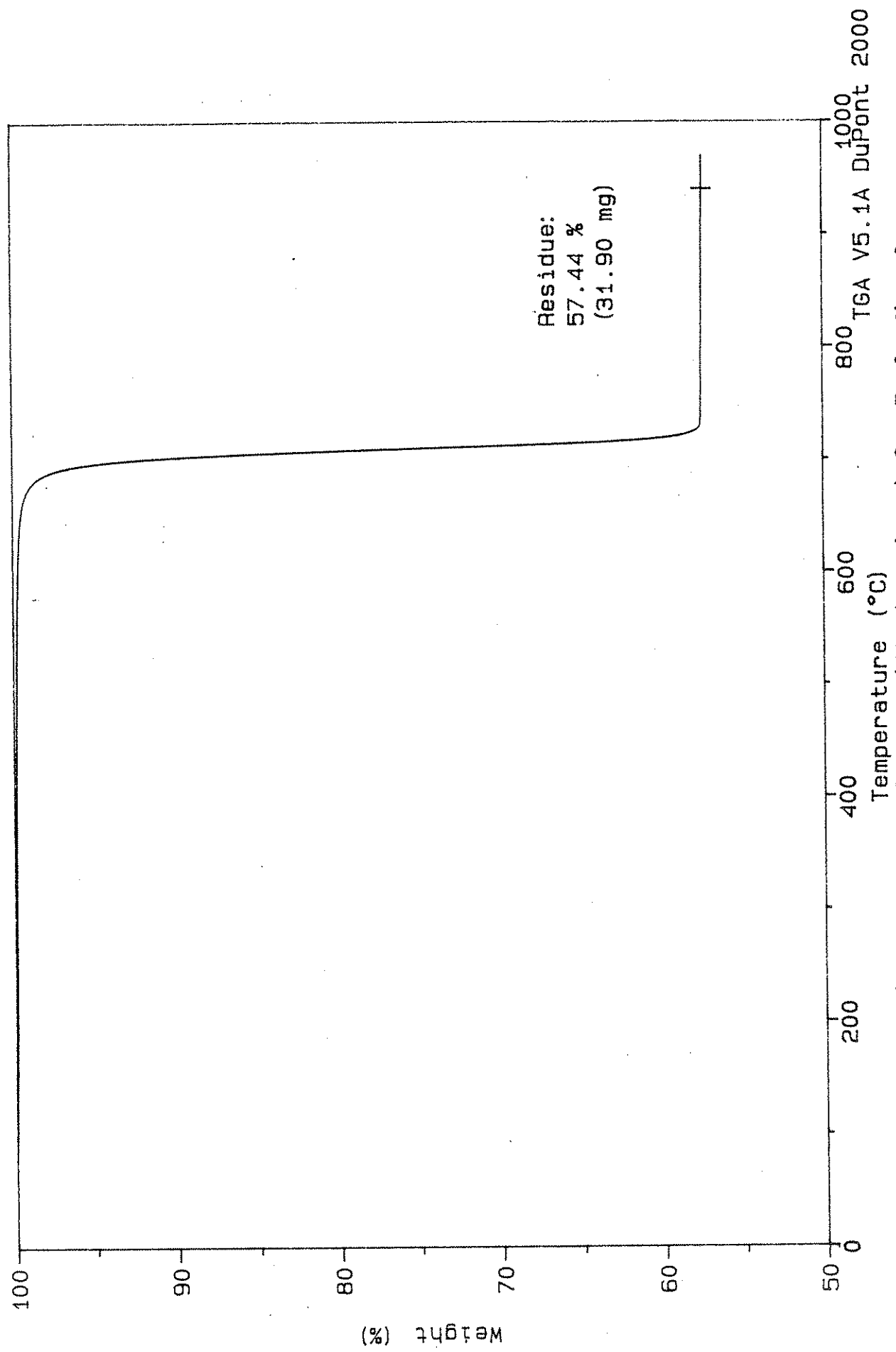


Figure 26, Appendix III. Thermal curve (N2 atmosphere) for Early Chapel aggr.

Sample: HR-337 ELDORADO
Size: 55.5240 mg
Method: 40°C/min, Res 5
Comment: N2 purge @ 100 ml/min

TGA

File: C:SCOTT.081
Operator: J. AMENSON
Run Date: 22-Feb-92 03:00

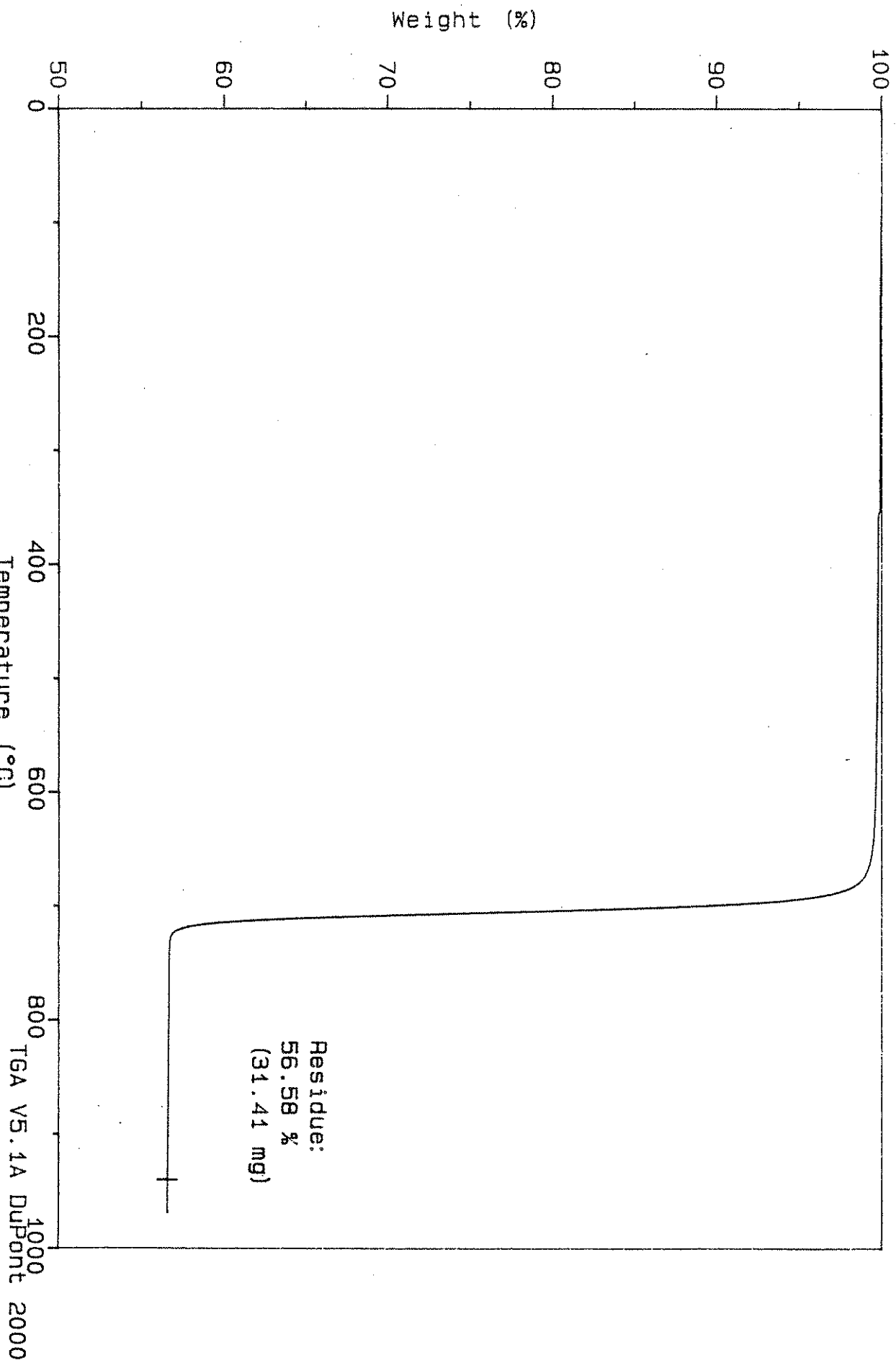


Figure 27, Appendix III. Thermal curve (N2 atmosphere) for Eldorado aggregate.

TGA V5.1A DuPont 2000

TGA

File: C: SCOTT.109
Operator: J. AMENSON
Run Date: 27-Feb-92 17:41

Sample: HR-337 MENLO
Size: 55.5640 mg
Method: 40°C/min, Res 5
Comment: N2 purge, 100 ml/min

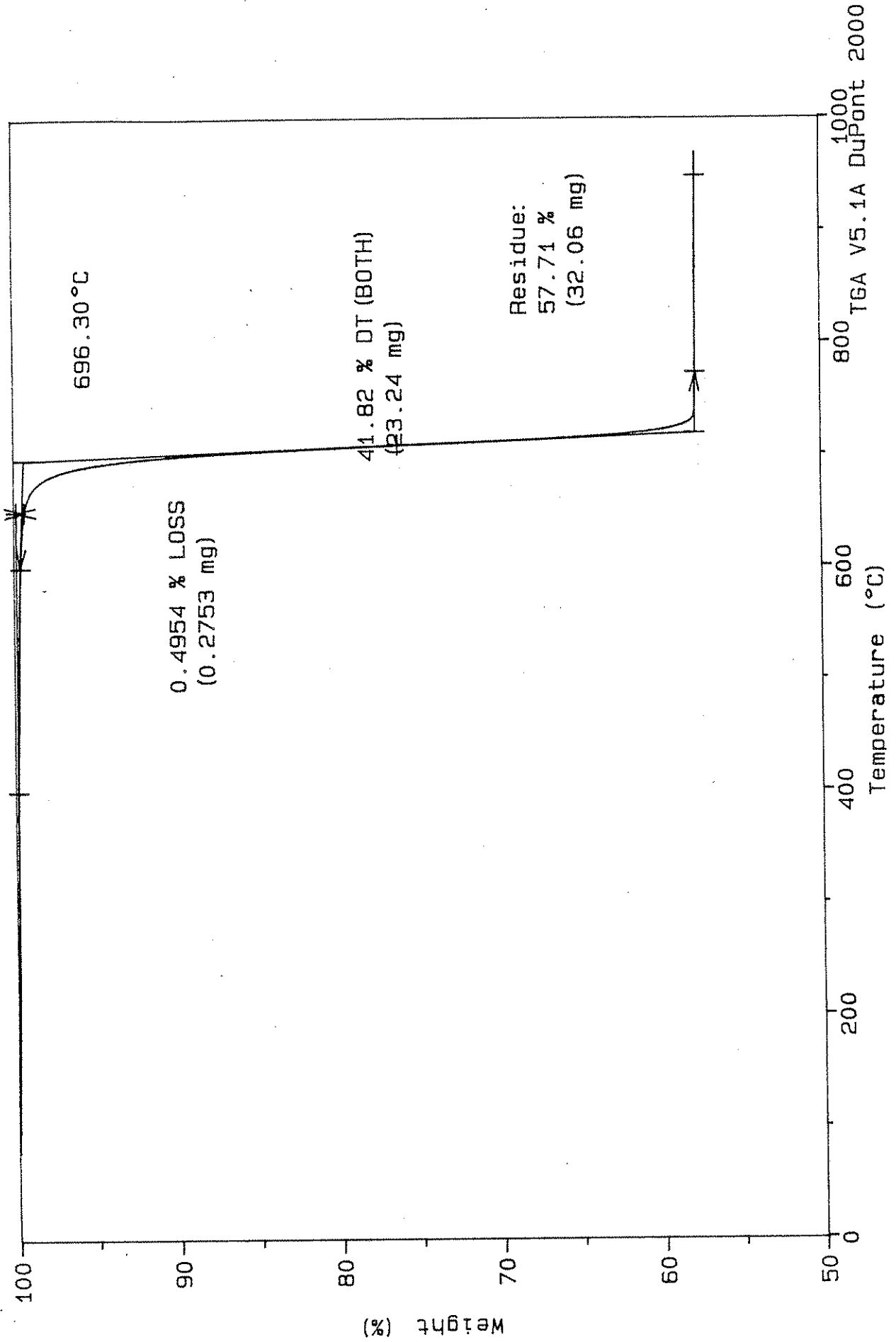


Figure 29, Appendix III. Thermal curve (N2 atmosphere) for Menlo aggregate.

Sample: HR-337 MONTOUR
Size: 55.3040 mg
Method: 40°C/min, Res 5
Comment: N2 purge @ 100 ml/min

TGA

File: C:SCOTT.086
Operator: J. AMENSON
Run Date: 22-Feb-92 11: 48

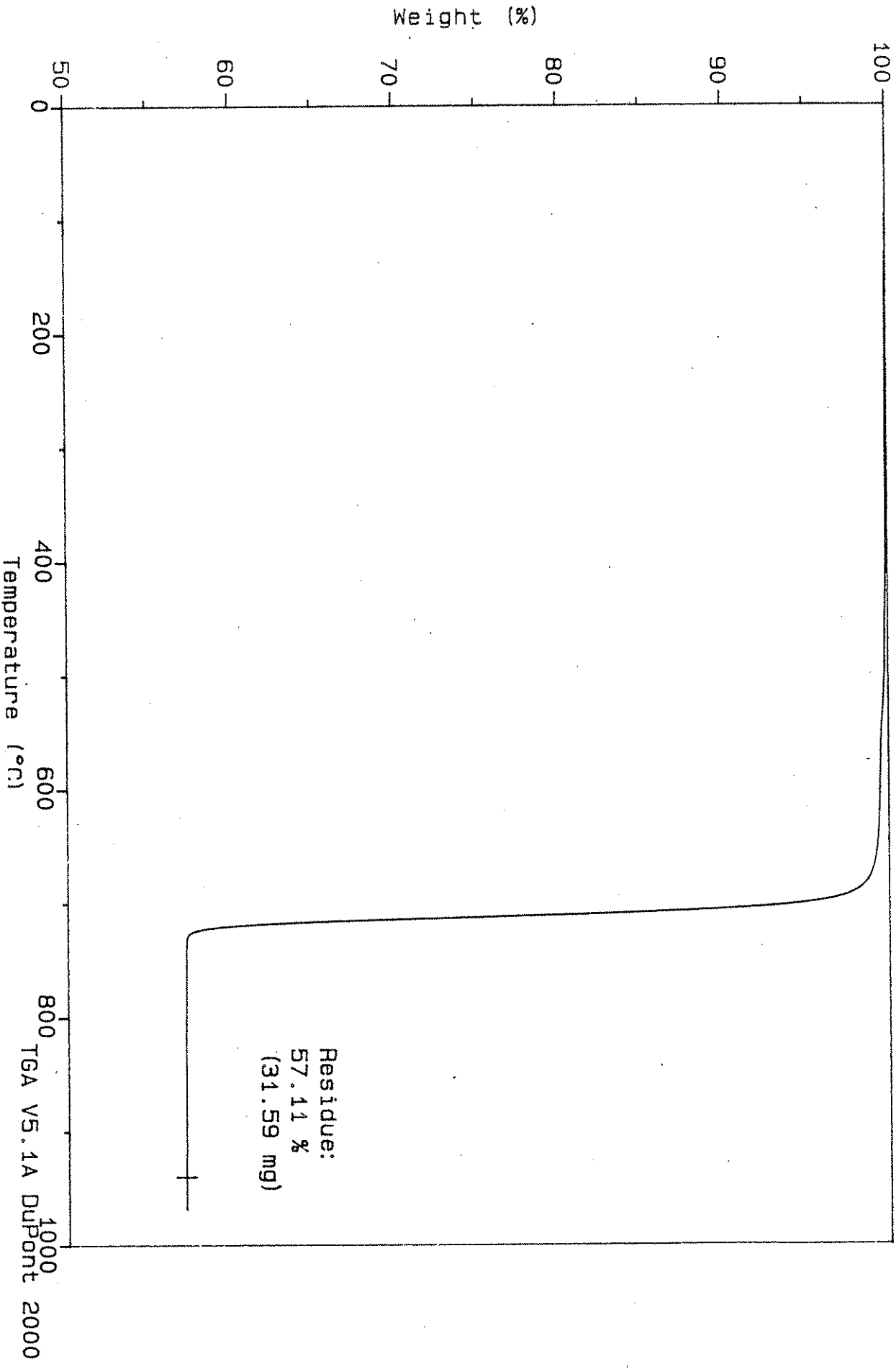


Figure 30, Appendix III. Thermal curve (N2 atmosphere) for Montour aggregate.

Sample: HR-337 SKYLINE
Size: 55.4860 mg
Method: 40°C/min, Res 5
Comment: N2 purge, 100 ml/min

TGA

File: C:SCOTT.110
Operator: J. AMENSON
Run Date: 27-Feb-92 19:20

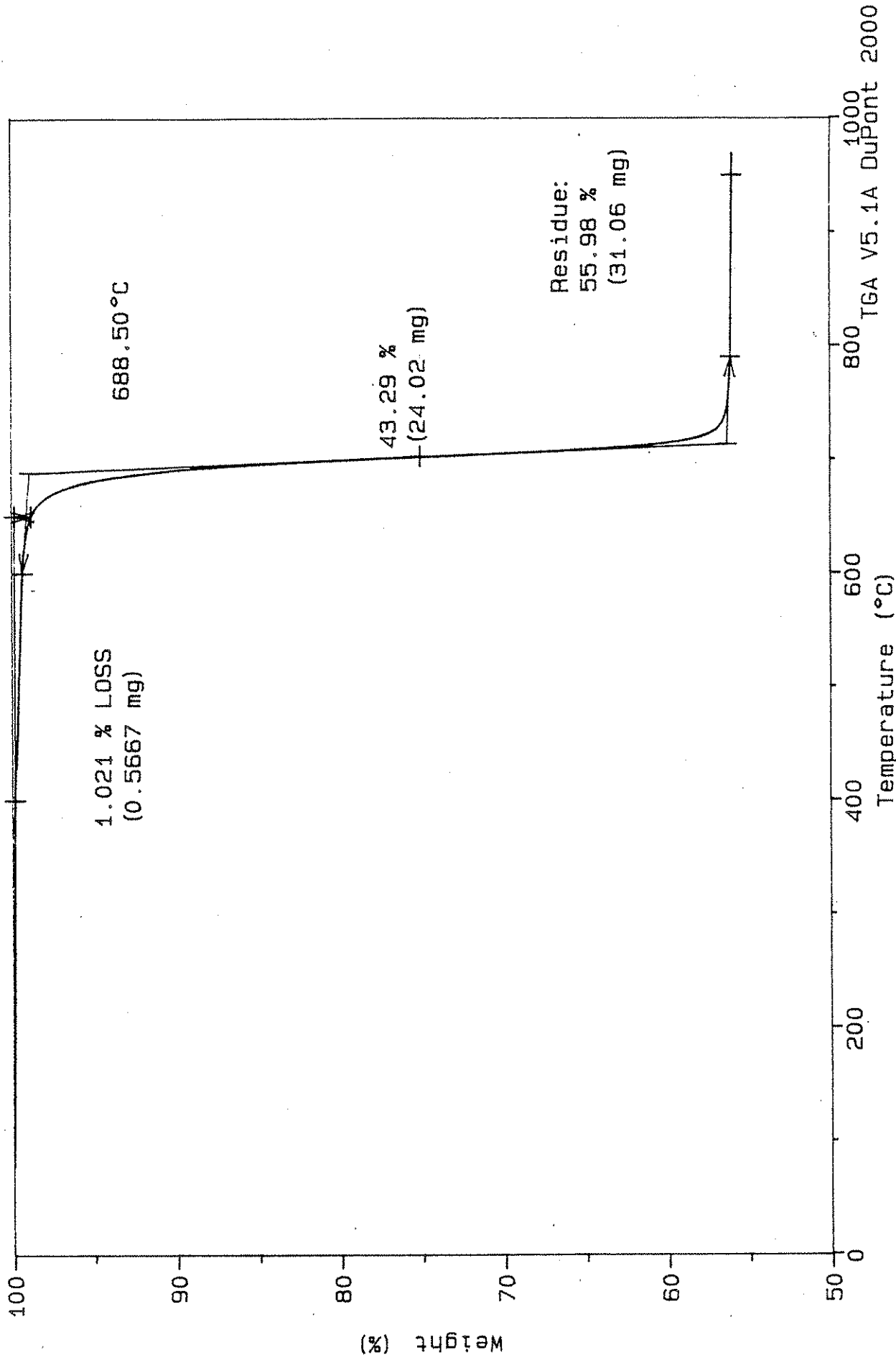


Figure 31, Appendix III. Thermal curve (N2 atmosphere) for Skyline aggregate.

Sample: HR-337 HUNTINGTON
Size: 55.5370 mg
Method: 40°C/min, Res 5
Comment: N2 purge @ 100 ml/min

TGA

File: C:SCOTT.074
Operator: J. AMENSON
Run Date: 21-Feb-92 14:47

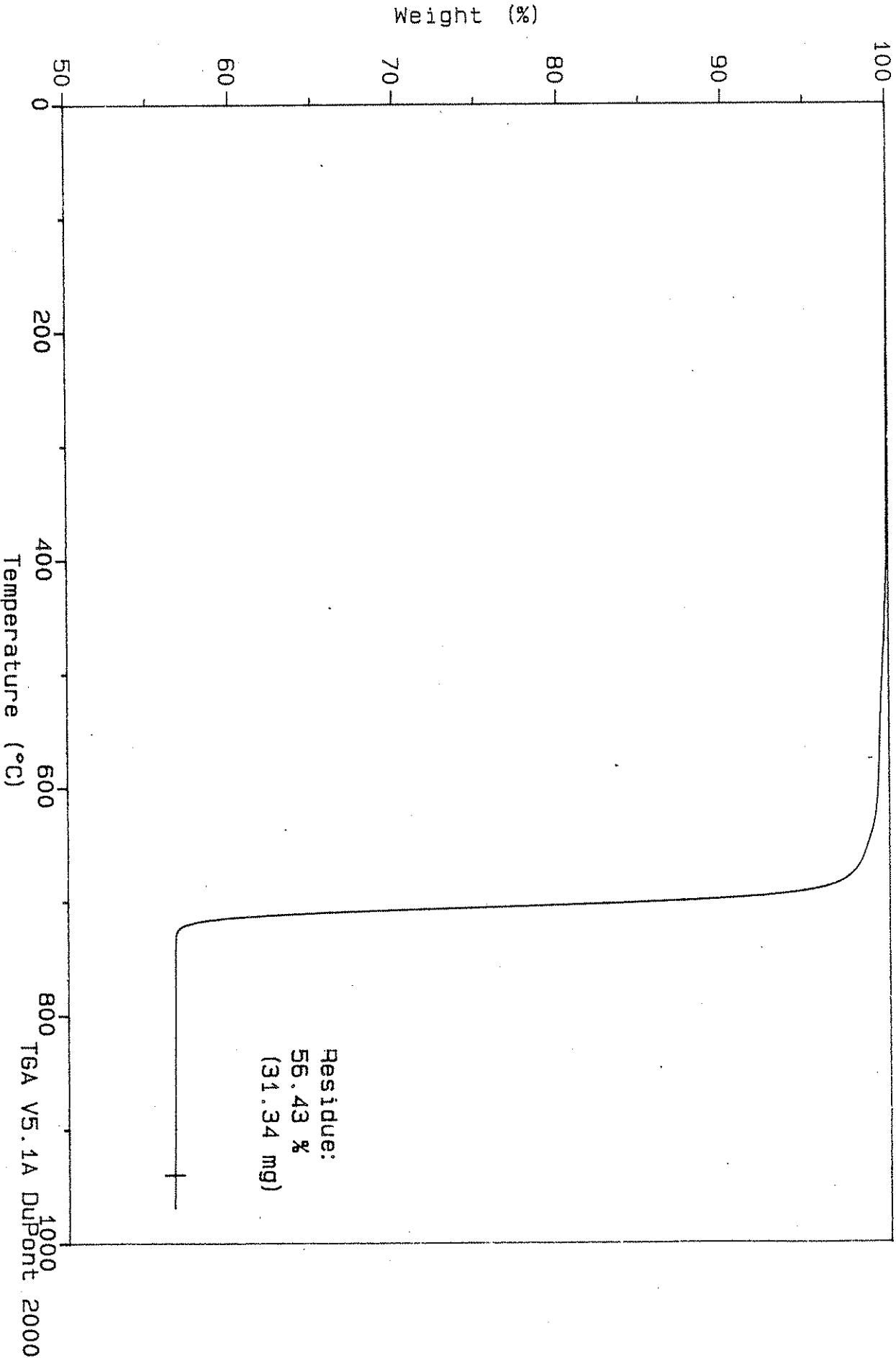


Figure 32, Appendix III. Thermal curve (N2 atmosphere) for Huntington aggregate

Sample: HR-337 FSCO CALCITE
Size: 55.3290 mg
Method: 40°C/min, Res 5
Comment: N2 purge, 100 ml/min

TGA

File: C:SCOTT.115
Operator: J. AMENSON
Run Date: 28-Feb-92 04:08

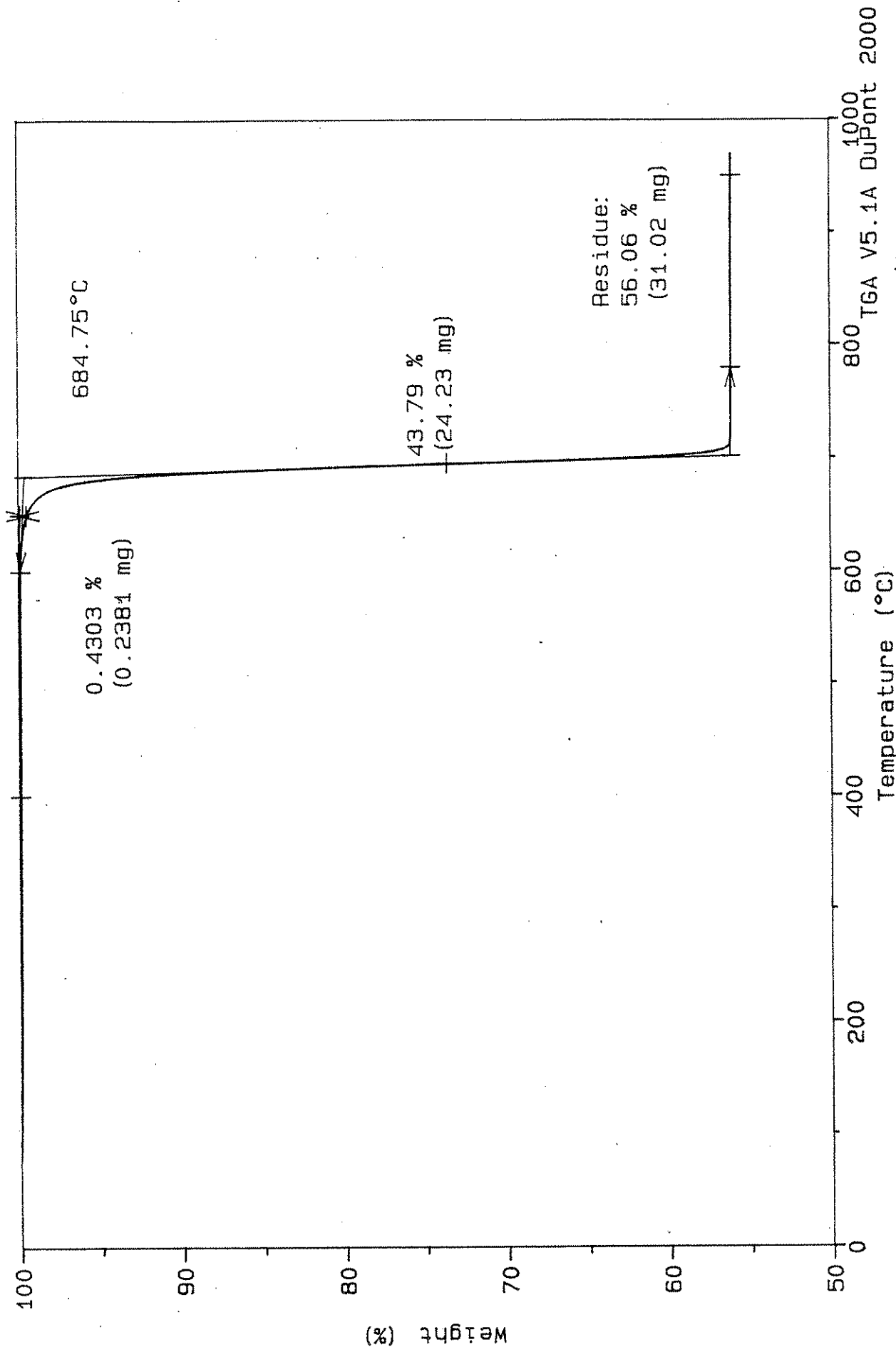


Figure 33, Appendix III. Thermal curve (N2 atmosphere) for Fisher Calcite.

Sample: HR-337 FSC0 CALCITE
Size: 55.3290 mg
Method: 40°C/min, Res 5
Comment: N2 purge, 100 ml/min

TGA

File: C:SCOTT.115
Operator: J. AMENSON
Run Date: 28-Feb-92 04:08

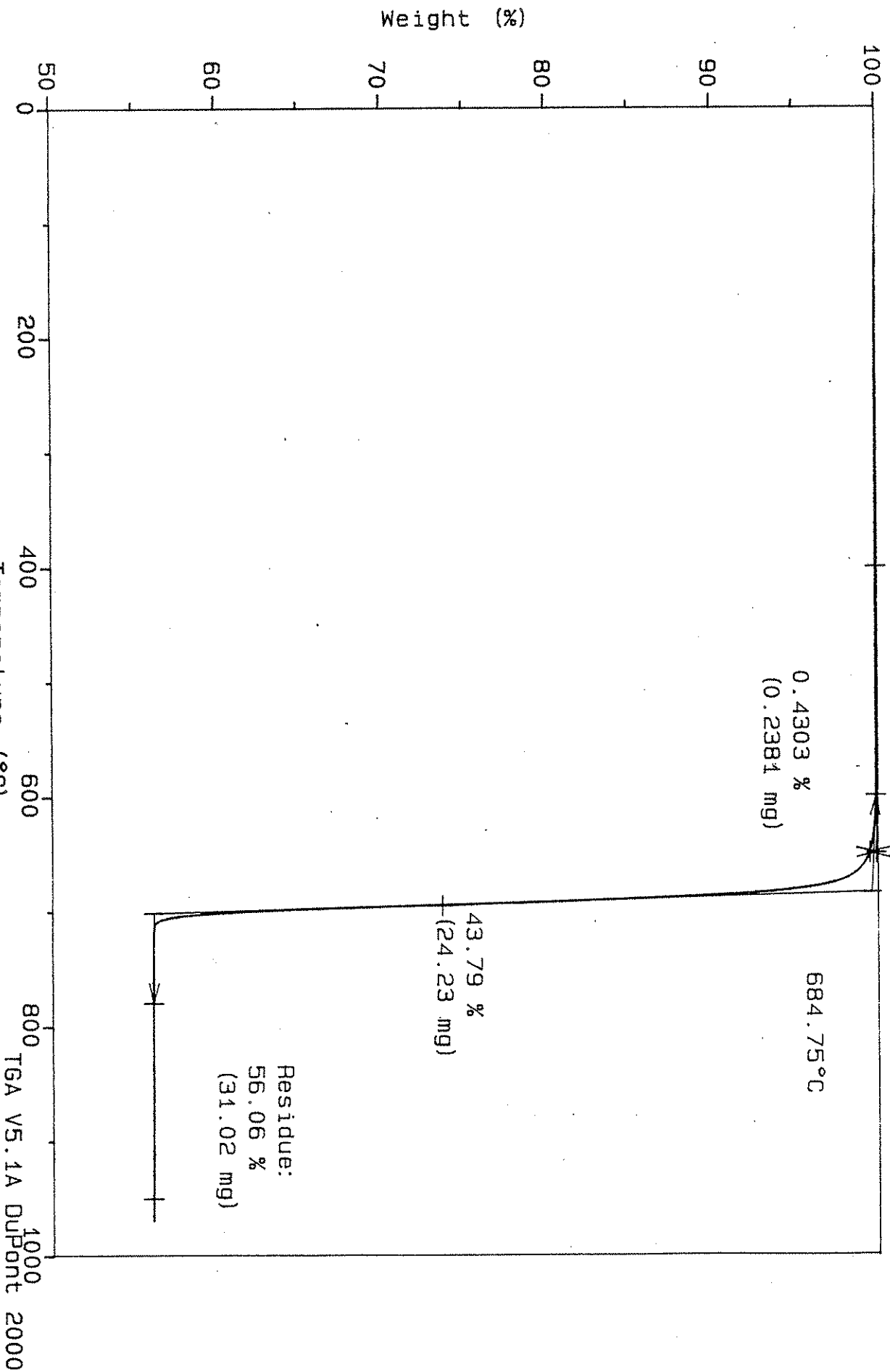


Figure 33, Appendix III. Thermal curve (N2 atmosphere) for Fisher Calcite.

Sample: HR-337 MARYVILLE
Size: 55.5450 mg
Method: 40°C/min, Res 5
Comment: N2 purge @ 100 ml/min

TGA

File: C:SCOTT.085
Operator: J. AMENSON
Run Date: 22-Feb-92 09:46

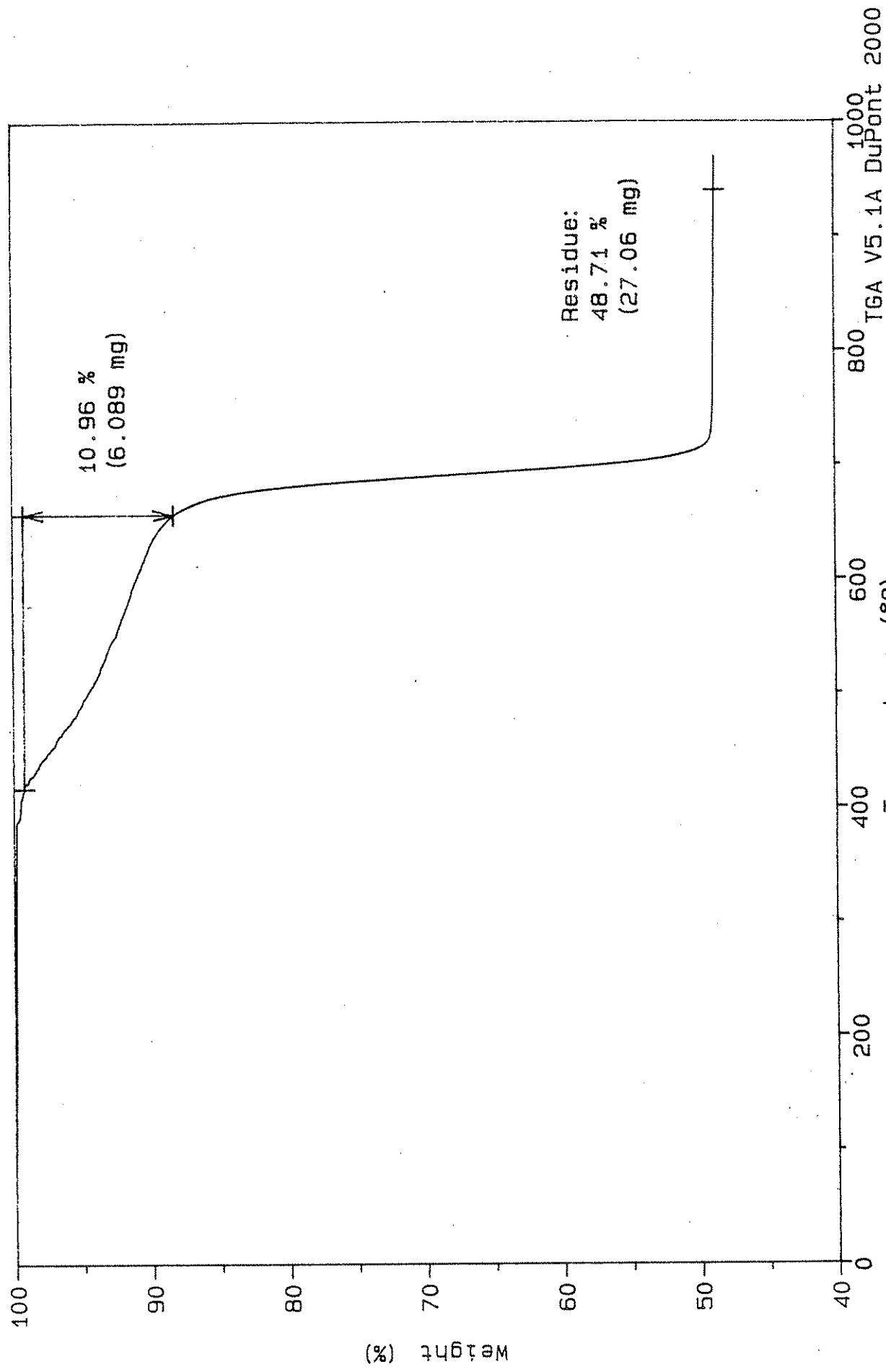


Figure 35, Appendix III. Thermal curve (N2 atmosphere) for Maryville aggregate.

Sample: HR-337 CEDAR RAPIDS (SOUTH-GRAY)
Size: 55.4910 mg
Method: 40°C/min, Res 5
Comment: N2 purge @ 100 ml/min

TGA

File: C:SCOTT.075
Operator: J. AMENSON
Run Date: 21-Feb-92 16:29

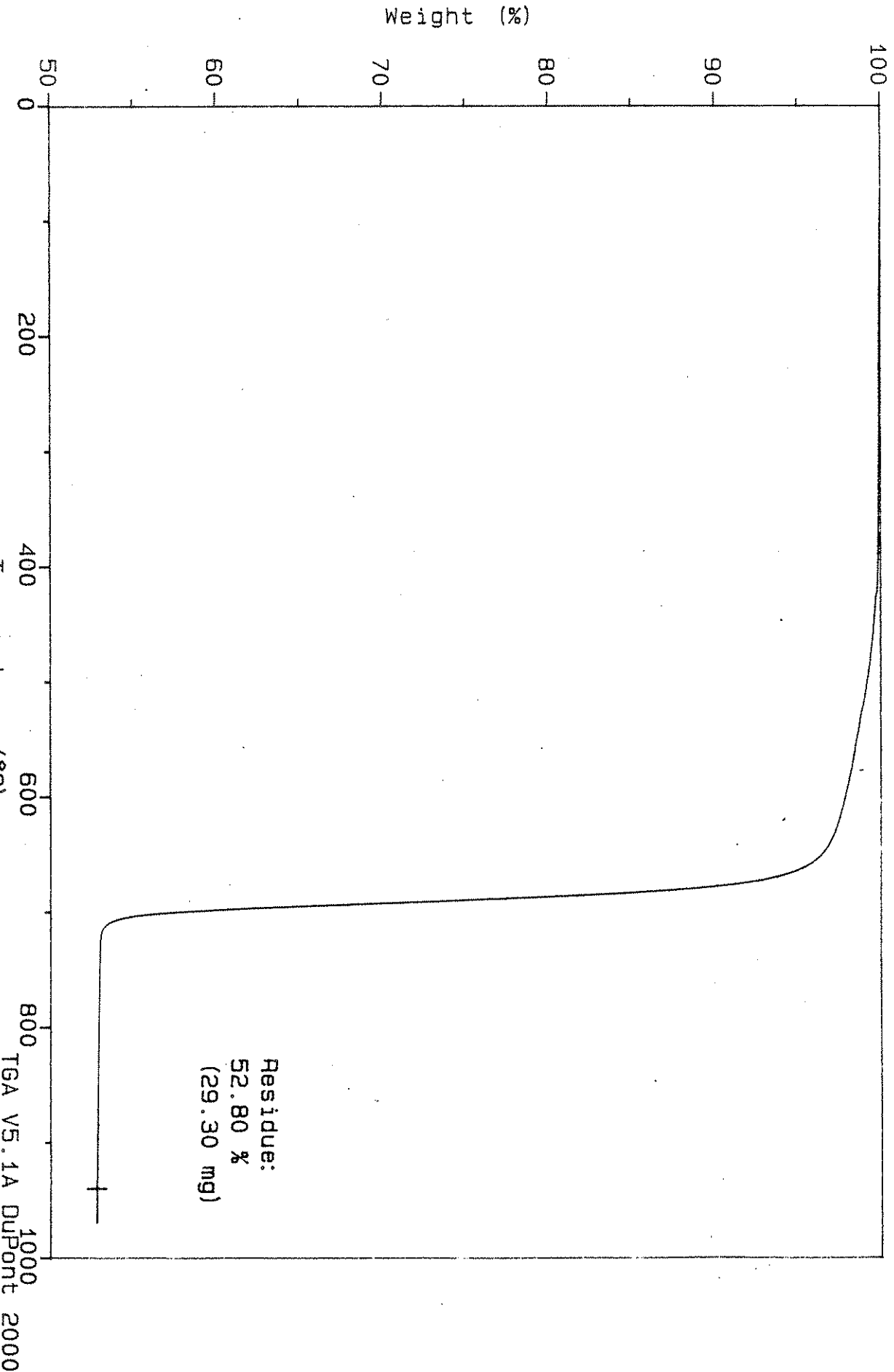


Figure 37, Appendix III. Thermal curve (N2 atmosphere) for Ced. Rap. Gray aggr.

Sample: HR-337 WARDS CALCITE (GROUND)
Size: 55.7630 mg
Method: 40°C/min, Res 5
Comment: N2 purge, 100 ml/min

TGA

File: C:SCOTT.114
Operator: J. AMENSON
Run Date: 28-Feb-92 02:27

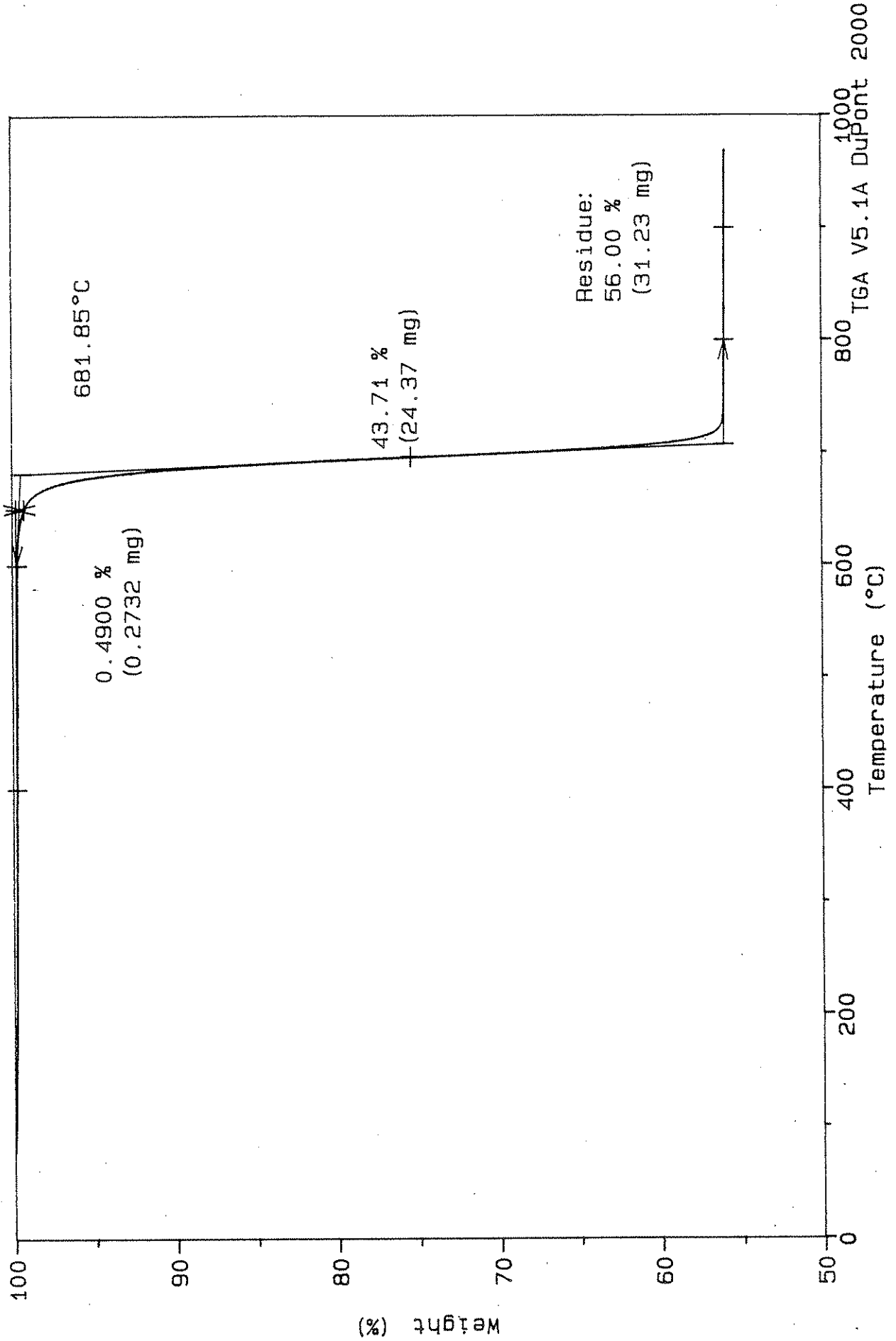


Figure 34, Appendix III. Thermal curve (N2 atmosphere) for Ward's Calcite.

Sample: HR-337 MARYVILLE
Size: 55.5450 mg
Method: 40°C/min, Res 5
Comment: N2 purge @ 100 ml/min

TGA

File: C:SCOTT.085
Operator: J. AMENSON
Run Date: 22-Feb-92 09: 46

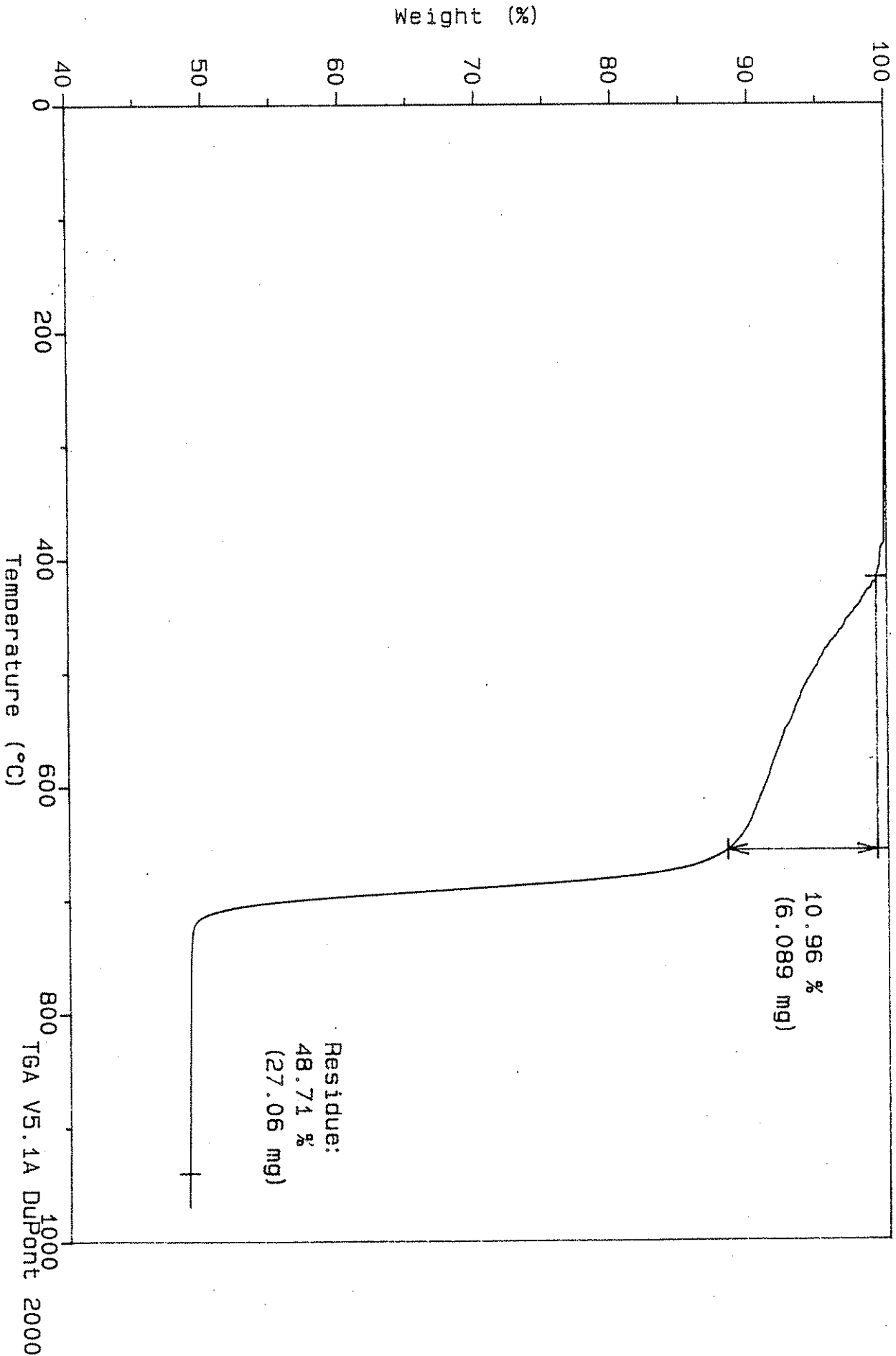


Figure 35, Appendix III. Thermal curve (N2 atmosphere) for Maryville aggregate.

Sample: HR-337 BRYAN
Size: 55.5170 mg
Method: 40°C/min, Res 5
Comment: N2 purge @ 100 ml/min

TGA

File: C:SCOTT.084
Operator: J. AMENSON
Run Date: 22-Feb-92 08:00

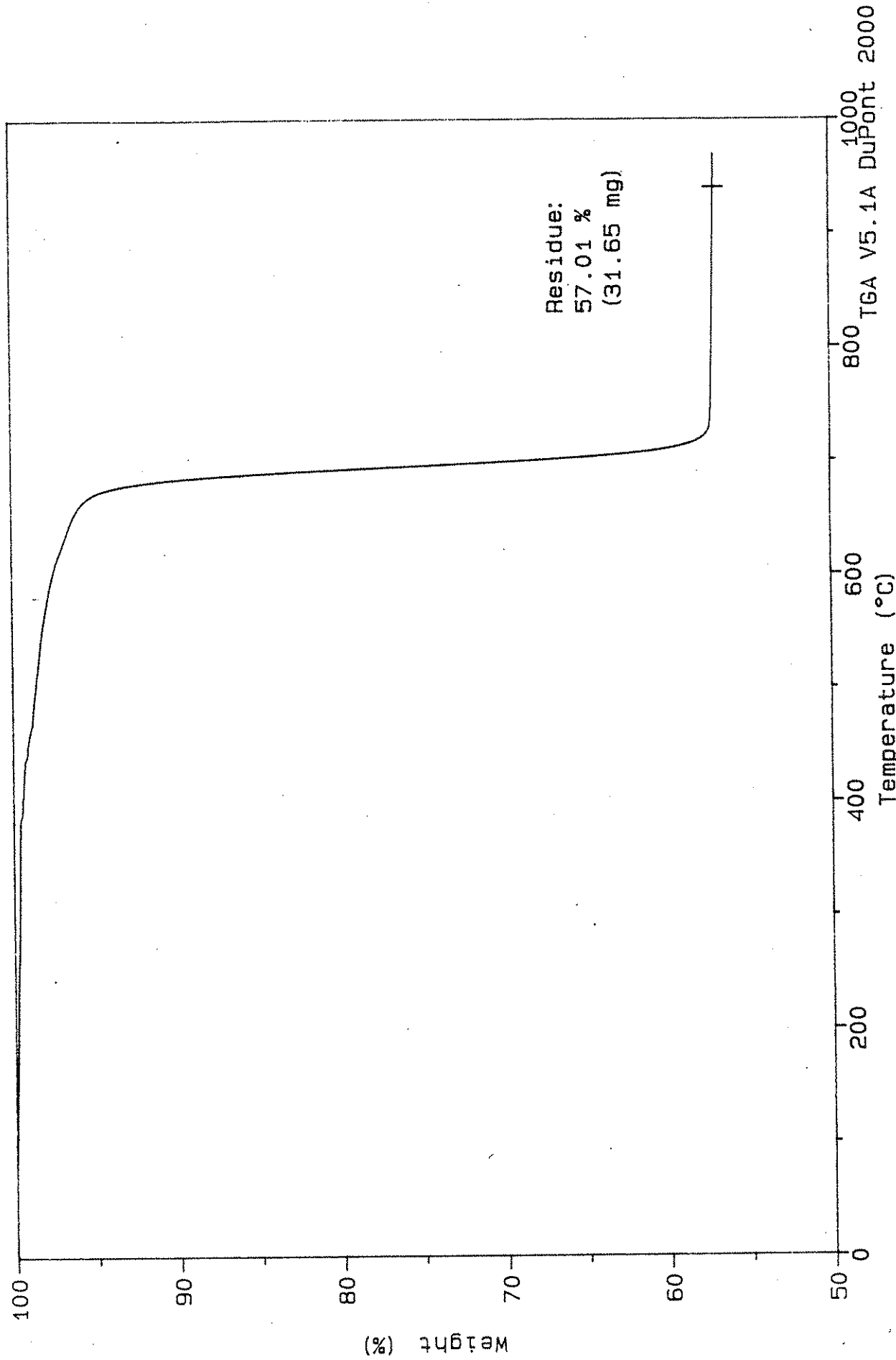


Figure 36, Appendix III. Thermal curve (N2 atmosphere) for Bryan aggregate.

Sample: HR-337 CEDAR RAPIDS (SOUTH-GRAY)
Size: 55.4910 mg
Method: 40°C/min, Res 5
Comment: N2 purge @ 100 ml/min

TGA

File: C:SCOTT.075
Operator: J. AMENSON
Run Date: 21-Feb-92 16:29

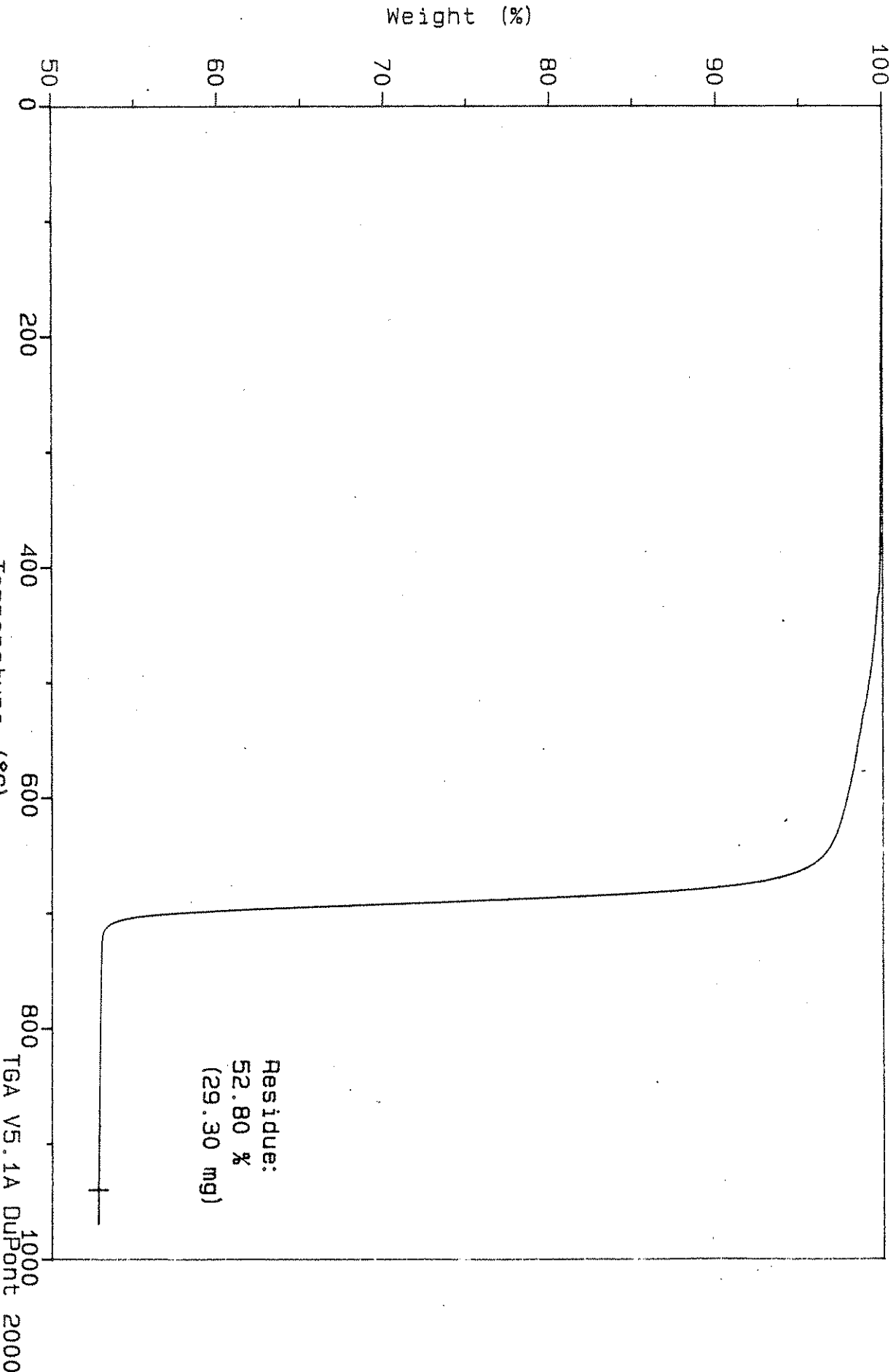


Figure 37, Appendix III. Thermal curve (N2 atmosphere) for Ced. Rap. Gray aggr.

Sample: HR-337 CEDAR RAPIDS (TAN-SOUTH) TGA

File: C: SCOTT.077
Operator: J. AMENSON
Run Date: 21-Feb-92 20:19

Size: 55.5040 mg
Method: 40°C/min, Res 5
Comment: N2 purge @ 100 ml/min

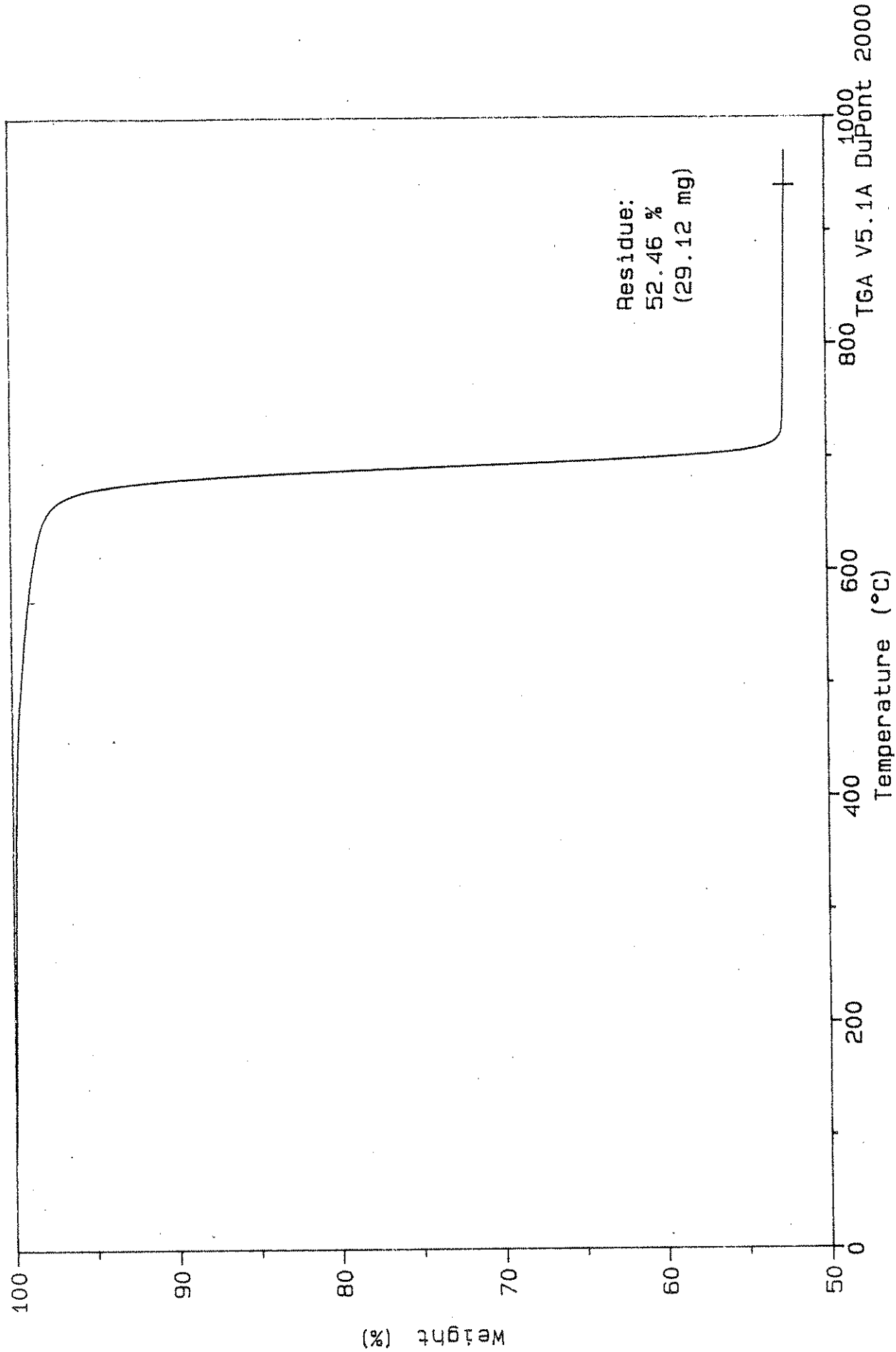


Figure 38, Appendix III. Thermal curve (N2 atmosphere) for Ced. Rap. Tan aggr

Sample: HR-337 GARRISON
Size: 55.6490 mg
Method: 40°C/min, Res 5
Comment: N2 purge, 100 ml/min

TGA

File: C:SCOTT.111
Operator: J. AMENSON
Run Date: 27-Feb-92 21: 04

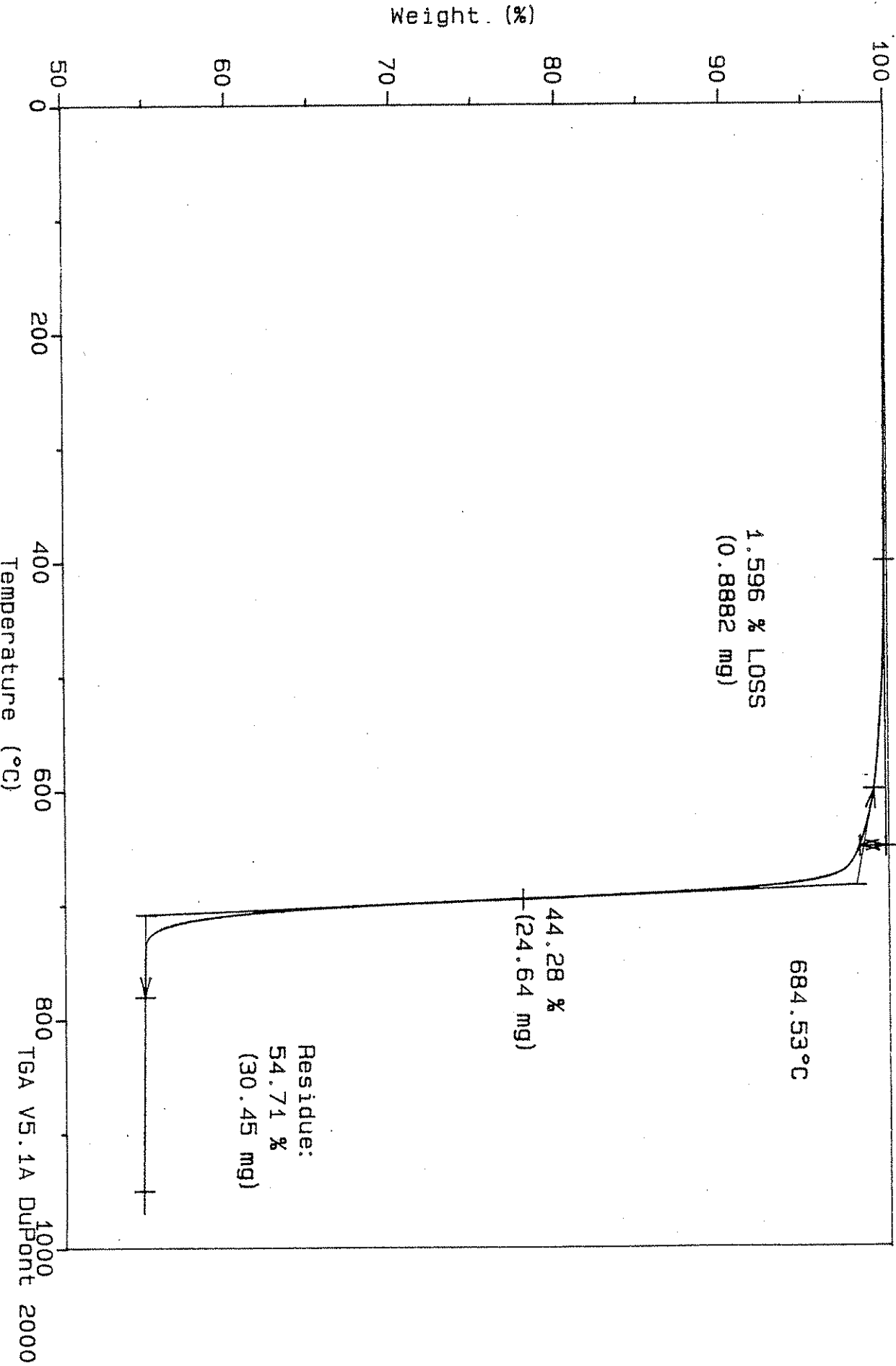


Figure 39, Appendix III. Thermal curve (N2 atmosphere) for Garrison aggregate.

Sample: HR-337 GASSMAN
Size: 55.4500 mg
Method: 40°C/min, Res 5
Comment: N2 purge @ 100 ml/min

TGA

File: C: SCOTT.076
Operator: J. AMENSON
Run Date: 21-Feb-92 18: 17

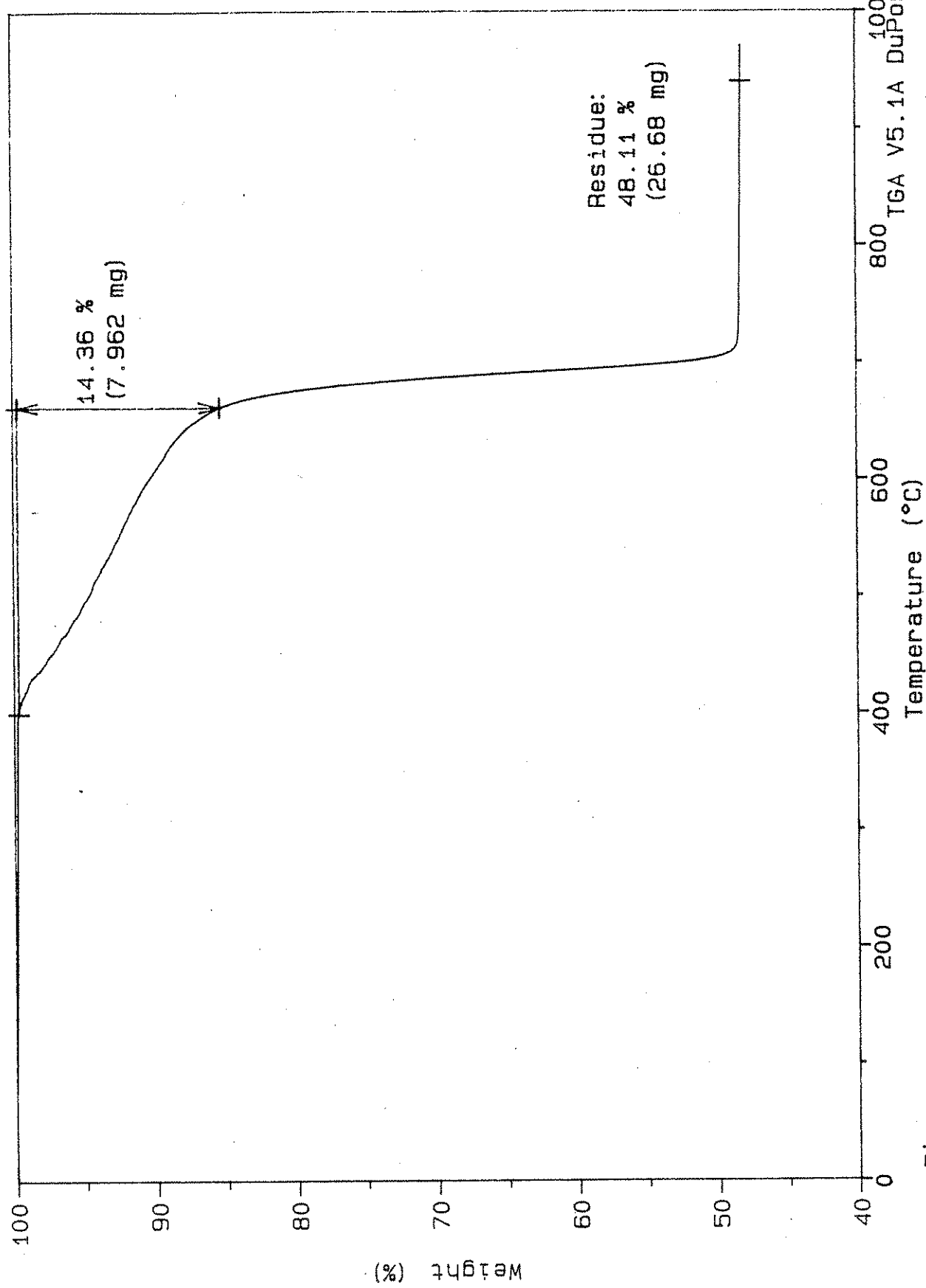


Figure 40, Appendix III. Thermal curve (N2 atmosphere) for Gassman aggregate.

Sample: HR-337 LAMONT
Size: 55.5040 mg
Method: 40°C/min, Res 5
Comment: N2 purge, 100 ml/min

TGA

File: C:SCOTT.108
Operator: J. AMENSON
Run Date: 27-Feb-92 15:35

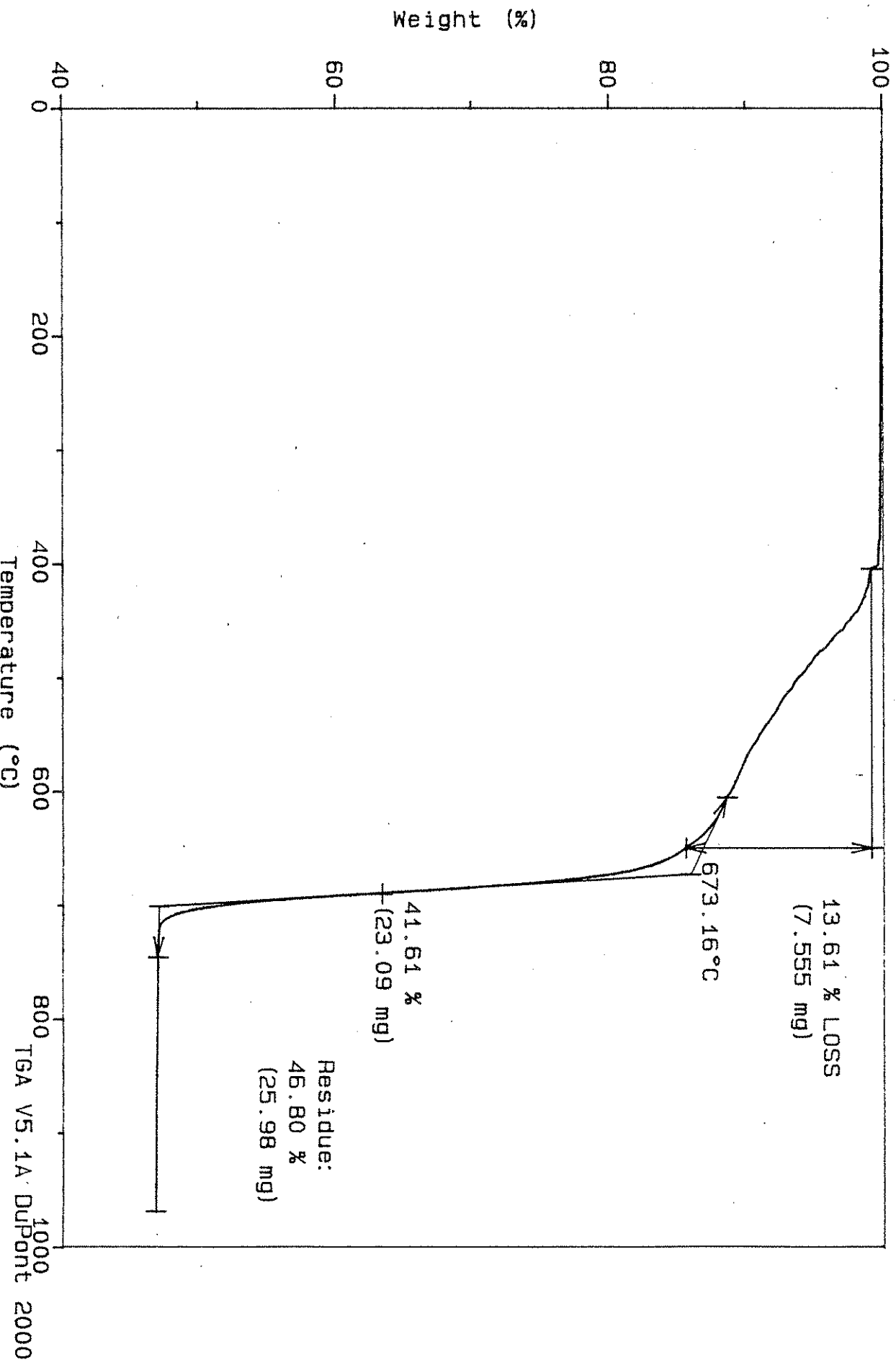


Figure 41, Appendix III. Thermal curve (N2 atmosphere) for Lamont aggregate.

Sample: HR-337 LE CLAIRE,
Size: 55.5820 mg
Method: 40°C/min, Res 5
Comment: N2 purge @ 100 ml/min

TGA

File: C:SCOTT.087
Operator: J. AMENSON
Run Date: 22-Feb-92 13:25

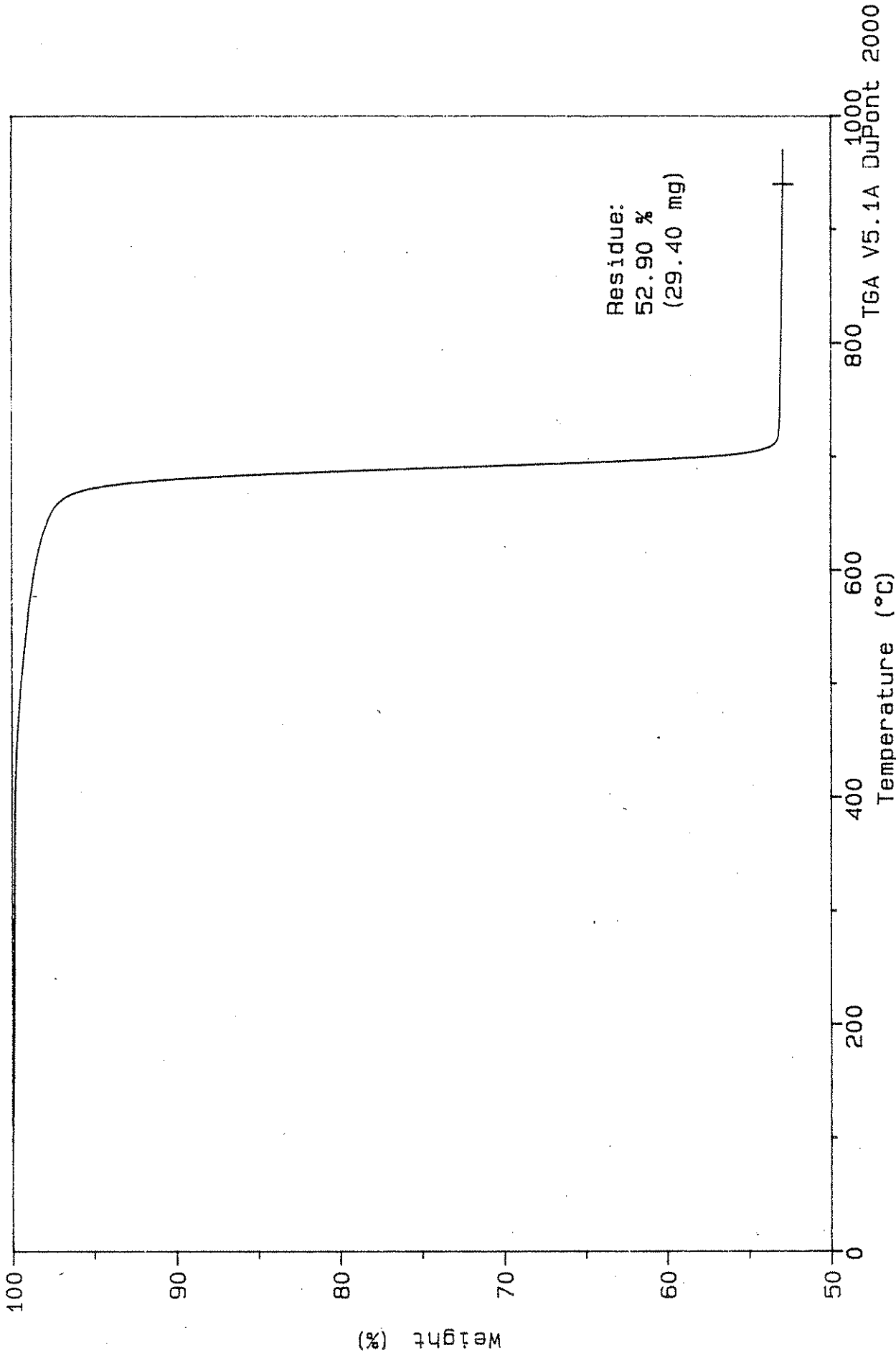


Figure 42, Appendix III. Thermal curve (N2 atmosphere) for LeClaire aggregate.

Sample: HR-337 PESKY
Size: 55.5290 mg
Method: 40°C/min, Res 5
Comment: N2 purge @ 100 ml/min

TGA

File: C:SCOTT.083
Operator: J. AMENSON
Run Date: 22-Feb-92 06:16

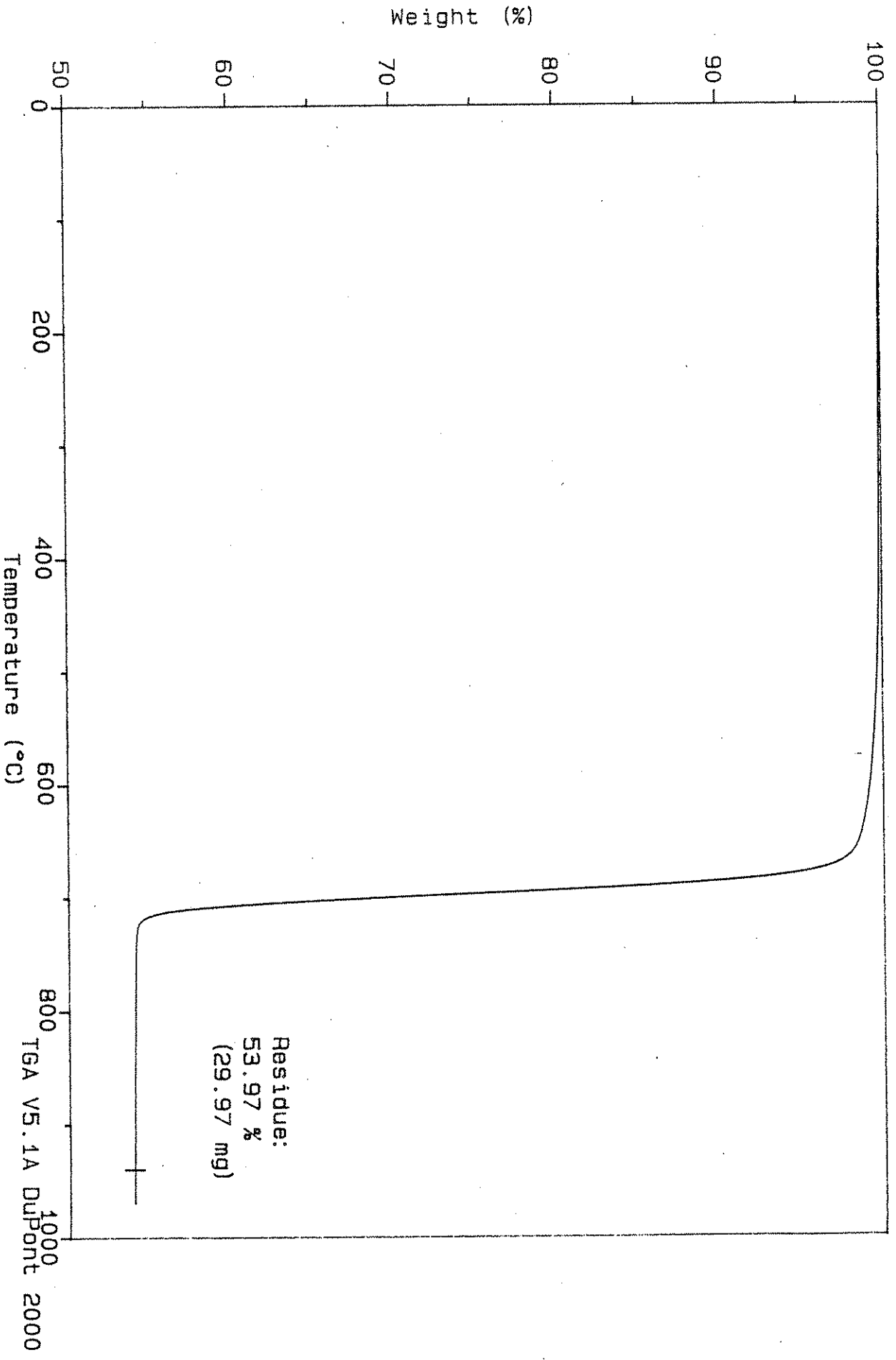


Figure 43, Appendix III. Thermal curve (N2 atmosphere) for Pesky aggregate.

Sample: HR-337 PLOWER
Size: 55.4650 mg
Method: 40°C/min, Res 5
Comment: N2 purge @ 100 ml/min

TGA

File: C:SCOTT.089
Operator: J. AMENSON
Run Date: 22-Feb-92 16:48

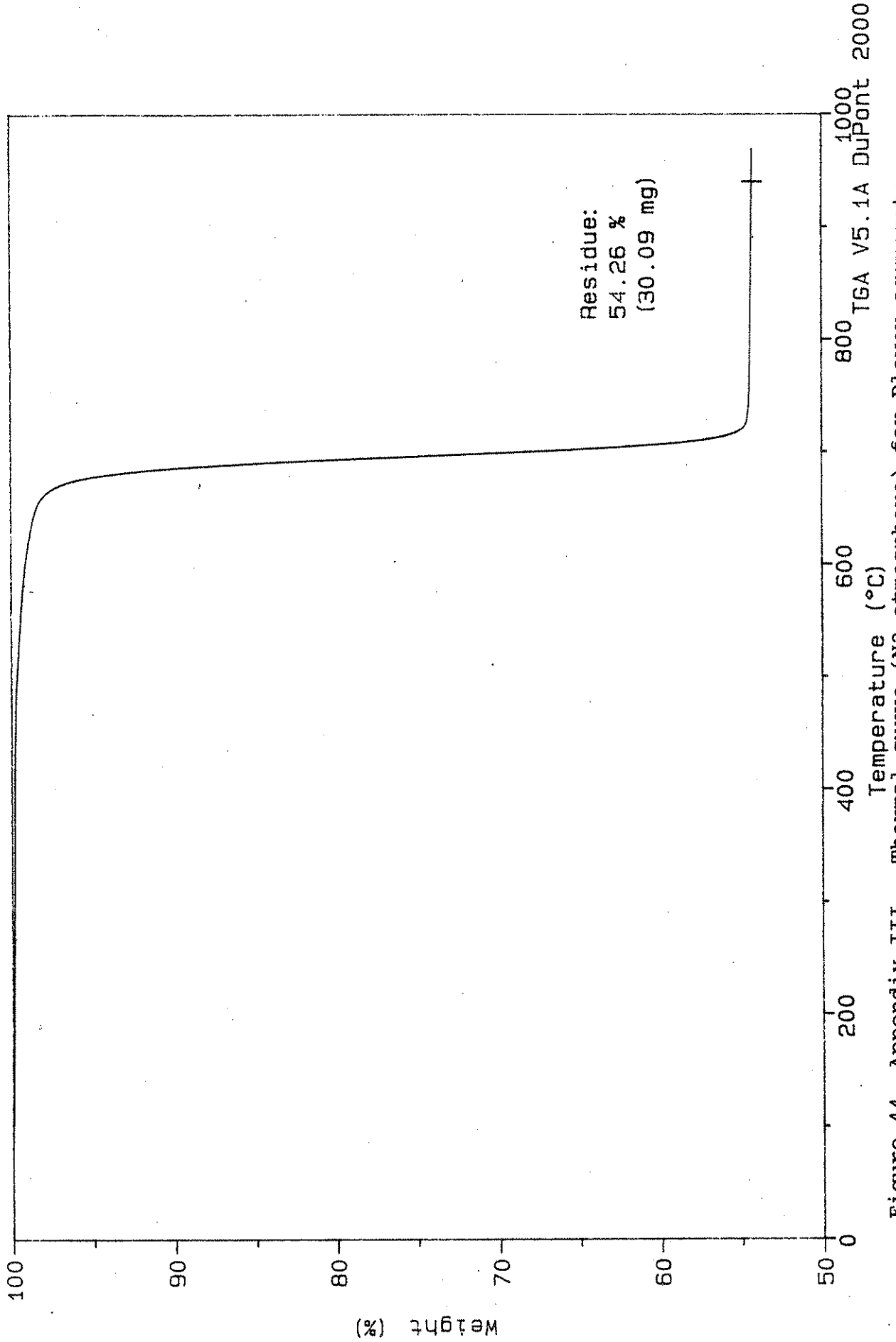


Figure 44, Appendix III. Thermal curve (N2 atmosphere) for PLOWER aggregate.